LBL-12879
UC-25 c.2

Lawrence Berkeley Laboratory
UNIVERSITY OF CALIFORNIA

Materials & Molecular Research Division

AUG 6
DOCUME

A STUDY OF ELECTROPOLISHING OF FERROUS ALLOYS USING ROTATING DISK ELECTRODES

T. Hryniewicz, R.H. Muller, and C.W. Tobias

June 1981

TWO-WEEK LOAN COPY

This is a Library Circulating Copy which may be borrowed for two weeks. For a personal retention copy, call Tech. Info. Division, Ext. 6782

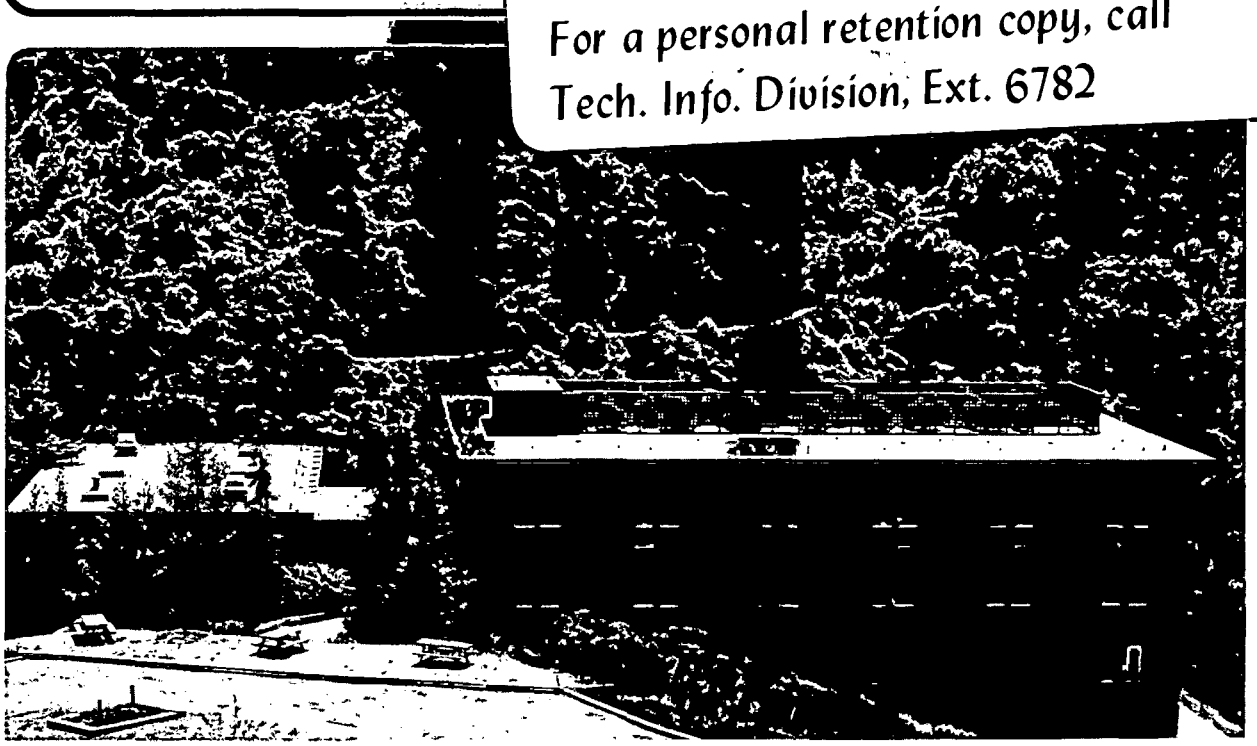

LBL-12879 c.2

Prepared for the U.S. Department of Energy under Contract W-7405-ENG-48

DISCLAIMER

This document was prepared as an account of work sponsored by the United States Government. While this document is believed to contain correct information, neither the United States Government nor any agency thereof, nor the Regents of the University of California, nor any of their employees, makes any warranty, express or implied, or assumes any legal responsibility for the accuracy, completeness, or usefulness of any information, apparatus, product, or process disclosed, or represents that its use would not infringe privately owned rights. Reference herein to any specific commercial product, process, or service by its trade name, trademark, manufacturer, or otherwise, does not necessarily constitute or imply its endorsement, recommendation, or favoring by the United States Government or any agency thereof, or the Regents of the University of California. The views and opinions of authors expressed herein do not necessarily state or reflect those of the United States Government or any agency thereof or the Regents of the University of California.

LBL-12879

A STUDY OF ELECTROPOLISHING OF FERROUS ALLOYS USING ROTATING DISK ELECTRODES

T. Hryniewicz, R.H. Muller, C.W. Tobias

Materials and Molecular Research Division
Lawrence Berkeley Laboratory
University of California
Berkeley CA 94720

June 1981

This work was supported by the U.S. Department of Energy under Contract No. W-7405-ENG-48.

Contents

		Page
	Abstract	1
1.	Introduction	3
2.	Objectives and Scope of This Research	3
3.	Experimental Method	4
	Specimen Materials	5
	RDE Apparatus and Procedure	6
4.	Electrical Investigation	8
5.	Mass Loss Study	10
	Effect of Rotation Speed	10
	Effect of the Duration of ECP	11
	Discussion	11
6	Current Efficiency Investigation	12
	Effect of Rotation Speed	12
	Discussion	13
7.	Effect of Initial Roughness on the ECP Leveling Time	13
8.	Potentiostatic Current Density Changes vs Rotation Speed	14
9.	Examinations of Comparable Surface Appearance	15
10.	Microscopic Observations	16
11.	Auger Spectroscopy	17
	Discussion and Conclusions	19
	Secondary Electron Micrography	20
12.	Discussion of Results and Conclusions	20
	Acknowledgments	24
	References	25
	Tables	29
	Figure Captions	32
	Figures	41

LBL- 12879

A STUDY OF ELECTROPOLISHING OF FERROUS ALLOYS USING ROTATING DISK ELECTRODES

T. Hryniewicz, R.H. Muller, C.W. Tobias

Materials and Molecular Research Division
Lawrence Berkeley Laboratory
University of California
Berkeley CA 94720

June 1981

Abstract: Electropolishing metals provides smooth, bright, and reflective surfaces that exhibit superior corrosion resistance compared to untreated metals. These features may be achieved also in the case of electropolishing of plain carbon steels or low-alloy steels.

This work deals with an elucidation of electropolishing of ferrous materials ranging from pure iron through carbon steels, with increasing carbon content, to a few low-alloy steels. The characteristics of electropolishing stainless and acid-proof steels are well known, and for this reason were not considered in this research.

Studies were performed on the rotating disk electrode system under controlled electrochemical and hydrodynamic conditions. The purpose was to establish conditions at which the best surface finish, after electropolishing of different types of ferrous alloys, may be achieved.

The work involved investigations over a wide range of applied current density, mass loss, and current efficiency. Changing the rotating speed of the sample influences the current density in

potentiostatic operations; this results in different surface finishes. Electropolishing conditions may be reached even at a very high rotating speed (above 3000 RPM), which indicates that a viscous layer is not a necessary criterion for the process to occur.

Microscopic observations showed that, contrary to what has been reported in the literature, there is no direct dependence between the carbon content in steel and the surface finish after electropolishing. Rather than this, several groups of similar appearances after electropolishing may be distinguished: 1) ideal glossy surface, 2) glossy but with needles (or other traces) on the surface, resulting from the steel microstructure, 3) bright orange-peel appearance, 4) fairly good but milky finish.

Composition of the surface layer before and after electropolishing has been evaluated using Auger spectroscopy. As expected, after electropolishing oxygen is the dominant component in the top 10 Å, with some carbon and silicon; the latter probably was introduced by the mechanical polishing prior to ECP.

1. Introduction

Most of the research on electropolishing (ECP) steels has been directed toward the polishing of stainless steels, since these are difficult to polish by mechanical methods and relatively easy to treat by ECP. A wide variety of electrolytes have been proposed for polishing stainless steels [3,4,5,9,21,29,30,32], but only a few of these are of practical interest [4,21,22,34]. Solutions for ECP of stainless steels have been correlated with their throwing power [4,20]. Thus, ECP of stainless steels is widely used for industrial purposes. However, there are many different ferrous alloys for which it would be desirable to use ECP. There are a large number of references on the electrolytes and conditions of the process of ECP, but no comprehensive knowledge of the steel surface finish is available.

Earlier literature, particularly the Russian [2,6,8,32], indicates that increasing the amount of carbon in steel usually worsens the electropolish. Therefore, it is impractical to electropolish cast iron. However, many references show that the plain carbon steels electropolish better with increasing carbon content [4,5,16,28]. This is one of the many problems that should be investigated further. Overall luster and brilliance is not as good on the plain carbon steels as it is on the low-alloy steels [4].

2. Objectives and Scope of this Research

The purpose of this research is to contribute to the knowledge of the ECP of ferritic materials, on the macroscopic and microscopic scales.

A rotating disk electrode system has been used to study the phenomenon of surface layer formation during ECP in order to control the mass-transport process. The experiments included polarization measurements and dissolution in different parts of the polarization curve (on the plateau c.d. and higher).

The effects of rotating speed and duration of ECP on the mass loss in dissolution is discussed in Sec. 5. Following this, the current efficiency of the ECP of ferrous alloys is discussed, based on the mass-loss study.

In Sec. 7 the effect of initial roughness on the ECP leveling time is considered.

Changes in current density vs rotating speed of electrodes under potentiostatic studies are very significant. This is presented in Sec. 8. These changes influence the surface appearance of the electropolished material.

Section 9 deals with the visual appearance of the surface.

In Sec. 10 the results of observations of the optical microscope are presented, and Sec. 11 deals with analysis of the surface layers of the specimen after ECP.

3. Experimental Method

Experiments were planned in such a way that ferrous alloys with varying contents of carbon (starting from pure iron), as well as other elements (low-alloy steels), were used. To establish proper ECP

conditions for each material, polarization curves were determined for different temperatures in the range of 20°C to 80°C.

Three electrolytic compositions were chosen from earlier studies [1,3,4,5,9,16,18,21,22,28,29,34,35], but two of these were later excluded after preliminary investigations because they produced etched finishes only. All experiments were carried out using a rotating disk electrode system (100-3000 RPM). The cell contained up to 1000 ml of polishing solution.

Specimen materials. Ten different ferritic materials were chosen for anodes. These are presented in Table I. Numbers in the table correspond to sample numbers. Materials for samples were prepared in such a way that (apart from sample 1,2,3,4) they were of similar hardness (about 50 HRC). Each sample of the same material, three times repeated, had a diameter of 19.05 mm and was 5 mm thick. Following machining, the sample was bonded by silver epoxy to a base-holder (Fig. 3-1) made from stainless steel to fit with the extension rod (Fig. 3-3) through the screws. The samples were coated on sides and back with epoxy resin (Fig. 3-2) to leave only the front surface accessible for investigation.

During the experiments, the samples were ground with a 240-grit wet-grinding paper before a run and then rinsed with running water and dried in air to receive, generally, one value of initial roughness.

The extension for the anode (Fig. 3-3) was made of 304-stainless steel coated with Kynar to isolate its external surface from the electrolyte.

The cathode (Fig. 3-4) was also made from a round stainless steel sheet fitted into the bottom of a beaker with the surface being about 45 times larger than the anode.

The reference electrode was made of glass with a Pt wire into a sealed bottom. $Hg/Hg_2SO_4/SO_4^{2-}$ was employed [7,11] as the reference electrode to measure the anode potential. 0.1N H_2SO_4 concentration was used and potential relevant to NHE equaled to +0.6151 V at 25°C with electrode reaction: $2\ Hg + SO_4^{2-} \rightleftharpoons Hg_2SO_4 + 2e$.
In the present work, the cathode potential was not measured.

The samples and the cell used in the experiments are presented in Fig. 3-5. The electrochemical cell consisted of a round glass beaker of 100 mm depth and 115 mm diameter, with an 8.5 mm hole diameter in its bottom. Into a beaker a 304 stainless steel cathode was placed and sealed by means of O-rings. For the initial stages of experiment, three electrolyte solutions were prepared (Table II). After the first runs, it appeared that only electrolyte E1 gives the expected results in the surface polishing. Two other compositions caused etching rather than ECP, so they were excluded from further investigation.

RDE apparatus and procedure. The experimental setup is shown in Fig. 3-6. The rotating anode surface was positioned on the central axis of the beaker, 30-50 mm above the cathode. With this configuration, the anode surface faces down. The anode surface is 2.834 cm^2.

Constant current was supplied by a Potentiostat Galvanostat Model 371 power supply. The anode current, as well as the cell current, when running galvanostatically, was measured by a Keithley 179 TRMS

Digital Multimeter, or by the voltmeter-ammeter built into Potentiostat Galvanostat Model 371 when its value exceeded 2 amperes.

The rotating disk assembly was powered by a variable speed DC motor, model STE-231T-1C, controlled by Servo-Tek with Rectifier Model ST-554-1. The RDE speed calibration was made earlier by D. Roha and was not repeated here. Calibration results are presented in Table III.

The electrical circuit in the potentiostatic mode is shown in Fig. 3-7. This figure also includes the wiring diagram for the electrochemical cell and the reference electrode.

The weight loss of the anode specimen resulting from anodic dissolution was measured to a precision of ±0.1 mg on a Mettler Type H6T balance after washing and drying at room temperature.

The change of shape on the anode surface was mesured after each run on a Bausch and Lomb Optical Gage DR-2TB. Starting from the center of the sample, measurements were carried out in four perpendicular directions to avoid the effect of misalignment of the specimen surface. The center of a sample was protected from dissolution by a small piece of tape that served as the reference point for the surface profile. In each case, four different sets of values were averaged to determine the thickness of the metal layer removed by ECP.

Microscopic observations of the anode surfaces under magnifications 6x and 40x were performed after washing and drying. Micrographs were taken on the periphery and near the center of the sample.

To analyze the composition of surface layers at 10 Å, 400 Å, and 500 Å depth, an Auger spectrometer was employed. Samples for the analysis were separated from the holder, cleaned mechanically and ultrasonically, washed in acetone and in alcohol, and then dried.

Roughness measurements of the anode surfaces were discontinued after having obtained similar results on many samples (Fig. 3-8).

4. Electrical Investigations

This section is devoted to two main problems: polarization curves and studies at low-current density (i.e., under the plateau current density).

Polarization curves. Results showing current density vs anode overpotential are presented in Figs. 4-1 to 4-6. Experiments were carried out with the same rotation speed, 500 RPM, and four different temperatures, 20, 40, 60, and 80°C. In each case, a plateau density is observed.

Polarization curves in Fig. 4-7 were obtained at 80°C and 1000 RPM and are presented together to compare all four materials. In the case of sample 9, there was no noticeable current plateau.

The effect of different rotation speeds on the shape of the polarization curve is presented in Fig. 4-8. At very low speed (100 RPM) the curve is slightly different from those obtained at higher speeds.

Studies at the low-density range. Four materials (samples 2, 4, 6, and 9) were studied below the plateau current density on the polarization curve (low-applied voltage). All studies were carried out at the same

rotation speed, 500 RPM. Dependence of the current density on time of electrolysis is shown in Fig. 4-9. The same dependence is presented in Figs. 4-10 and 4-11 after repeated polishing.

From the last two figures (sample 6), it can be seen that the changes in current density at steady potential exists, but these fluctuations are of minor importance. Very similar results were obtained for sample 4 (see Figs. 4-12 and 4-13). The beginning stage of change is shown in Fig. 4-13.

The dependence of current density on time at narrow voltage changes is shown in Fig. 4-16. One curve in this figure (corresponding to 0.34 V) is presented in Fig. 4-15 as a function of $it^{0.5} = f(t^{0.5})$. It appeared that, after the initial steep change, the function in Fig. 4-15 is close to liner.

Other examples of current vs time curves obtained for toolsteel H13 (sample 9) and Armco iron (sample 2) are shown in Figs. 4-16, 4-17, 4-18, and 4-19, respectively.

It is noticed that in each case, after switching on the voltage, there is a quick drop in current density, which then rises again to a steady value depending on the amount of voltage applied.

Discussion. Experiments show that for most alloys a plateau current density exists. In the case of high-carbon steel and low-alloy steel, however, the plateau current density extends over only a very short range of overvoltage, and sometimes may not occur (sample 9).

The behavior of the polarization curves cannot be connected with the surface finish attainable after ECP.

The rotation speed of the anode surface has a minor effect, if any, on the polarization curve. The temperature of the electrolyte strongly influences the polarization curve.

Investigations at low-current density have shown fluctuations. The mechanisms may be connected with the formation and disappearance of the surface layer. It results in a drop and then an increase of the anodic current density.

One curve from Fig. 4-14 is replotted as a function of square-root time. In Fig. 4-15 it shows that at a certain value of the potential applied (0.34 V in this case), the process starts to be diffusion-controlled. It may result in the formation of a solid film on the treated surface [13].

5. Mass-Loss Study

Two problems were of importance during the study of mass loss: 1) the effect of different rotation speed on mass transfer rates, and 2) the effect of the duration of ECP.

Effect of rotation speed. Metal removal thickness vs distance from the center of the sample for three materials are shown in Fig. 5-1. Different results were obtained depending on the material used. These results were obtained at 1500 RPM and without rotation (0 RPM).

Mass loss during ECP is higher when the RDE is rotating than at zero speed. The study at various rotation speeds (Figs. 5-2, 5-3, 5-4) has shown, however, that dependence on rotation speed values is not always the same. To establish an exact dependence, more experiments will have to be done.

Such a study was performed for all ten materials at two different rotation speeds--100 and 1000 RPM. Experiments were done galvanostatically at 3 V, which resulted in two different current densities--100 and 85 A/dm^2 (Fig. 5-5). In spite of the lower current density at 1000 RPM, the average mass loss was higher than at 100 RPM. This was indicated also by the higher current efficiency at 1000 RPM (36 percent), as compared with the current efficiency at 100 RPM (27 percent).

Effect of the duration of ECP. The effect of the duration of ECP on the mass loss was determined under the following ECP conditions: 3 V, 100 A/dm^2, 500 RPM, and 66°C for carbon steel (sample 6). Before each run the sample was reground with a 240-grit wet-grinding paper, then rinsed with running water and dried. One-minute and 5-minute ECP intervals were employed. Results of mass loss vs ECP time are presented in Fig. 5-6.

Discussion. The results obtained in the mass loss study during ECP with the RDE system may be compared with the results obtained by Marathe and Newman [25] for the metal deposition reaction. For an RDE system, the tendency toward nonuniformity of the current distribution exists, as well as deviations of electrode kinetics and mass transfer in the diffusion layer. In the case of ECP with the RDE system, the higher the rotating speed the greater the mass loss rate.

Different mass losses resulted in different current efficiencies. One may notice from Fig. 5-6 that mass loss was different during each minute of ECP. The cause of this phenomenon may be as follows:

1) Different preparation of the anode surface for ECP resulting from different regroung conditions

2) Different activities of the electrolyte, minute by minute

3) Different phases of steel resulting from heat treatment (sample 6) exposed to dissolution.

It is interesting that uniformity of dissolution measure in the mass loss was much greater if the samples were not reground before a run, as presented in Sec. 6.

6. Current Efficiency Investigation

Three different materials were electropolished for a total period of 18 minutes without regrinding after each interruption. The mass loss was measured after each run, lasting 1, 2, 3, or 4 minutes. The experiment was carried out potentiostatically with one rotation speed, 500 RPM. The results are presented in Fig. 6-1.

Pure iron has the highest current efficiency (sample 1), η_{CE}^{1} = 30.9 percent; the next lower was toolsteel (sample 10), η_{CE}^{10} = 28.2 percent; and the lowest was carbon steel (sample 5), η_{CE}^{5} = 24.6 percent.

Effect of rotation speed. Three groups of materials--pure iron (sample 1), carbon steel (samples 5,6,7), and toolsteel (sample 9)--were electropolished to examine the effect of rotation speed on the current efficiency. Studies were performed potentiostatically at 3 V and 5 V. Results are presented in Figs. 6-2 and 6-3. Figure 6-2 shows results of all samples together, therefore it is difficult to withdraw proper conclusions. More conclusions may be reached by analyzing Fig. 6-4.

Discussion. One may notice from the figures presented that, generally, the higher the voltage applied the lower the current efficiency. Current efficiency changes with the rotation speed of the sample. Up to 1500 RPM, the changes are minor (Fig. 6.3); at higher RPM, the current efficiency in each case started to increase (except for sample 1 at 3 V).

Comparing Figs. 6-1 and 6-3, one notices that the results coincide with each other. At most of the rotation speeds employed, the best current efficiency was achieved for pure iron (sample 1). In the case of low-alloy steels (toolsteels), the results are somewhat mixed, especially at the low voltage applied (3 V); but this is generally due to the etching rather than to the ECP action under this voltage.

Among the three groups of ferritic material (pure iron, carbon steels, and low-alloy steels), the current efficiency was lowest for carbon steels.

From Fig. 6-4, it appears that at the higher rotation speed there is less scatter in the dependence of current efficiency on applied voltage.

7. Effect of Initial Roughness on the ECP Leveling Time

This experiment was performed under the following conditions: samples 1, 3, 4, and 5 were ground and polished with 240-, 400-, or 600-grit paper(s) and 00-grit emery paper and the procedure described earlier was followed.

ECP at 3 V, 100 A/dm^2, 73°C, 1000 RPM was caried out until the specimen surface reached comparable appearance and comparable level of smoothness. Results are shown in Fig. 7-1.

The approach to the evaluation of the surface after ECP indicates that the finer the grit of paper used to prepare the surface, the shorter the time required for leveling and polishing. It is obvious that the dependence is not linear. The shape of the curve is very close to that usually obtained for decreasing roughness vs time of ECP.

8. Potentiostatic Current Density Changes vs Rotating Speed

Four materials were chosen to study a correlation between the current and rotating speed of the sample, depending on the voltage applied. Experiments were performed with pure iron (sample 1), carbon steels (samples 5 and 7), and toolsteel (sample 9) at applied voltages of 1, 2, 3, 4, and 5 V. Rotation speeds were changed gradually, from 0 to 3000 RPM, and higher.

In Fig. 8-1, 8-2, 8-3, and 8-4, the dependence of current on rotation speed is shown. The lowest current is observed without rotation (0 RPM). When the speed is increased, a considerable increase up to the maximum value is observed. Sometimes there are two maxima--one at about 1000 RPM and the other at a speed between 1500 and 1800 RPM. One then observes a drop in the current.

Figures 8-5, 8-6, 8-7, and 8-8 present the change in current density vs square root of an angular speed of the sample. These changes in current density are of interest from a phenomenological viewpoint.

The sudden rises and drops observed in the current density when rotation speed is increased are probably caused by disruption and rebuilding of the surface layer. Results presented in Figs. 8-1 through 8-8 indicate that the range of quick changes in the current density may be significant for the level of surface finish after ECP. Thus, these regions should be examined thoroughly, taking into account the surface appearance.

9. Examinations of Comparable Surface Appearance

Three materials were studied potentiostatically to discover the effect of rotation speed and overpotential on the surface finish. Experiments were performed with pure iron (sample 1), carbon steel (sample 5), and low-alloy steel (sample 9). Results are presented in Figs. 9-1, 9-2, and 9-3.

Spatial graphs show the areas of a good finish, depending on the rotation speed and voltage applied. The increasing area of good appearance is indicated by thin dotted lines with arrows.

It is obvious that to produce satisfactory ECP results the current density should be at least on the plateau of the polarization curve for each point of electropolished surface. In practice, a higher voltage than that derived from the polarization curve must usually be applied. Thus, in each case discussed at 2 V, the surface finish was rather poor (see Figs. 9-1, 9-2, and 9-3).

10. Microscopic Observations

Observations of the specimen surfaces were performed with the optical microscope. The purpose of this investigation was to determine the surface quality of different ferritic materials after ECP, as well as to examine the entire surface.

Two typical examples of electropolished surfaces are shown in Fig. 10-1. In the case of Armco iron (sample 2), a fine grain structure was revealed; and for toolsteel (sample 9) traces of previous treatment were visible, especially since the voltage applied (2 V) was relatively low (Fig. 10-1,b).

Milky stains may sometimes occur on the electropolished surface (Fig. 10-2) when conditions of ECP or rinsing/washing after it are improper.

Under some conditions of ECP using the RDE system, a nonpolished spot forms in the center of the rotating specimen (Fig. 10-3). Formation of the spot was, however, not reproducible under the same external conditions, i.e., rotation speed, voltage applied, and electrolyte temperature.

A similar spot formed on the low-alloy steels (Fig. 10-4) specimens, but the phenomenon was also not reproducible.

The surface of pure iron after ECP at magnification 40X is presented in Fig. 10-5. Under the conditions applied (1500 RPM), traces of spirals were very distinct.

In the case of Armco iron (Fig. 10-6), pits can be seen on the micrographs after ECP.

The surface finish of low-alloy carbon steel (Fig. 10-7) is fairly good under rotation (a); but without rotation pitting occurs that results in the decreasing of the surface finish attainable (b). In particular, the positioning of the sample facing down causes bubbles to form on the surface.

Anode surfaces (samples 4 through 9) under two different conditions of ECP, (a) 3 V, 1500 RPM, and (b) 2 V, 500 RPM, are presented in Figs. 10-8 through 10-13.

In the case of (a), photographs were taken near the center of the sample surface; in the case of (b), a periphery of the sample was photographed (where the effect of ECP was better than in the center of the sample).

In Fig. 10-14, only case (a) is presented because at 2 V no ECP action was observed.

In three cases (samples 2, 5, and 7), a very similar effect of ECP occured (Figs. 10-6, 10-9, and 10-11), the surface having a bright orange-peel appearance.

11. Auger Spectroscopy

Auger electron spectroscopy was employed to study the composition of the surface layer. Three materials were chosen for this study: pure iron (sample 1), carbon steels (samples 5 and 6), and low-alloy steel (sample 9).

In Fig. 11-1 the composition of the surface layer of pure iron after ECP (sample 1) at a depth of 10 Å is presented. Composition of the

same specimen after one-minute sputtering (400 Å depth) is shown in Fig. 11-2. In Figs. 11-3 and 11-4 peak-to-peak and percentage contents of major elements (sample 1) are shown as a function of sputtering time. In the superficiel layer, oxygen dominates and is then replaced by iron; but a surprisingly high content of carbon is visible.

The composition of the surface layer of carbon steel (sample 5) before ECP (after mechanical polishing) is presented in Fig. 11-5 (10 Å depth) and Fig. 11-8 (400 Å depth). In this case, iron also replaces oxygen in the deeper layers of the metal. The next two figures, Fig. 11-7 (10 Å depth and Fig. 11-8 (500 Å depth) present the surface layer of the same carbon steel (sample 5) after ECP. Figs. 11-9 and 11-10, showing peak-to-peak and percentage contents of major elements (sample 5), enable us to see how thin the surface layer is after ECP.

Figures 11-11 (10 Å depth) and 11-12 (500 Å depth) present spectrography of carbon steel (sample 6) after etching rather than after ECP, to compare the composition of the surface layer with that after ECP. lthough on the surface the composition of the etched layer (Fig. 11-11) is similar to that (apart from carbon content) received after ECP (Fig. 11-7), Figs. 11-13 through 11-16 show there is quite a difference going into the depth (below the surface). Figs. 11-13 through 11-16, which show peak-to-peak and percentage contents of the major elements (sample 6 after etching) after the first and second minutes of sputtering, enable us to see a major difference between etching and ECP results.

Two more spectrographs are presented for low-alloy steel (sample 9) in Figs. 11-17 d(10 Å depth) and 11-8 (500 Å depth), respectively. Compering these with previous results, a relatively high amount of phosphorus and sulfur is visible.

Discussion and conclusions. As could be expected, in all the examined materials (pure iron, carbon steel, and low-alloy steel), oxygen dominates in the superficial layer. Then as we go deeper, oxygen is replaced by iron as the major element of the steel.

Relatively high amounts of carbon (as well as traces of silicon) on the surface of all samples results probably from the previous preparation process, i.e., mechanical polishing using silicon carbide. The reason for the presence of zinc is not clear. Phosphorus and sulfur follow from the procedure of ECP in the electrolyte containing mainly H_3PO_4 and H_2SO_4. After sputtering, some amounts of oxygen and residual argon usually remain on the surface.

Auger electron spectroscopy shows the differences that exist in the surface layer between electropolished, etched, and mechanically polished surfaces. Comparing Figs. 11-3 and 11-4 (sample 1) with Figs. 11-9 and 11-10 (sample 5), one may notice that the depth of change is different. In the case of pure iron (sample 1), the surface layer is much thicker (over 500 Å) than in the case of carbon steel (sample 5, ~50 Å)

It appears that the main reason is the hardness of the material used for ECP (pure iron, below 130 HB; carbon steel ~50 HRC). It results in different depths of influence during ECP. It is obvious that to reach a proper conclusion, more research should be performed.

Secondary electron microphotography. Figures 11-19 and 11-20 show secondary electron micrographs of the samples used in Auger spectroscopy. Electropolished surfaces of pure iron (Fig. 11-19a) and carbon steel (Fig. 11-20b, sample 5) are presented at magnification 500x. Figure 11-20a presents the surface of carbon steel (sample 5) after mechanical polishing (magnification 500x), and Fig. 11-19b shows the surface of carbon steel (sample 6) after etching at magnification 130x.

12. Discussion of Results and Conclusions

In the course of the research, several groups of results were obtained. Experiments covering ten different ferritic materials were carried out over wide ranges of the parameters: 1) current density, 2) rotation speed of the anode sample, and 3) bulk electrolyte temperature. Thus the results are concerned with:

(a) The effect of the temperature of the bulk electrolyte on the behavior of the polarization curve

(b) The effect of time and voltage applied (overvoltage) on the current density and charging of the surface layer under the plateau current density

(c) The effect of rotating speed and duration of ECP on the mass loss and current efficiency

(d) The effect of initial roughness on the ECP leveling time

(e) Potentiostatic changes in current density vs rotating speed, and the voltage applied to these influencing a surface appearance after ECP

(f) Microscopic surface evaluation after ECP

(g) Spectrometric analysis of the surface layer.

Ad. (a): Polarization curves were obtained for all ten materials. It was found that the shape of the polarization curve does not depend on the rotation speed of the anode surface. It strongly depends, however, on the bulk electrolyte temperature.

Ad. (b): At a very low voltage applied, no formation of viscous layer or solid film is observed and only dissolution of the anode surface takes place. With a certain overpotential applied, a fast drop in current density occurs initially, after which the viscous layer grows to a steady-state value. Such behavior may be caused by the initial formation of oxides or hydroxides very close to the dissolving surface. However, unless there is film formation, no polishing action is observed.

Ad. (c): Generally, increasing the rotation speed causes an increase in mass loss. Uniformity of dissolving of the electropolished surface depends on the material treated. Different mass losses result in different current efficiencies. Among the materials investigated, pure iron has the highest current efficiency (η_{CE}^{1} = 30.9 percent), toolsteel has lower current efficiency (η_{CE}^{1} = 8.2 percent), and carbon steel has the lowest current efficiency (η_{CE}^{5} = 24.6 percent). It has been stated that during ECP the higher the voltage applied the lower the current efficiency. At higher rotation

speed of the anode, there is less discrepancy with results obtained in current efficiency dependency on the voltage applied.

Ad. (d): The reverse approach to the surface polishing problem, taking into account the grit of paper used instead of roughness measurement, indicates that the finer the grit of the paper used to prepare the surface, the shorter the time needed for leveling and polishing.

Ad. (e): Potentiostatic control of current density as a function of rotation speed leads to the conclusion that these factors must influence the surface finish after ECP. It was found that, depending on the rotation speed and voltage applied, there is an area of the factors in which a good surface finish is achieved. One further conclusion resulting from this study is that even at a very high rotation speed (high Reynolds number) ECP conditions can be found. This finding may mean that it is sufficient to generate a thin film without a sticky layer, for ECP to occur.

Ad. (f): Microscopic studies allowed us to evaluate the finish of the sample surface after ECP. Results of these observations show that, contrary to what has been reported in the literature, there is no direct dependence between the carbon content in steel and the surface finish after ECP. Rather than this, several groups of similar appearances of steel after ECP may be distinguished: 1) ideal glossy surface

(samples 1, 4, and 8), 2) glossy needles (or other traces resulting from the steel structure after heat treatment) on the surface (samples 6 and 9), 3) bright orange-peel appearance (samples 2, 5, and 7), and 4) fairly good but milky finish (samples 3 and 10).

Ad. (g): Auger electron spectroscopy was used to study the surface layer after ECP to compare the results obtained with other treatments. In each case of treatment (ECP, etching, mechanical polishing) in the superficial layer, oxygen dominated (10 Å depth) and was then replaced by iron as a major element of steel.

The thickness of the surface layer (for carbon steel) is about 15 to 20 times lower on the ECP surface (50-60 Å) compared with the etched one (700-800 Å). Also, comparing the electropolished samples 1 and 5, the thickness of the surface layer on pure iron (~500 Å) is about 10 times greater than on carbon steel, which may be caused by different hardnesses of these two materials.

Acknowledgments

I would like to express my appreciation and gratitude to Professor Charles Tobias for his direction throughout this work. I would also like to thank Dr. Rolf Muller for his many helpful suggestions and critiques during the course of this research. J. Holthuis and W. Giba are acknowledged for preparation of the samples. All my nearest colleagues, expecially C. Coughanowr, J. Faltemier, and T. Tsuda are gratefully acknowledged for their help and practical advice during this work.

This work was supported by the Director, Office of Energy Research, Office of Basic Energy Sciences, Materials Sciences Division of the U.S. Department of Energy under Contract No. W-7405-ENG-48.

References

1. G. Bacquais, Electrolytic polishing of common and precious metals, Oberfläche Surf., July 1979, 20(7), 166-168 [in French].
2. V.L. Chejfec, N.P. Fedoťev, and S.Ja. Griliches. Sostojanie poverchnosti stali pri elektrochimičeskom polirovanii, Žurnal Prikl. Chimii, 29(12) (1956) 1822-1827.
3. R.S. Crouse. Metallography appendix of MEI, Oak Ridge TN, 1970, p. 87.
4. C.L. Faust, Electropolishing-electroplating engineering handbook, Ed. by A.K. Graham, 3rd Edition, Van Nostrand Reinhold, New York, 1971.
5. C.L. Faust, Electropolishing-metals engineering handbook, Vol. 2, ASM Metals Park OH, 1964, 484-488.
6. N.P. Fedot'ev and S.Ja. Griliches, "Zavisimosť anodnogo potenciala stali ot sostava elektrolita pri eleletrochimičeskom polirovanii, Žurnal Prikl. Chimii, 30(2), 1975, 233-239.
7. I. Fried. The electrochemistry of electrode processes, Academic Press, London-New York, 1973.
8. S.Ja. Griliches and N.P. Fedoťev, O mechanizme processa eletrochimičeskogo polirovanija metallov, Žurnal Prikl. Chimii, 30(4), 1957, 528-533.
9. J. Heyes, Electrolytic polishing of steel-perchloric acid type electrolytes, Metal Finishing 60(12), 1962, 36-41.
10. J.P. Hoare, Anodic polarization studies on soft iron in some concentrated salt solutions, NATURE 219, September 1968, 1034-1035.

11. D.J.G. Ives and G.J. Janz, Reference electrodes theory and practice, Academic Press, New York and London, 1961.

12. S.K. Kang and K.V. Gow, An improved metallographic technique for the study of nonmetallic inclusions in steel metallography 11(2), 1978, 219-222.

13. R. Kirchheim, K. Maier, and G. Tolg, Diffusion and solid-film formation during electropolishing of metals, J. Electrochem. Soc. 128(5), 1981, 1027-1034.

14. K. Kojima, A study of the mechanism of electropolishing of copper, PhD dissertation, University of California, Berkeley, February 1972. (LBL-140)

15. G. Kortüm. Treatise on electrochemistry, Elsevier Publ. Co., Amsterdam-London-New York, 1965.

16. R.H. Krishnan, R. Subramanian, and N.V. Parthasaradhy, Electropolishing mild steel-phosphoric-sulfuric-lactic acid electrolyte, Metal Finishing 7, 42-47, 1968.

17. N.M. Kulešova and N.S. Fedorova, Vlijanie naturalnoj konvekcii pri elektropolirovke metallov, Žurnal Fiz. Chimii, February 1979, 53(2), 388-391.

18. L.M. Kurviakova, T.E. Kulikova, and S.C. Grišina, Sravnenie elektrolitov dla polirovki uglerodistych stalej, Zašcita Metallov, January-February 1978, 14(1), 113-115.

19. L.M. Kurviakova, T.E. Kulikova, G.I. Medvedev, and S.C. Grišina, Vlijanie materiala katoda na elektropolirovku uglerodistych stalej, Zašcita Met., May-June 1978, 14(3), 340-342.

20. F.A. Lowenheim, Glossary - Electroplating engineering handbook, Ed. by A.K. Graham, 3rd Edition, Van Nostrand Reinhold, New York, 1971.

21. G.P. Majtak and G.S. Tretakova, Elektrolity da elektrochimičeskogo polirovanija stali, Žurnal Prikl. Chimii, 32(5), 1060-1065, 1959.

22. G.P. Majtak and G.S. Treťakova, Nekotorye fiziko-chimičeskie i technologičeskie svojstva elektrolitov dla elektrochimičeskogo polirovanija stalej, Žurnal Prikl. Chimii, 32(10), 2242-2247, 1959.

23. K.W. Mao, Anodic polarization study of mild steel in NaCl solution during electrochemical machining, J. Electrochem. Soc. 120(8), 1056-1060, 1973.

24. K.W. Mao, ECM study in a closed-cell system: I. $NaClO_3$. J. Electrochem Soc. 118, 1971, 1870-1876.

25. K.W. Mao, ECM study in a closed-cell system: II. NaCl, $NaClO_4$, and $NaNO_3$, J. Electrochem. Soc. 118, 1971, 1876-1879.

26. V. Marathe and J. Newman, Current distribution on a rotating disk electrode, J. Electrochem. Soc. 116(12), 1706-1707, 1969.

27. P. Neufeld and D. Southall, Gas evolution and pitting in electropolishing, Trans. Inst. Met. Finish., spring 1976, 54(1), 40.

28. I. Rajagopalan, Electropolishing steels, Finishing Industries 2(9), 26-32, 1978.

29. S. Ramachandran and R. Subramanian, Electropolishing of steel, influence of addition agents, Metal Finishing 62(10), 68-69, 73, 75, 1964.

30. P.V. Shigolev, Electrolytic and chemical polishing of metals, Freund Publ., Tel-Aviv, Israel, 1974.

31. J. Swain, Industrial developments in electropolishing, Prod. Finishing (London), November 1979, 31(11), 31, 33-34, 36.

32. V.M. Sztanko, P.P. Kariazin, and J.N. Lipkin, Nekotorye osobennosti stalej v elektrolitach s dobavkoj poverchnostno-aktivnych veščestv, Žurnal Prikl. Chimii, 66(1), 192-195, 1973.

33. V.M. Sztanko, P.P. Kariazin, V.G. Mosolova, and S.N. Širotkin, K voprosu o vlijanii anodnogo okislenija poverchnostno-aktivnych veščestv na process elektrochimiceskoj polirovki metallov, Žurnal Prikl. Chimii, 68(8), 1761-1764, 1975.

34. K.N. Tankov and A.M. Pleskač, Experiment planning in the development of a polishing electrolyte, Ind. Lab. (U.S.S.R.), October 1978, 44(10), 1417-1418.

35. W.J. McG. Tegart, The electrolytic and chemical polishing metals in research and industry, Pergamon Press Ltd., London, 1956.

Table I. Materials Used for Experiments

Sample	Name	Properties	Times used
1	Iron (Fe)	99.91 percent purity	1',1'',1'''
2	Armco iron	Max 0.1 C+Mn+P+S+Si Max 0.01 P, max 0.03 S, max 0.15 Cu	2' 2'',2'''
3	Steel 1018	Cold finished, minimum 126HB Chem. composition: 0.15-0.10 C, 0.60-0.90 Mn, max 0.040 P, max 0.050 S	3',3'',3'''
4	Steel 1028	Cold finished Chem. composition: 0.15-0.31 C, 0.60-0.90 Mn, max 0.04 P, max 0.05 S	4',4'',4'''
5	Steel 1040	Hot rolled bars, 48-51 HRC martensite Chem. Composition: 0.37-0.44 C, 0.60-0.90 Mn, max 0.04 P, max 0.05 S	5',5'',5'''
6	Steel 1060	Hot rolled bars, 50-53 HRC tempered martensite Chem. composition: 0.55-0.65 C, 0.60-0.90 Mn, max 0.04 P, max 0.05 S	6',6'',6'''
7	Steel 1080	Hot rolled bars, 50-53 HRC tempered martensite Chem. Composition: 0.75-0,88 C, 0.60-0.90 Mn, max 0.04 P, max 0.05 S	7',7'',7'''
8	Steel 4141	Hot rolled, annealed, 50 HRC tempered Chem. Composition: 0.38-0.43 C, 0.75-1.0 Mn, max 0.04 P, max 0.05 S, 0.20-0.33 Si, 0.80-1.1 Cr, 0.15-0.25 Mo	8',8'',8'''
9	H13 toolsteel	Hot work die steel, free machining H13, 52 HRC tempered martensite Chem. Composition: 0.40 C, 1.0 Si, 0.80 Mn, 5.25 Cr, 1.35 Mo, 1.0 V	9',9'',9'''
10	01 toolsteel	Hot rolled, annealed, oil hardening type, 53-56 HRAC tempered martensite, as quenched Chem. Composition: 0.85-0.95 C, 1-1.3 Mn, max 0.50 Si, 0.40-0.60 Cr, 0.40-0.60 W, without vanadium	10',10'',10'''

Table II. Composition of Electrolytes

Number of electrolyte	Composition Content	% by wgt	Remarks
E-1	H_3PO_4	70	Primarily used
	H_2SO_4	12	
	CrO_3	9	
	H_2O	9	
E-2	H_3PO_4	65	Preliminary experiment
	H_2SO_4	20	
	H_2O	15	
E-3	H_3PO_4	62	Preliminary experiment
	H_2SO_4	18	
	CrO_3	6	
	H_2O	14	

Table III. RDE Calibration Results Using Tachometer (by D. Roha)

Item	Pot.setting	RPM	Item	Pot.setting	RPM
1	0.20	181.5	21	2.30	1684
2	0.30	250.2	22	2.40	1750
3	0.40	328.0	23	2.50	1827
4	0.50	393.5	24	2.60	1893
5	0.60	469.0	25	2.80	2041
6	0.71	500.0	26	3.00	2185
7	0.80	608.0	27	3.20	2326
8	0.90	680.3	28	3.40	2474
9	1.00	751.0	29	3.50	2544
10	1.20	896.0	30	3.60	2612
11	1.30	967.1	31	3.80	2762
12	1.40	1044.0	32	4.00	2902
13	1.50	1110.4	33	4.20	3050
14	1.60	1179.0	34	4.40	3190
15	1.70	1253.8	35	4.60	3335
16	1.80	1323.0	36	4.80	3475
17	1.90	1397.2	37	5.00	3625
18	2.00	1468.0	38	5.50	3980
19	2.10	1540.6	39	6.00	4300*
20	2.20	1607.0			off correlation

RPM = 35.09 + 716.91 (Pot.)

Figure Captions

Fig. 3.1 Rotating disk sample holder, dimensions in mm, material: 304 stainless.

Fig. 3.2 Sample connected to sample holder.

Fig. 3.3 Rotating disk extension (connecting) rod, dimensions in mm.

Fig. 3.4 Cathode, material: 304 stainless.

Fig. 3.5 Samples and cell used in the experiments: 1-beaker, 2-cathode, 3-extension (connecting rod), 4-O-ring, 5-samples after ECP, 6-sample after grinding (prior to ECP), 7-sample holder with Allen wrench (prepared for measurement).

Fig. 3.6 Experimental setup: 1-potentiostat-galvanostat model 371, 2-Keithley 179 TRMS digital multimeter, 3-Servo-Tek with rectifier model ST-554-1, 4-universal stand, 5-motor model STE-231T-1C with drive, 6-extension rod with sample, 7-beaker with electrolyte and thermometer inside, 8-reference electrode, 9-electrometer model 178.

Fig. 3.7 Electrical circuit for potentiostatic operation.

Fig. 3.8 Typical surface roughness (a) after grinding, prior to ECP; (b) after ECP.

Fig. 4.1 Polarization curves for sample 1 at 500 RPM, electrolyte temperatures (a) 20°C, (b) 40°C, (c) 60°C, (d) 80°C.

Fig. 4.2 Polarization curves for sample 2 at 500 RPM, electrolyte temperatures (a) 20°C, (b) 40°C, (c) 60°C, (d) 80°C.

Fig. 4-3 Polarization curves for sample 3 at 500 RPM; electrolyte temperatures (a) 20°C, (b) 40°C, (c) 60°C, (d) 80°C.

Fig. 4-4 Polarization curves for sample 4 at 500 RPM; electrolyte temperatures (a) 20°C, (b) 40°C, (c) 60°C, (d) 80°C.

Fig. 4-5 Polarization curves for sample 5 at 500 RPM; electrolyte temperatures (a) 20°C, (b) 40°C, (c) 60°C, (d) 80°C.

Fig. 4-6 Polarization curves for sample 6 at 500 RPM; electrolyte temperatures (a) 20°C, (b) 40°C, (c) 60°C, (d) 80°C.

Fig. 4-7 Polarization curves for samples 7, 8, 9, and 10 at 1000 RPM and electrolyte temperature 80°C.

Fig. 4-8 Polarizatioan curves for sample 1 and electrolyte temperature 60°C at (a) 100 RPM, (b) 500, 1000, and 1500 RPM.

Fig. 4-9 Dependence of current density on time. Conditions: sample 6, 500 RPM, 70°C, 0.3, 0.4, 0.5, 0.6, 0.7, 0.8 V, potentiostatic control.

Fig. 4-10 Dependence of c.d. on time with rpeated polarizations. Conditions: sample 6, 500 RPM, 65°C, 0.5, 0.6, 0.7, 0.8 V, potentiostatic control.

Fig. 4-11 Dependence of c.d. on time with repeated polarizations. Conditions: sample 6, 500 RPM, 65°C, 0.4 V, potentiostatic control.

Fig. 4-12 Dependence of c.d. on time with repeated polarizations. Conditions: sample 4, 500 RPM, 65°C, 0.4, 0.5 V, potentiostatic control.

Fig. 4-13 Dependence of c.d. on time--initial period of Fig. 4-12 enlarged. Conditions: sample 4, 500 RPM, 65°C, 0.4, 0.5 V, potentiostatic control.

Fig. 4-14 Dependence of c.d. on time--low-potential region. Conditions: sample 4, 500 RPM, 75°C, 0.30, 0.31, 0.32, 0.33, 0.34, 0.35 V, potentiostatic control.

Fig. 4-15 Dependence of $it^{0.5} = f(t^{0.5})$ for one of the curves from Fig. 4-14. Conditions: sample 4, 500 RPM, 75°C, 0.34 V.

Fig. 4-16 Dependence of c.d. on time. Conditions: sample 9, 500 RPM, 70°C, 0.5, 0.6, 0.7, 0.8, 0.9, 1 V, potentiostatic control.

Fig. 4-17 Dependence of c.d. on time--region of increase of c.d. with potential. Conditions: sample 9, 500 RPM, 70°C, 0.2, 0.3, 0.4, 0.44, 0.45, 0.46, 0.50, 0.60 V, potentiostatic control.

Fig. 4-18 Dependence of c.d. on time. Conditions: sample 2, 500 RPM, 70°C, 0.39, 0.40, 0.41, 0.42, 0.43, 0.445, 0.45, 0.46 V, potentiostatic control.

Fig. 4-19 Dependence of c.d. on time--region of increase of c.d. with potential. Conditions: sample 2, 500 RPM, 70°C, 0.2, 0.3, 0.35, 0.39, 0.395, 0.40, 0.41, 0.42, 0.46 V, potentiostatic control.

Fig. 5-1 Measured distribution of removal of material during ECP with RDE, effect of rotation speed. Conditions: 3 V (~100 A/cm^2), 64°C, time 5 min, 1500 RPM, r_o-sample radius, area 2.834 cm^2, a-sample 1, b-sample 5, c-sample 8. Mass loss of the samples is presented at: 1-without rotating (speed 0), and 2-1500 RPM.

Fig. 5-2 Measured distribution of removal of material during ECP with RDE, effect of rotation speed. Conditions: sample 1, 3 V (~100 A/dm^2), 64°C, time 5 min, r_0-sample radius, area 2.834 cm^2, a-100 RPM, b-500 RPM, c-1000 RPM, d-1800 RPM. Besides--relative mass loss of the sample.

Fig. 5-3 Measured distribution of removal of material during ECP with RDE, effect of rotation speed. Sample 5, rest of conditions as for Fig. 5-2.

Fig. 5-4 Measured distribution of removal of material during ECP with RDE, effect of rotation speed. Sample 8, rest of conditions as for Fig. 5-2.

Fig. 5-5 Mass loss after ECP measured for ten samples, electrode area 2.834 cm^2. Conditions: thin line--100 RPM, 3 V, 100 A/dm^2, 65°C, time 5 min, av. loss 0.0675g, current efficiency 27 percent; thick line--1000 RPM, 3 V, 85 A/dm^2, 65°C, time 5 min. av. loss 0.07409, current efficiency 35 percent, galvanostatic control.

Fig. 5-6 Mass loss on ECP time with regrinding after each run. Conditions: sample 6, 3 V, 100 A/dm^2, 500 RPM, 66°C, galvanostatic control.

Fig. 6-1 Mass loss on ECP time without regrinding. Conditions: samples 1, 5, and 10; 4 V, 70-82 A/dm^2, 500 RPM, 68°C.

Fig. 6-2 Relationships of current efficiency and rotating speed measured for five materials, four levels of speed, and two potentials--3 V and 5 V, potentiostatic control.

Fig. 6-3 The same relationships as in Fig. 6-2 for three groups of materials: a-pure iron (1), b-carbon steels(5,6,7), and c-low-alloy steel (9).

Fig. 6-4 Average current efficiency of data given in Fig. 6-2, showing decreasing role of the voltage applied with increasing rotation speed.

Fig. 7-1 Dependence of leveling time on paper grit number.

Fig. 8-1 Current vs rotation speed. Conditions: sample 1, 70°C, 1, 2, 3, 4, 5 V.

Fig. 8-2 Current vs rotation speed. Conditions: sample 5, 70°C, 1, 2, 3, 4, 5 V.

Fig. 8-3 Current vs rotation speed. Conditions: sample 7, 84°C, 1, 2, 3, 4, 5 V.

Fig. 8-4 Current vs rotation speed. Conditions: sample 9, 70°C, 1, 2, 3, 4, 5 V.

Fig. 8-5 Current density vs $\omega^{0.5}$. Conditions as in Fig. 8-1.

Fig. 8-6 Current density vs $\omega^{0.5}$. Conditions as in Fig. 8-2.

Fig. 8-7 Current density vs $\omega^{0.5}$. Conditions as in Fig. 8-3.

Fig. 8-8 Current density vs $\omega^{0.5}$. Conditions as in Fig. 8-4.

Fig. 9-1 Dependence of surface brightness on rotating speed and potential applied for sample 1.

Fig. 9-2 Dependence of surface brightness on rotating speed and potential applied for sample 5.

Fig. 9-3 Dependence of surface brightness on rotating speed and potential applied for sample 9.

Fig. 10-1 Specimen surfaces after ECP, magnification 6x, (a) Armco iron, sample 2, 3 V, 65°C, 5 min, 500 RPM; (b) toolsteel, sample 9, 2 V, 65°C, 5 min, 500 RPM.

Fig. 10-2 Stains on electropolished surface, magnification 6x, sample 4, 3 V, 65°C, 5 min, 1500 RPM.

Fig. 10-3 Spot in the specimen center after ECP, magnification 6x, (a) carbon steel, sample 4, 3 V, 68°C, 10 min, 500 RPM; (b) carbon steel, sample 7, 2 V, 65°C, 5 min, 500 RPM.

Fig. 10-4 Spot in the specimen center after ECP, magnification 6x, (a) low-alloy steel, sample 8, 2 V, 68°C, 5 min, 500 RPM; (b) toolsteel, sample 9, 3 V, 68°C, 10 min, 500 RPM.

Fig. 10-5 Surface of pure iron (sample 1) after ECP, magnification 40x, 3 V, 66°C, 10 min, 1500 RPM. (a) flow-lines near periphery of the sample, (b) flow-lines (spirals) near the center of the sample.

Fig. 10-6 Surface of Armco iron (sample 2) after ECP, magnificatin 40x, 3 V, 70°C, 10 min, 1500 RPM. (a) spirals near the center, (b) spirals near the periphery.

Fig. 10-7 Surface of low-carbon steel (sample 3) after ECP, magnification 40x, (a) fairly good finish, visible spirals, 3 V, 70°C, 10 min, 1500 RPM; (b) without rotation, visible pitting, 3 V, 68°C, 8 min, 0 RPM.

Fig. 10-8 Surface of carbon steel (sample 4) after ECP, magnification 40x, (a) better finish than sample 3, visible spirals, 3 V, 70°C, 10 min, 1500 RPM; (b) visible spirals but less than (a), 2 V, 60°C, 5 min, 500 RPM.

Fig. 10-9 Surface of carbon steel (sample 5) after ECP, magnification 40x, (a) spirals near center, bright orange-peel finish, 3 V, 70°C, 10 min, 1500 RPM; (b) spirals near periphery, poor finish, 2 V, 60°C, 5 min, 1500 RPM.

Fig. 10-10 Surface of carbon steel (sample 6) after ECP, magnification 40X, (a) spirals hardly seen, very good finish, 3 V, 70°C, 10 min, 1500 RPM; (b) periphery of sample, good finish, 2 V, 65°C, 5 min, 500 RPM.

Fig. 10-11 Surface of high-carbon steel (sample 7) after ECP, magnification 40x, (a) spirals near center, bright orange-peel finish, 3 V, 70°C, 10 min, 1500 RPM; (b) visible spirals and poor finish, 2 V, 68°C, 5 min, 500 RPM.

Fig. 10-12 Surface of low-alloy steel (sample 8) after ECP, magnification 40x, (a) spirals hardly marked, good finish, 3 V, 70°C, 10 min, 1500 RPM; (b) spirals hardly marked, good finish on periphery, 2 V, 70°C, 5 min, 500 RPM.

Fig. 10-13 Surface of toolsteel (sample 9) after ECP, magnification 40x, (a) traces of spirals, good finish but needles on the surface, 3 V, 70°C, 10 min, 1500 RPM; (b) spirals hardly marked, good finish with needles on the surface, 2 V, 70°C, 5 min, 500 RPM.

Fig. 10-14 Surface of toolsteel (sample 10) after ECP, magnificatin 40x, fairly good but milky finish, 3 V, 70°C, 10 min, 1500 RPM. There was no ECP action at 2 V so the picture is not presented.

Fig. 11-1 Spectrography of pure iron after ECP (sample 1, 10 Å).

Fig. 11-2 Spectrography of pure iron after ECP after 1 min sputtering (sample 1, 400 Å).

Fig. 11-3 Peak-to-peak content of major elements in the ECP surface layer (sample 1).

Fig. 11-4 Percentage content of major elements in the ECP surface layer (sample 1).

Fig. 11-5 Spectrography of carbon steel before ECP (after mechanical polishing)(sample 5, 10 Å).

Fig. 11-6 Specgrography of carbon steel before ECP (after mechanical polishing) after 1 min sputtering (sample 5, 400 Å),

Fig. 11-7 Spectrography of carbon steel after ECP (sample 5, 10 Å),

Fig. 11-8 Spectrography of carbon steel after ECP after 1.25 min sputtering (sample 5, 500 Å).

Fig. 11-9 Peak-to-peak content of major elements in the ECP surface layer (sample 5).

Fig. 11-10 Percentage content of major elements in the ECP surface layer (sample 5).

Fig. 11-11 Spectrography of carbon steel after etching (sample 6, 10 Å).

Fig. 11-12 Spectrography of carbon steel after etching, after 2 min sputtering (sample 6, 800 Å).

Fig. 11-13 Peak-to-peak content of major elements in the etched surface layer (sample 6, 0-400 Å).

Fig. 11-14 Percentage content of major elements in the etched surface layer (sample 6, 0-400 Å).

Fig. 11-15 Peak-to-peak content of major elements in the second minute of sputtering (sample 6, 400-800 Å). (See Fig. 11-13)

Fig. 11-16 Percentage content of major elements in the second minute of sputtering (sample 6, 400-800 Å). (See Fig. 11-14)

Fig. 11-17 Spectrography of low-alloy steel after ECP (sample 9, 10 Å).

Fig. 11-18 Spectrography of low-alloy steel after ECP after 1.25 min sputtering (sample 9, 500 Å).

Fig. 11-19 Secondary electron micrographs received: (a) after ECP of pure iron (sample 1, Magn. 500x), (b) after etching (instead of ECP) of carbon steel (sample 6, magn. 130x).

Fig. 11-20 Secondary electron micrographs received: (a) after mechanical polishing (before ECP) of carbon steel (sample 5, magn. 500x), (b) after ECP of carbon steel (sample 5, magn. 500x).

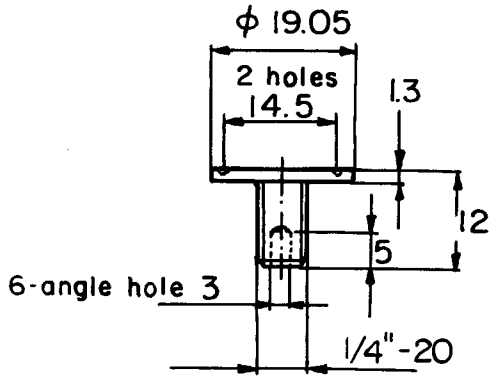

All dimensions in mm
except where noted

Mat. 304
Scale 1:1

Fig. 3-1

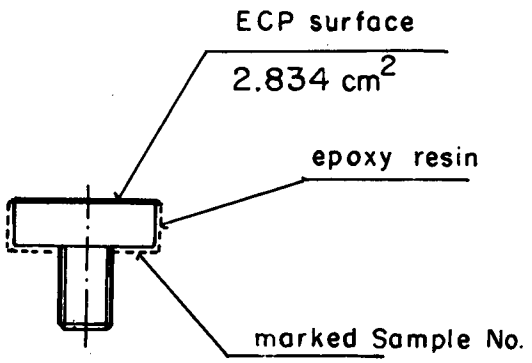

Fig. 3-2

XBL 815-5723

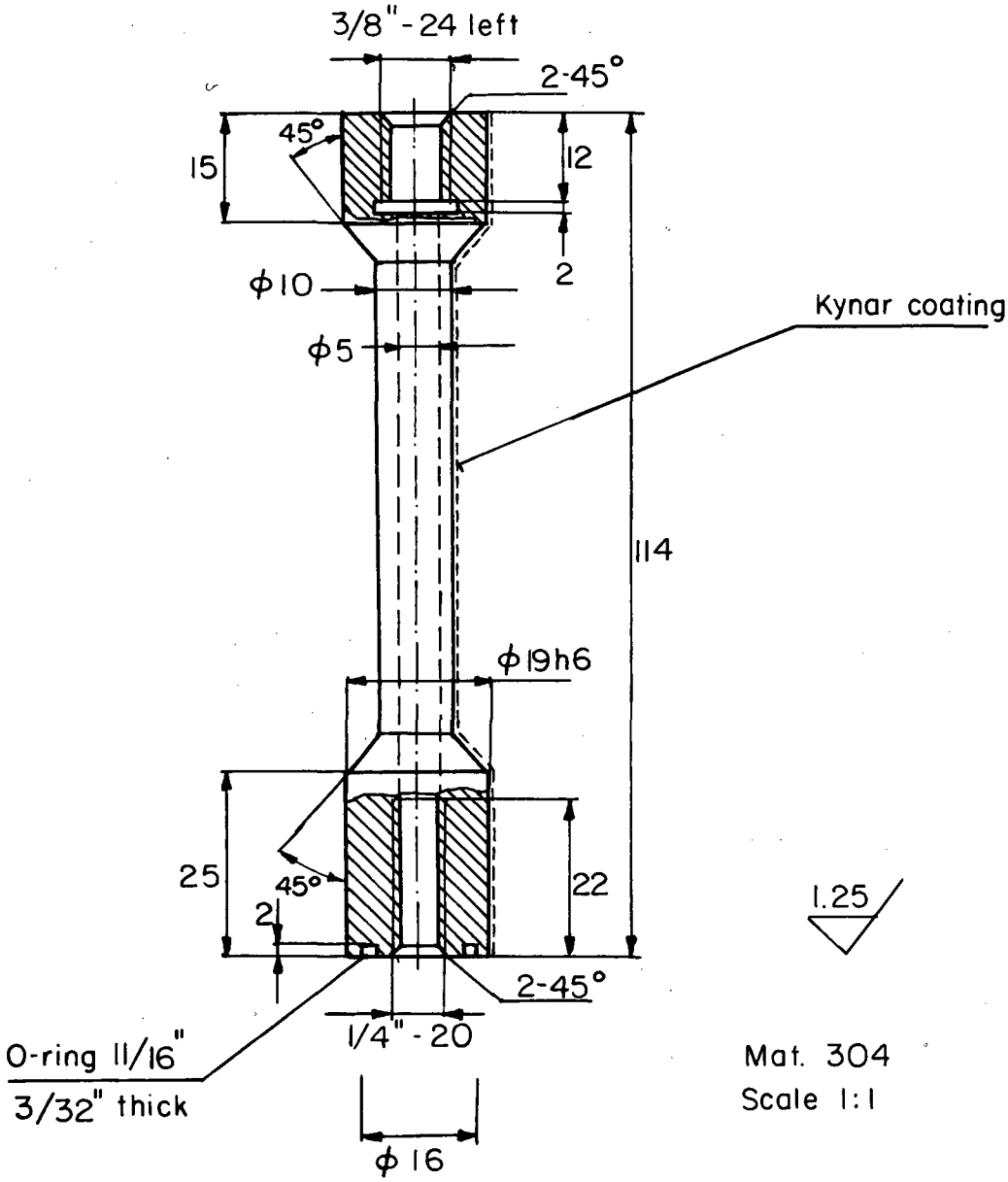

Fig. 3-3

XBL 815-5724

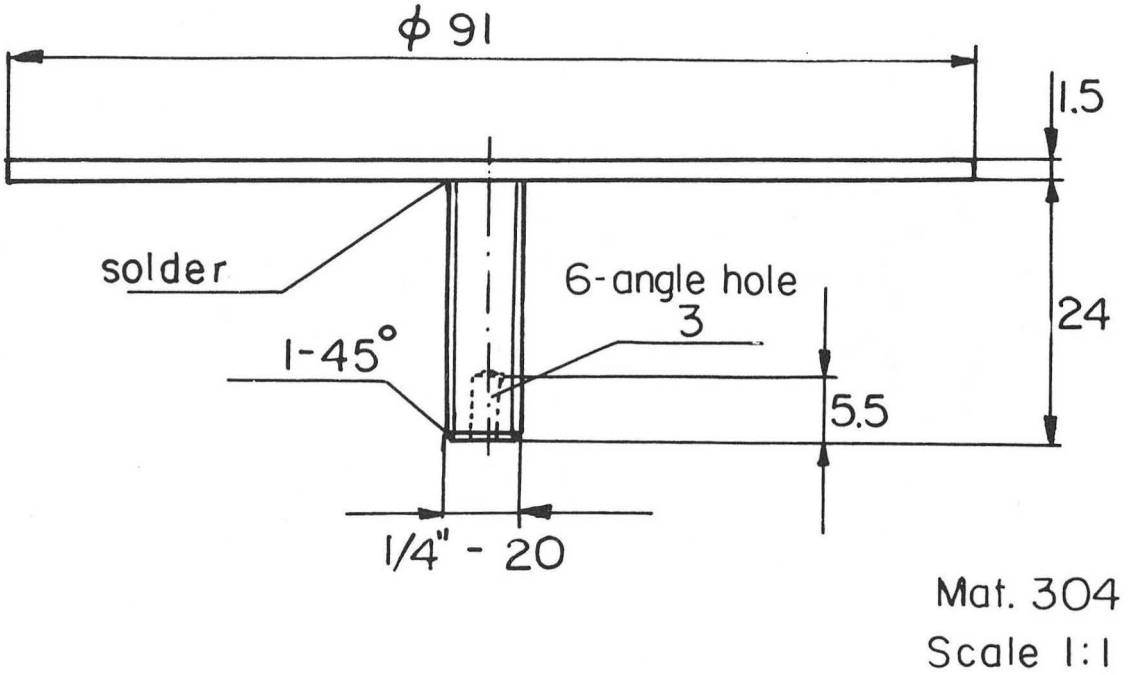

Fig. 3-4

XBL 815-5725

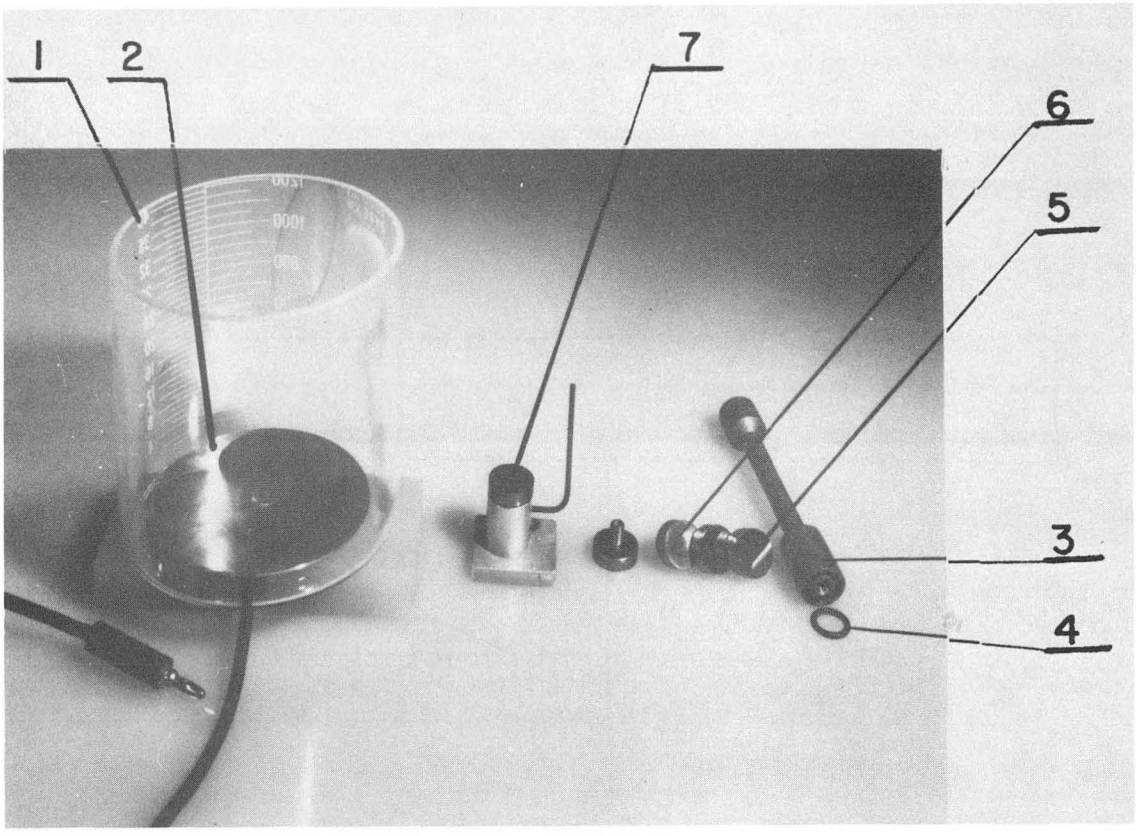

XBB 813-2171A

Fig. 3-5

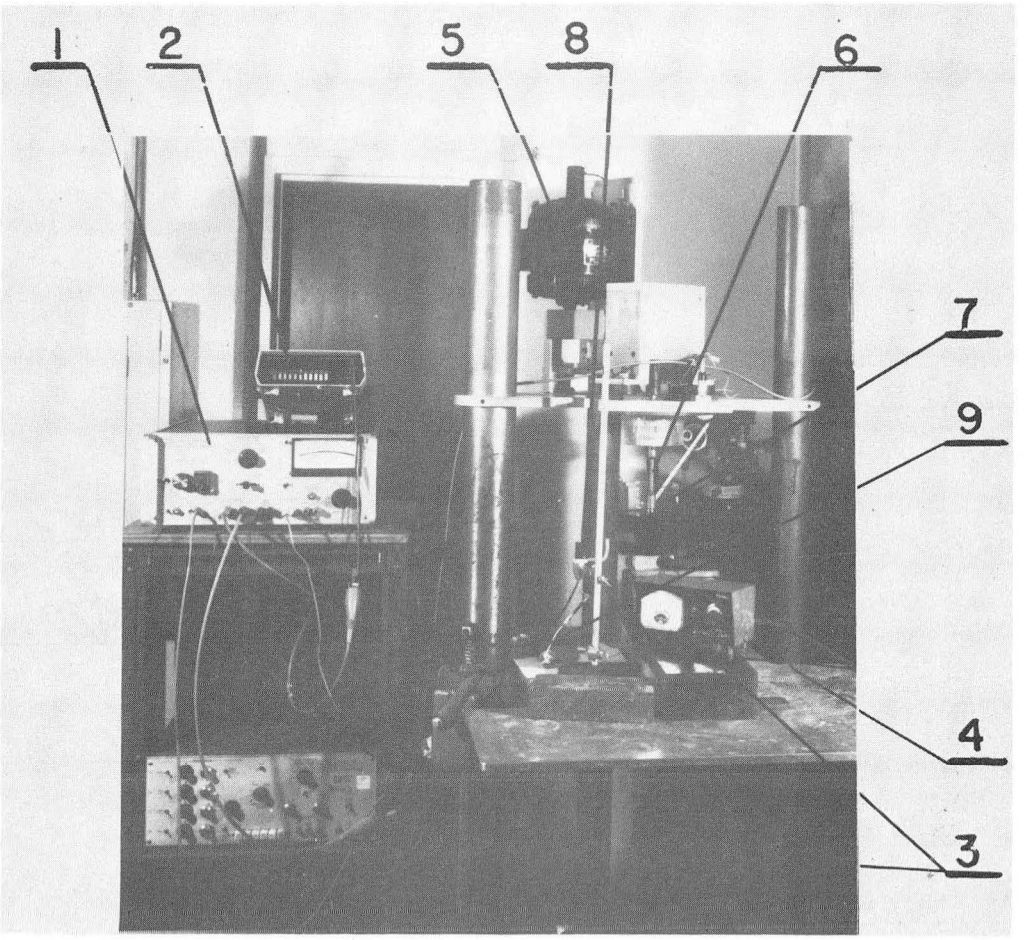

XBB 813-2169A

Fig. 3-6

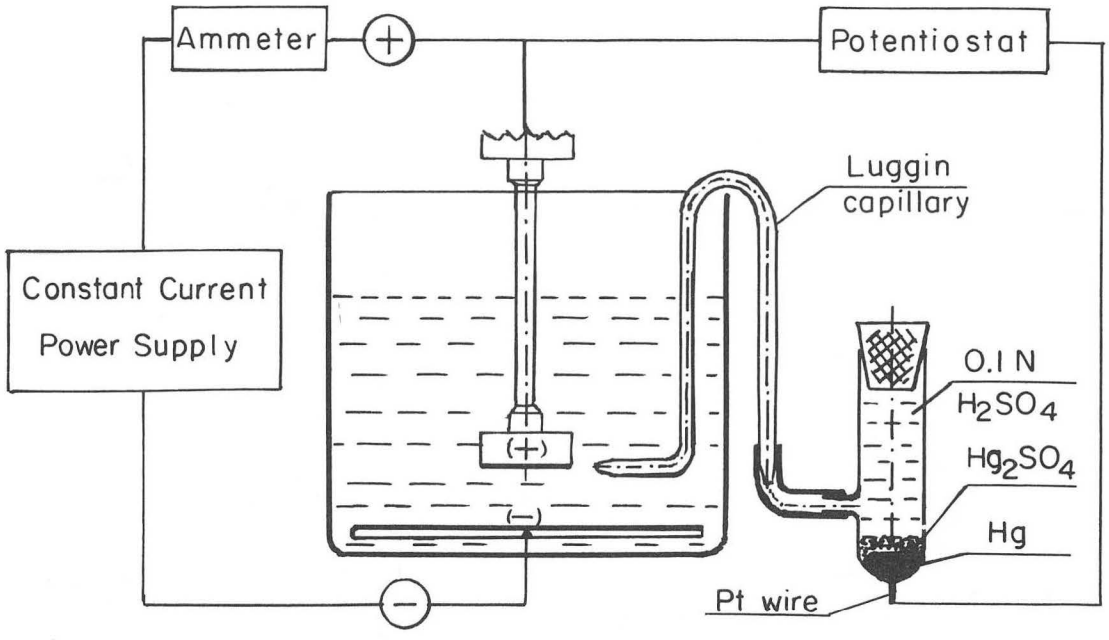

Fig. 3-7

XBL 815-5726

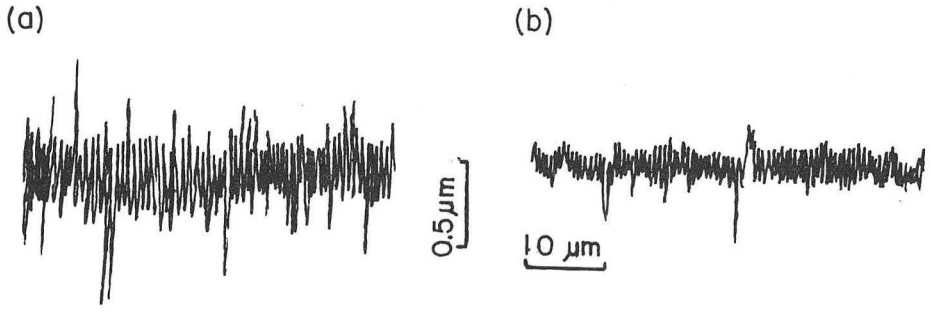

Fig. 3-8

XBL 815-5727

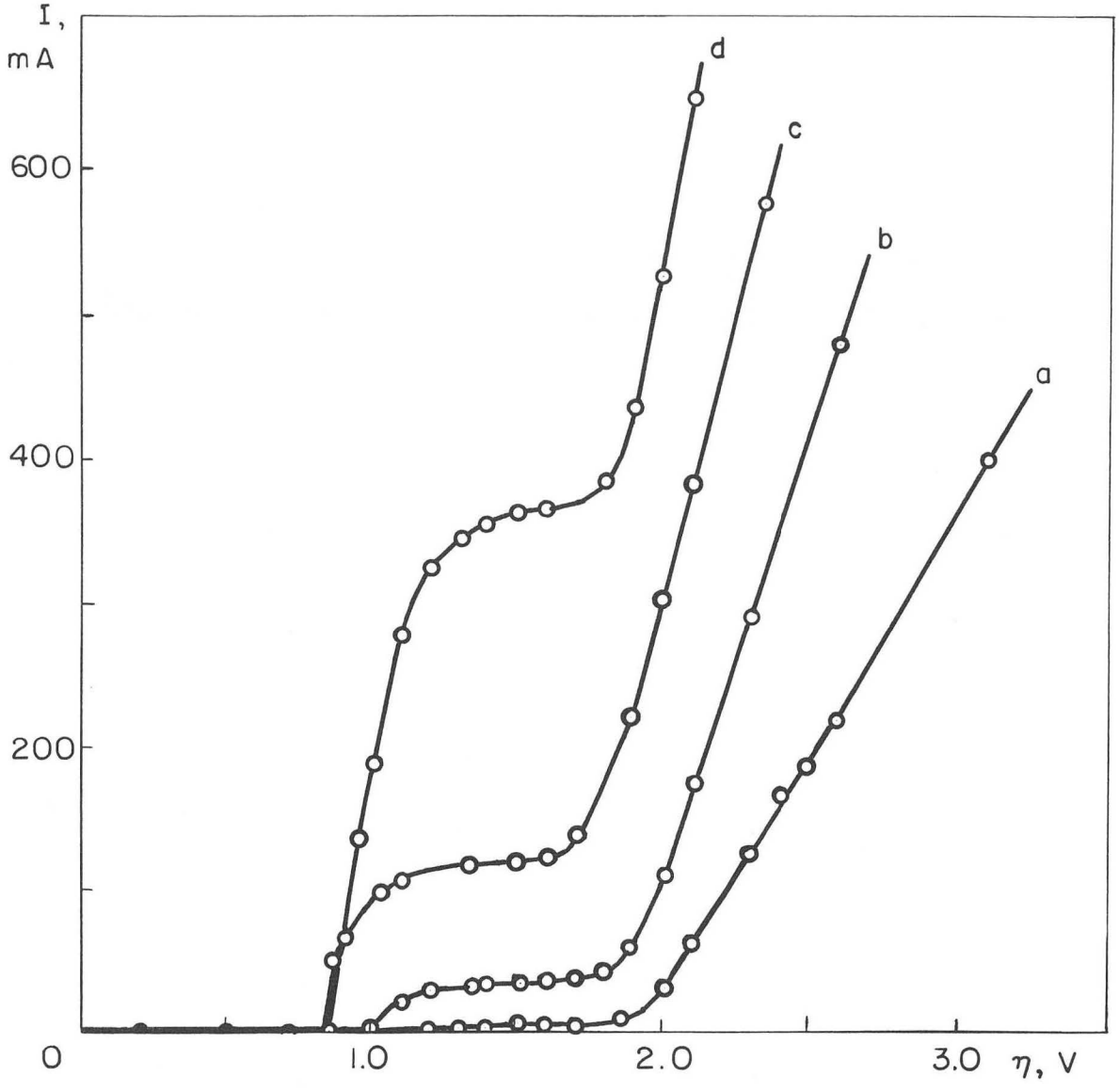

Fig. 4-1

XBL 815-5728

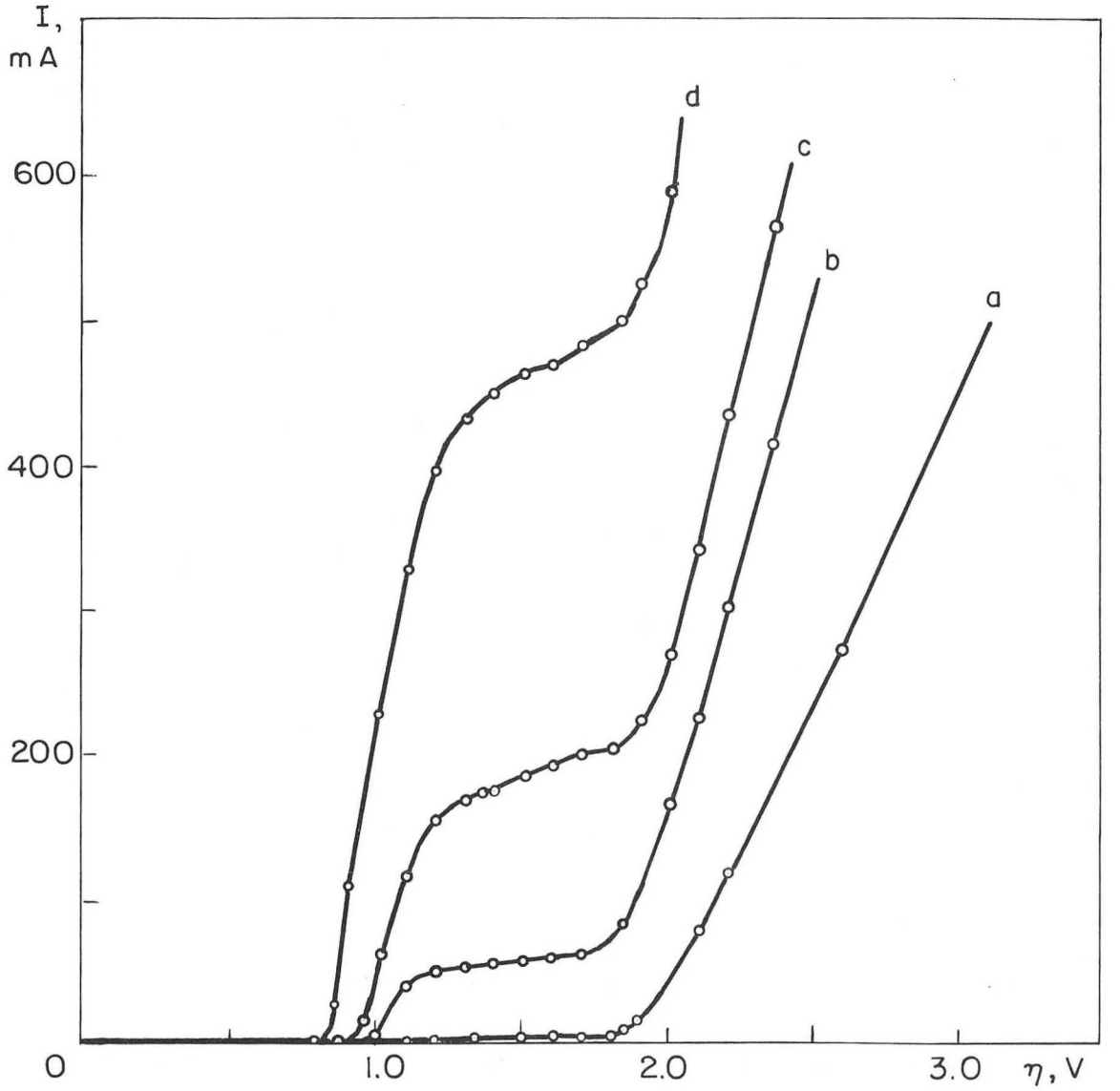

Fig. 4-2

XBL 815-5729

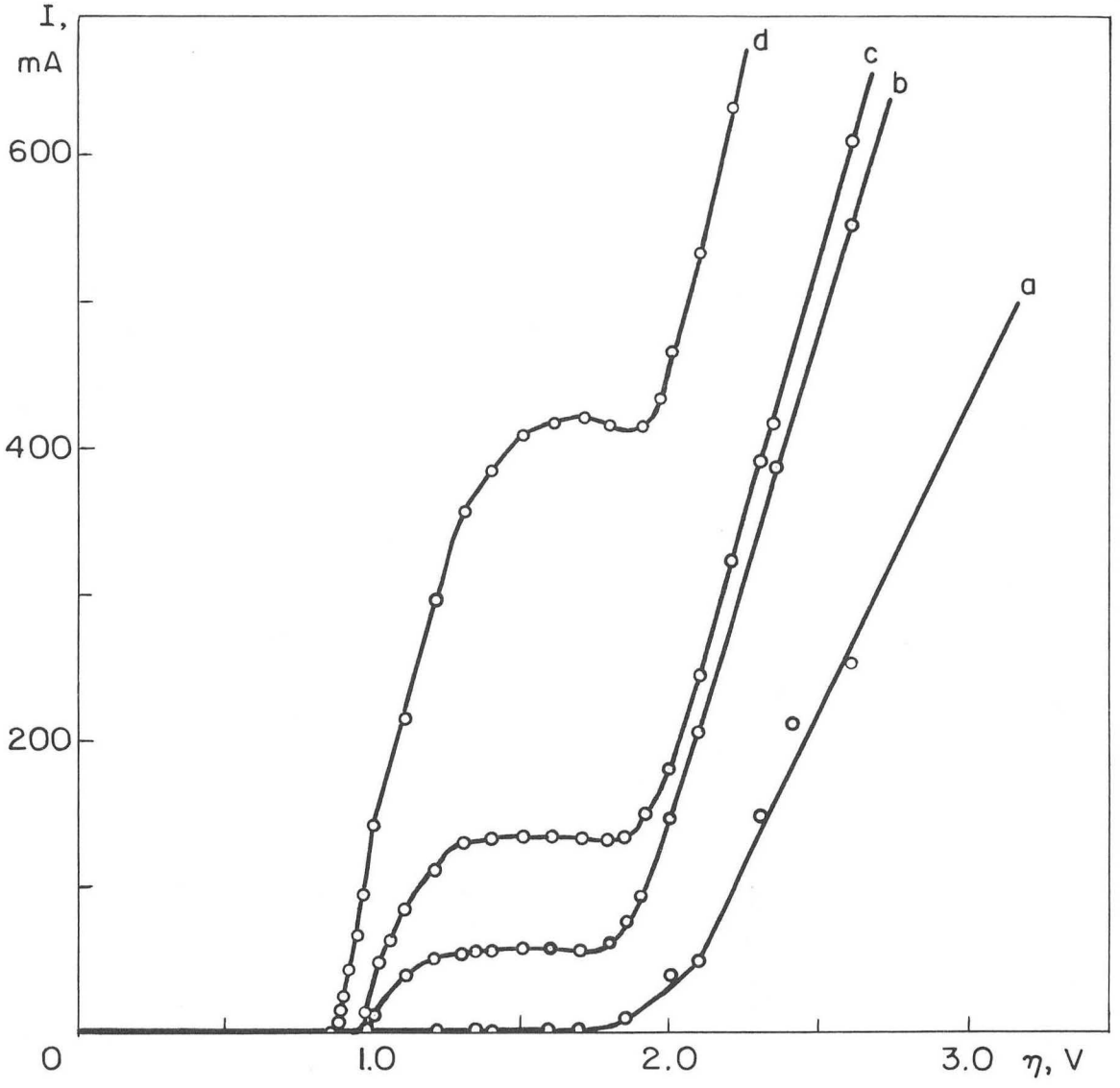

Fig. 4-3

XBL 815-5730

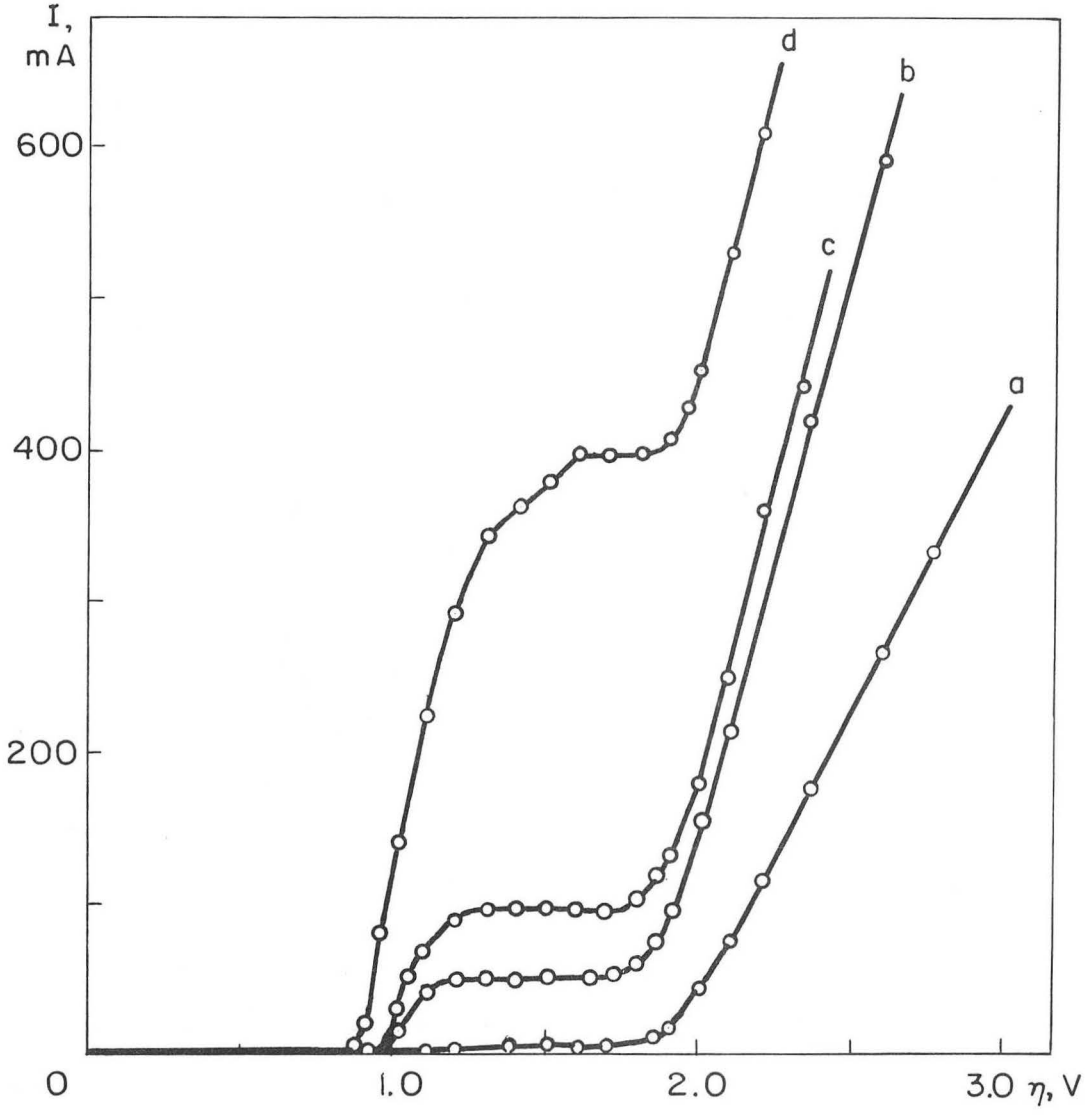

Fig. 4-4

XBL815-5731

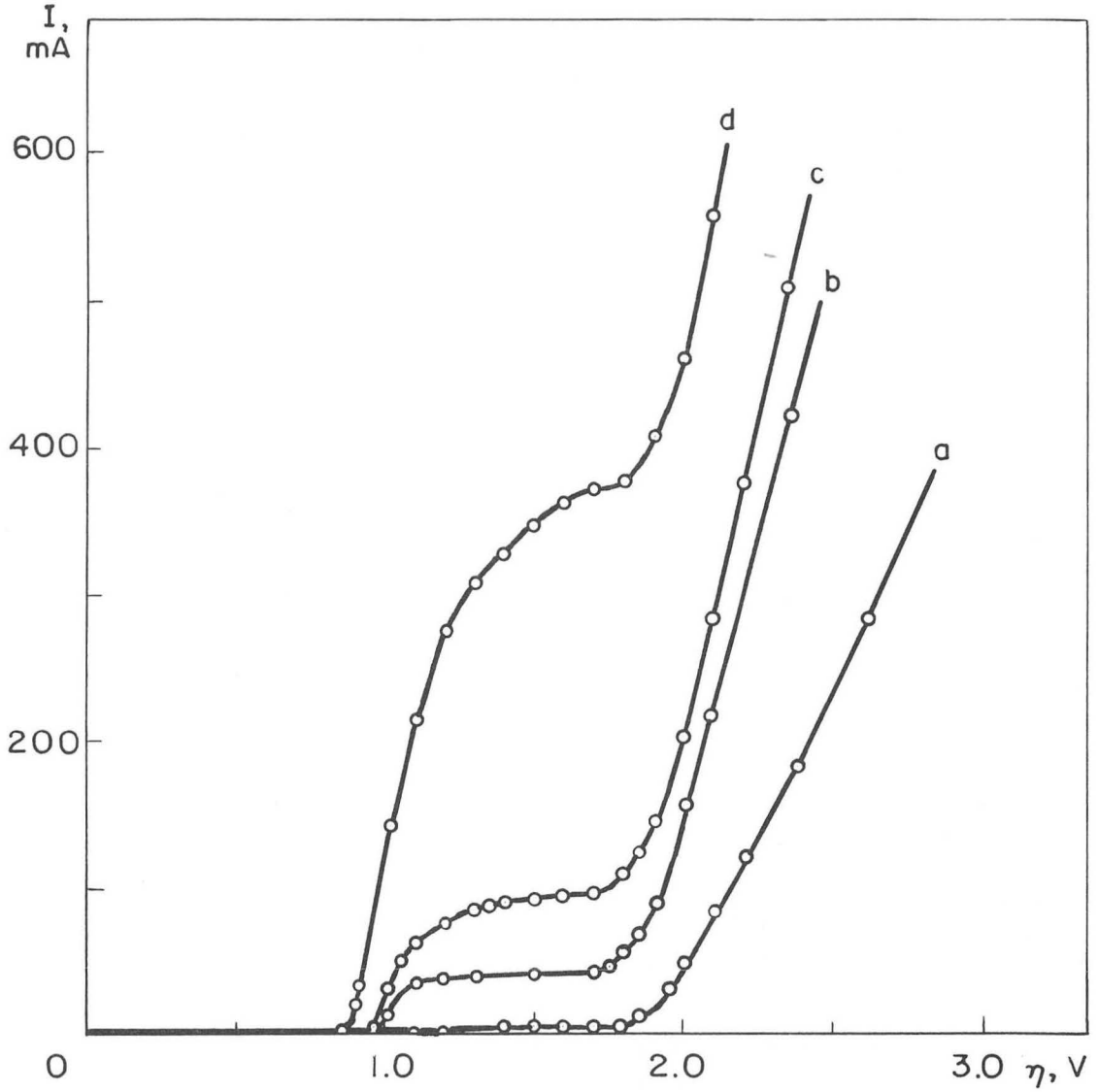

Fig. 4-5

XBL 815-5732

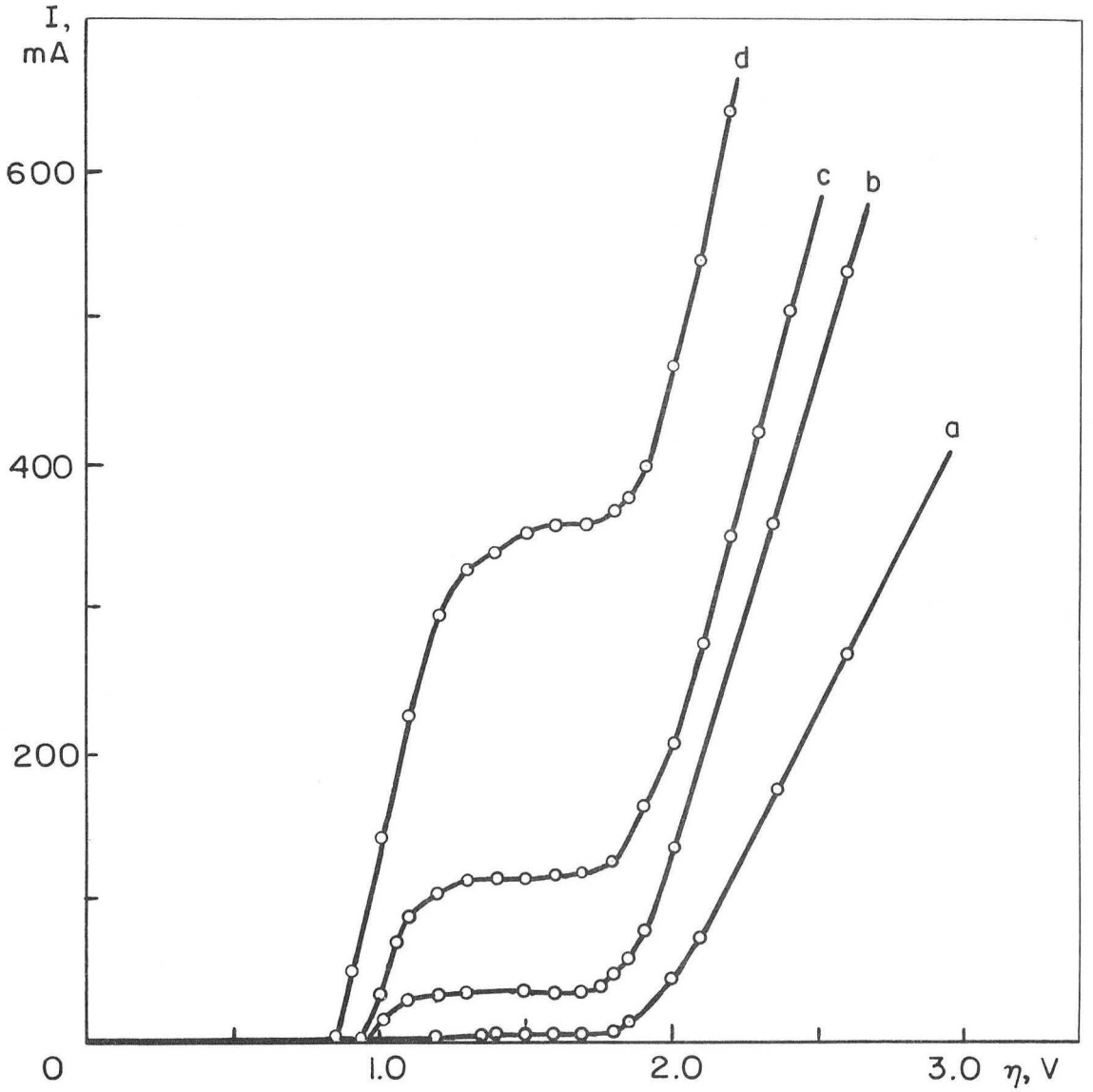

Fig. 4-6

XBL 815-5733

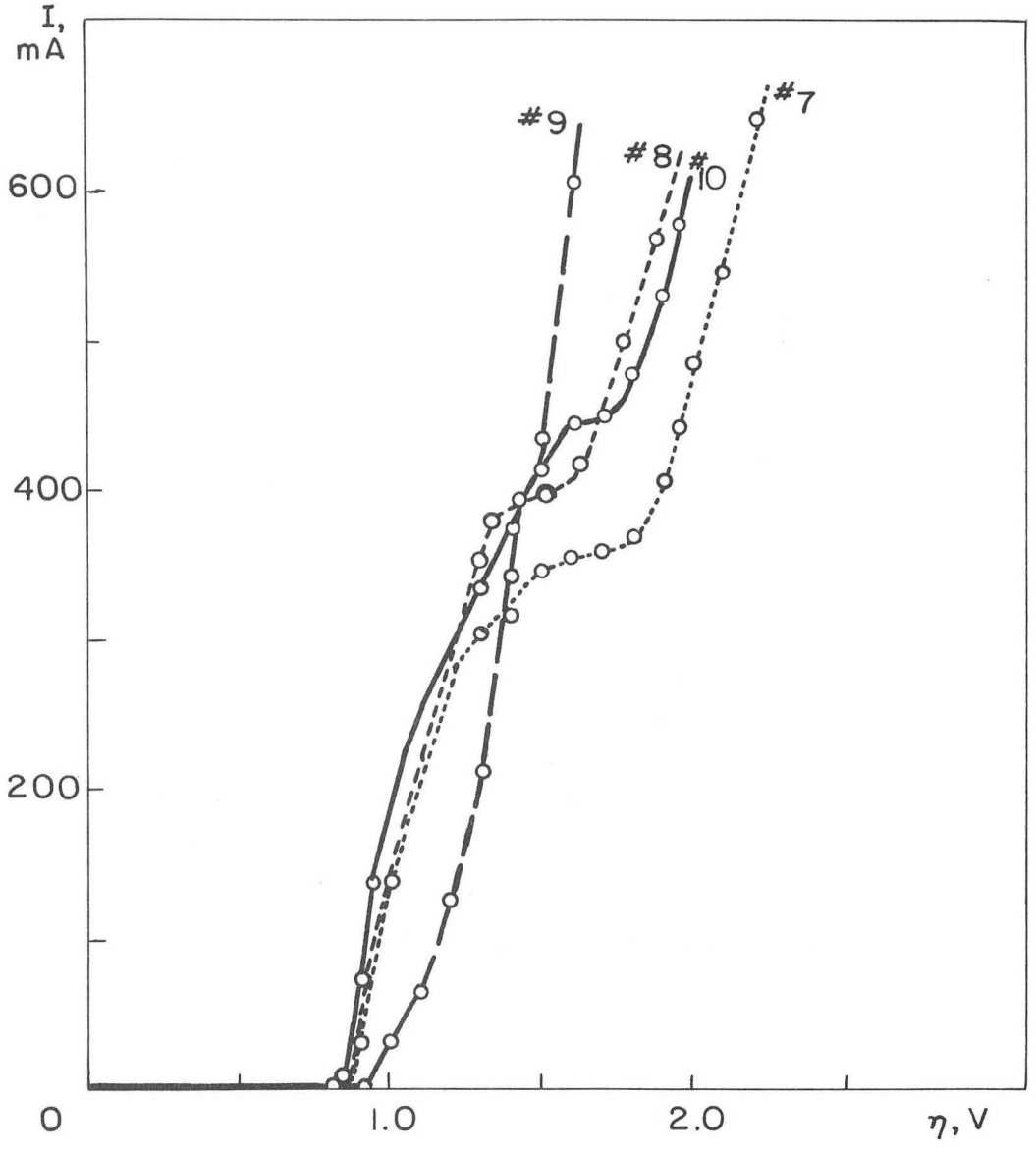

Fig. 4-7

XBL815-5734

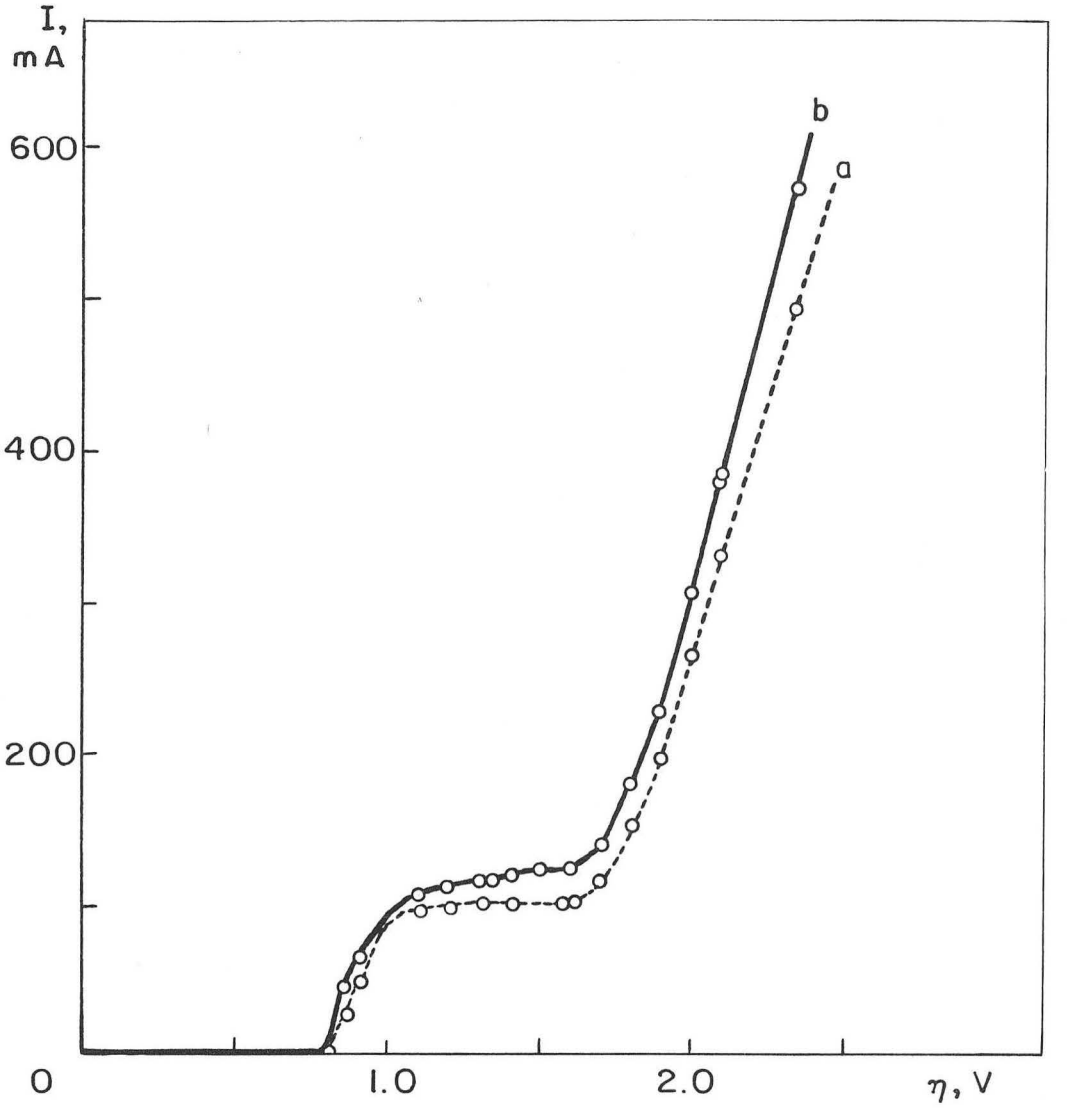

Fig. 4-8

XBL 815-5735

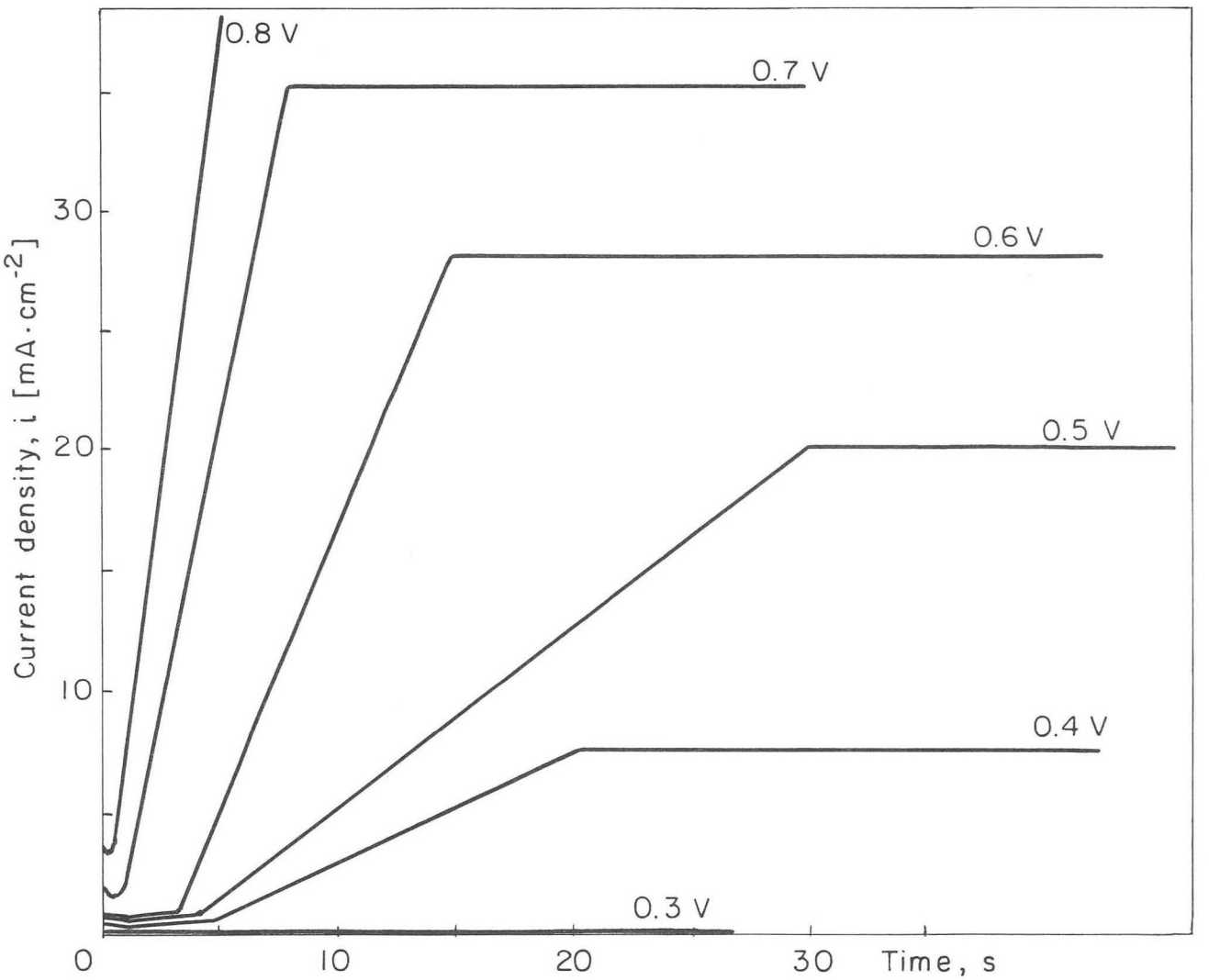

Fig. 4-9

XBL 815-5736

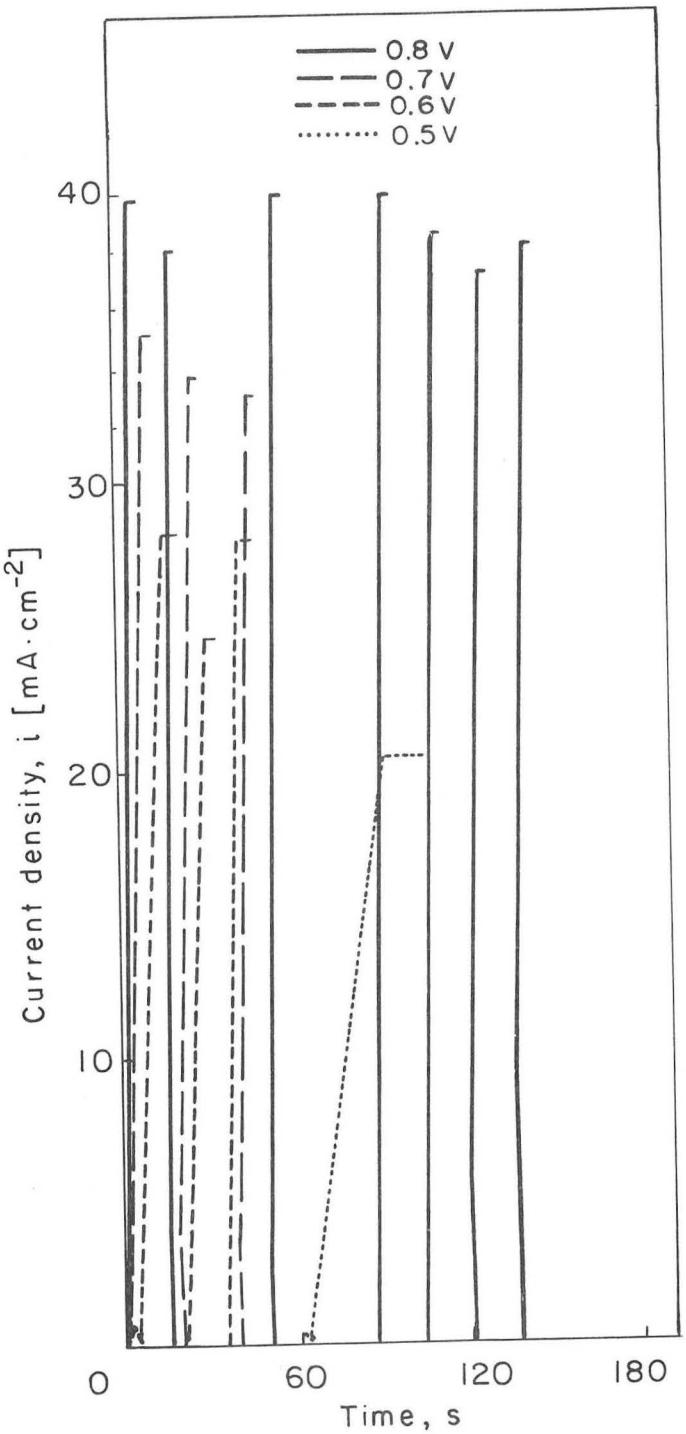

Fig. 4-10

XBL815-5737

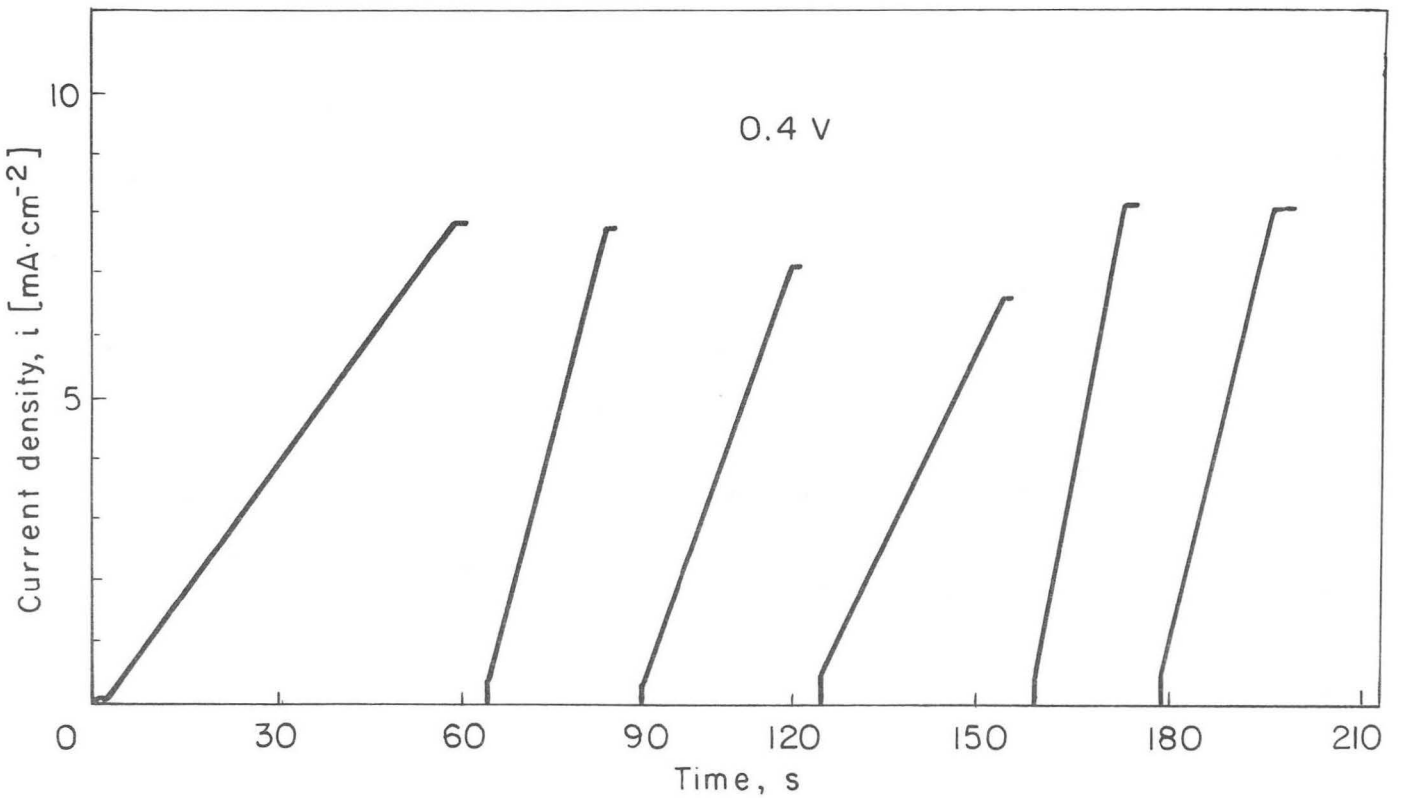

Fig. 4-11

XBL 815-5738

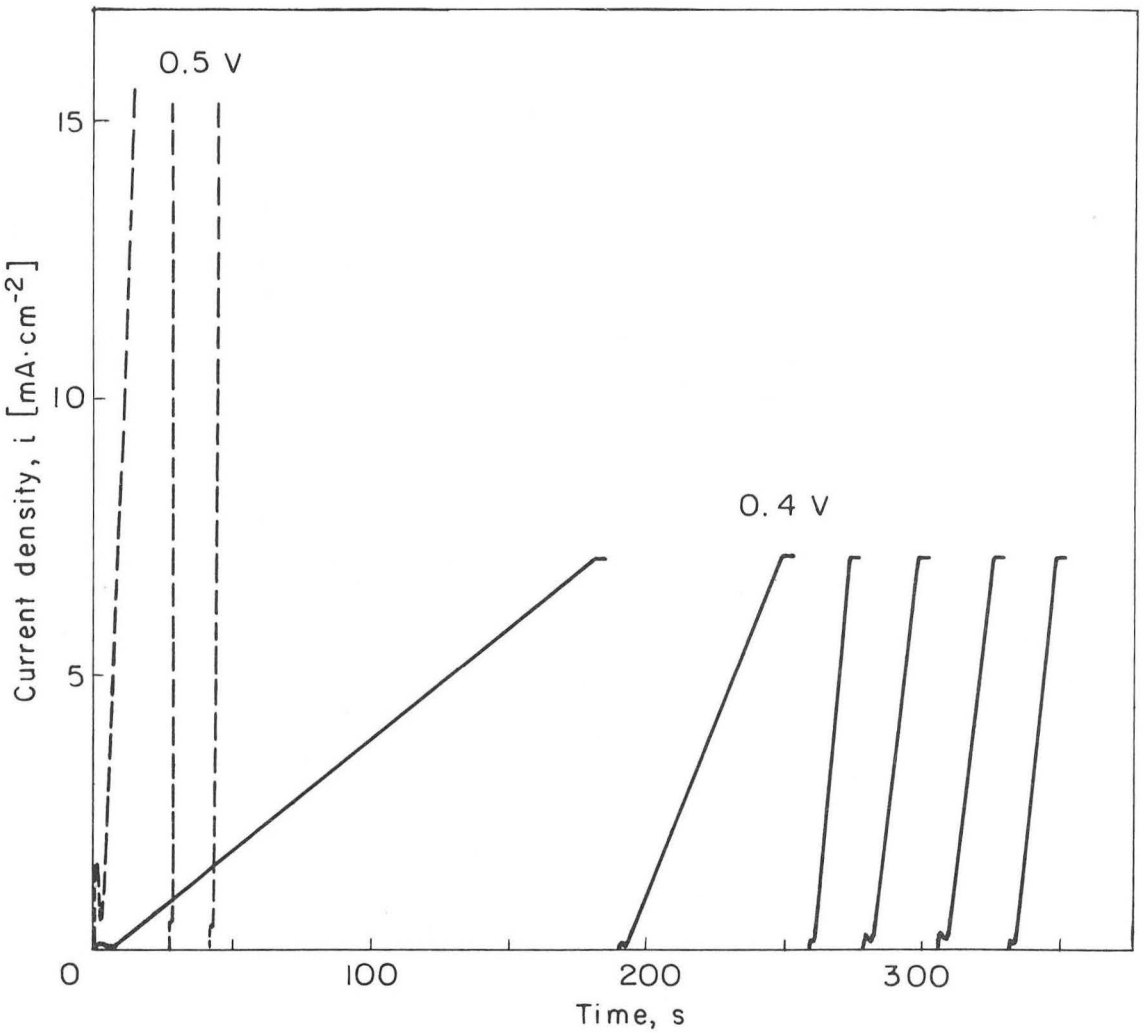

Fig. 4-12

XBL 815-5739

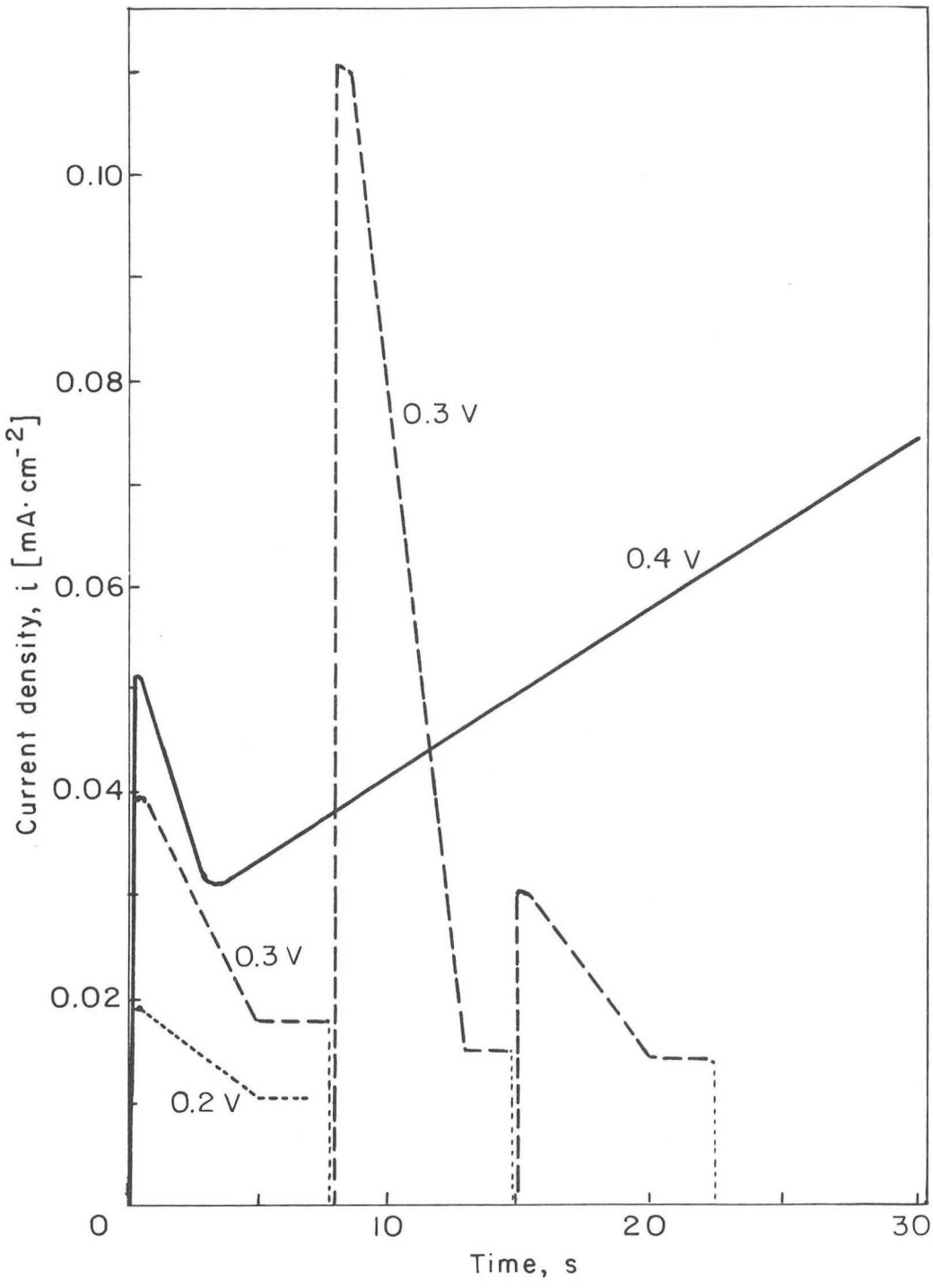

Fig. 4-13

XBL815-5740

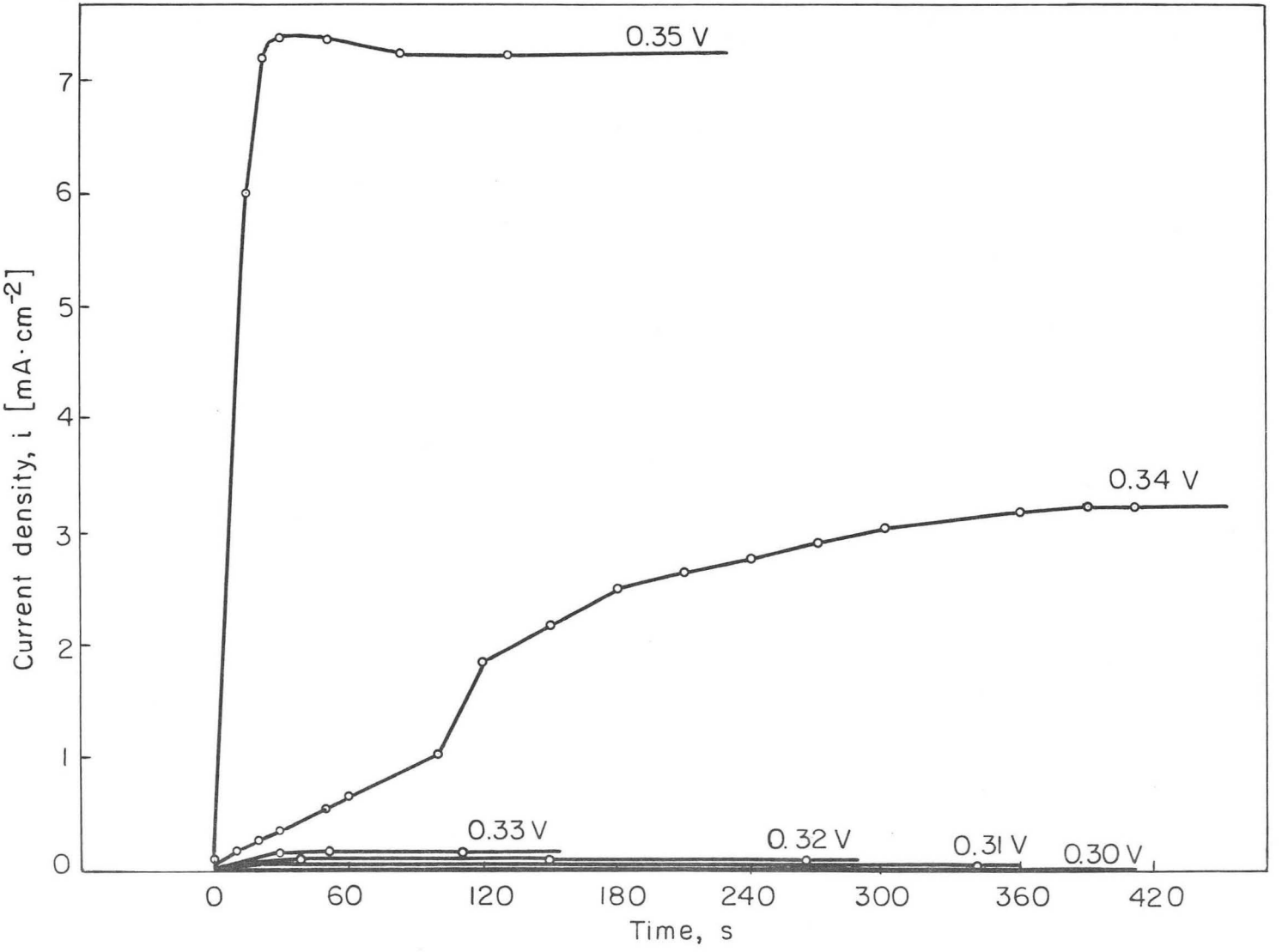

Fig. 4-14

XBL 815-5741

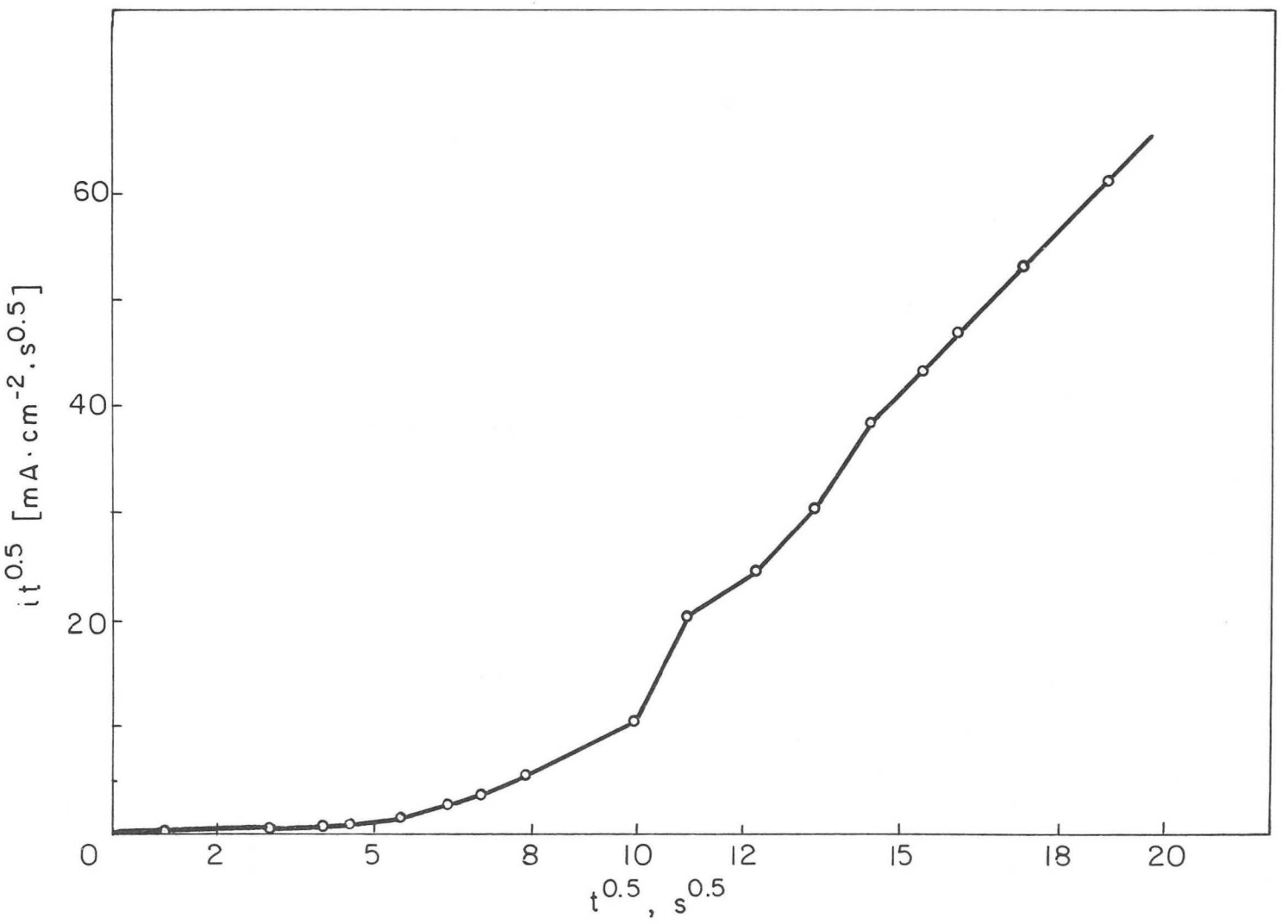

Fig. 4-15

XBL 815-5742

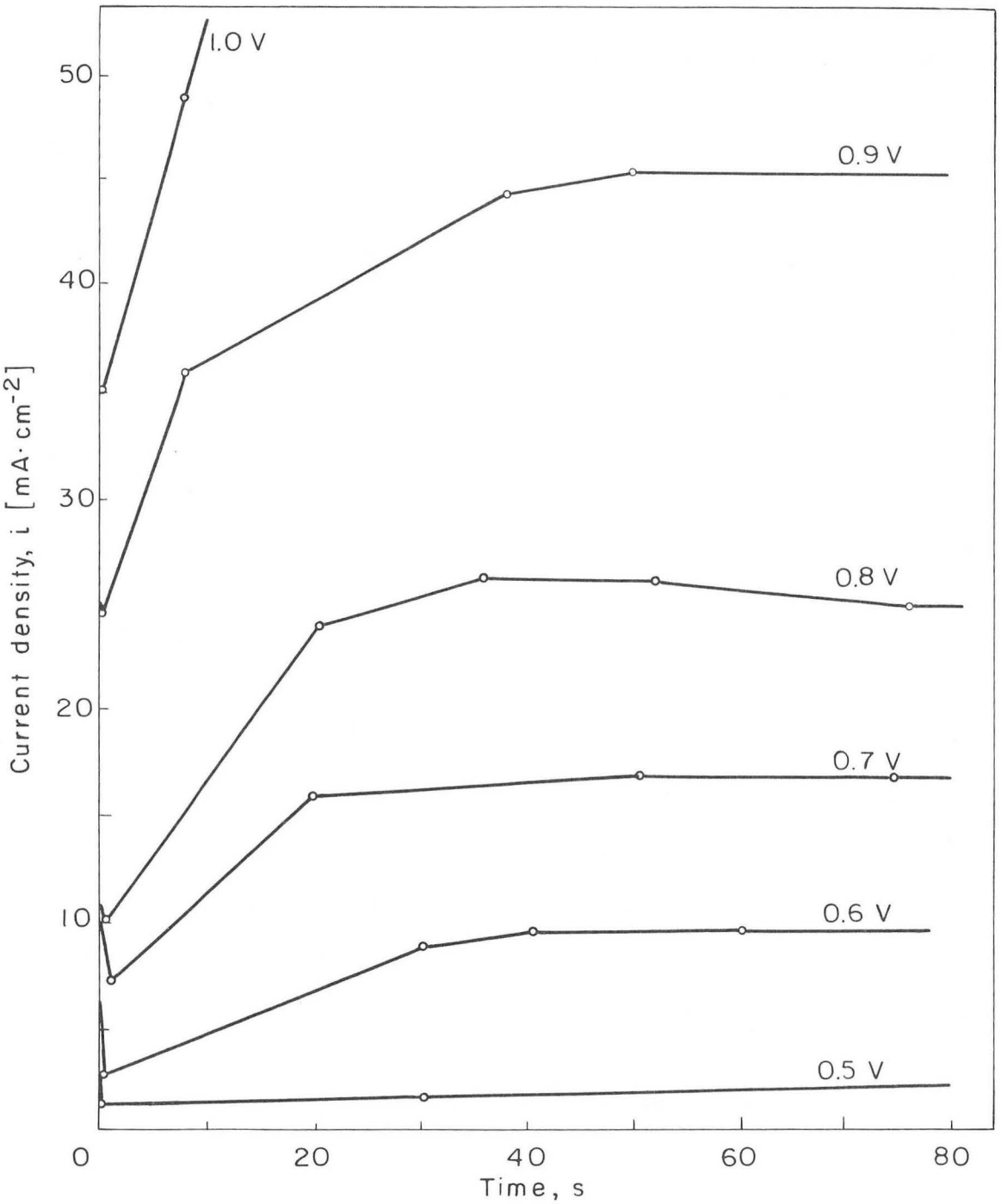

Fig. 4-16

XBL815-5743

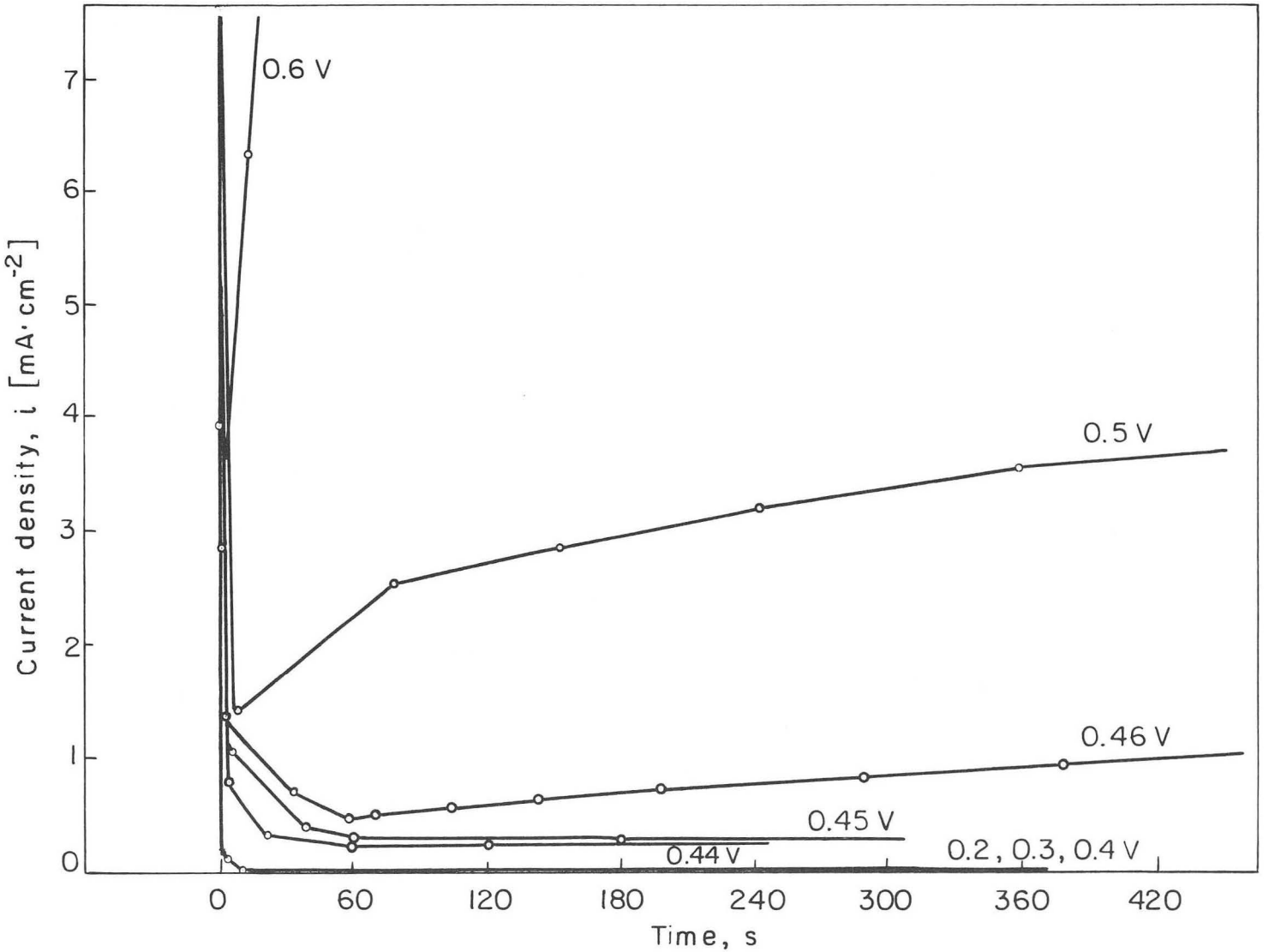

Fig. 4-17

XBL815-5744

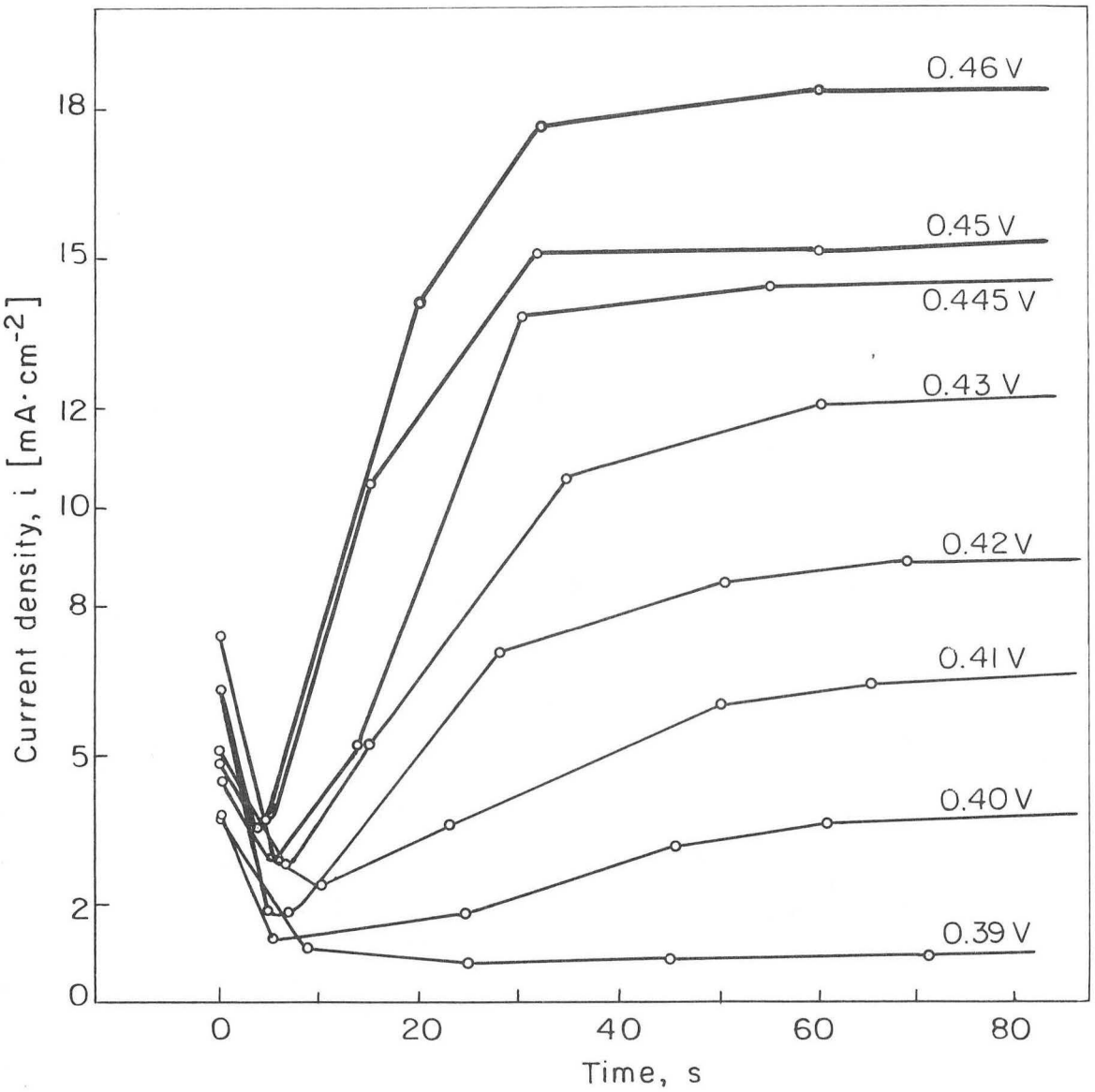

Fig. 4-18

XBL 815-5745

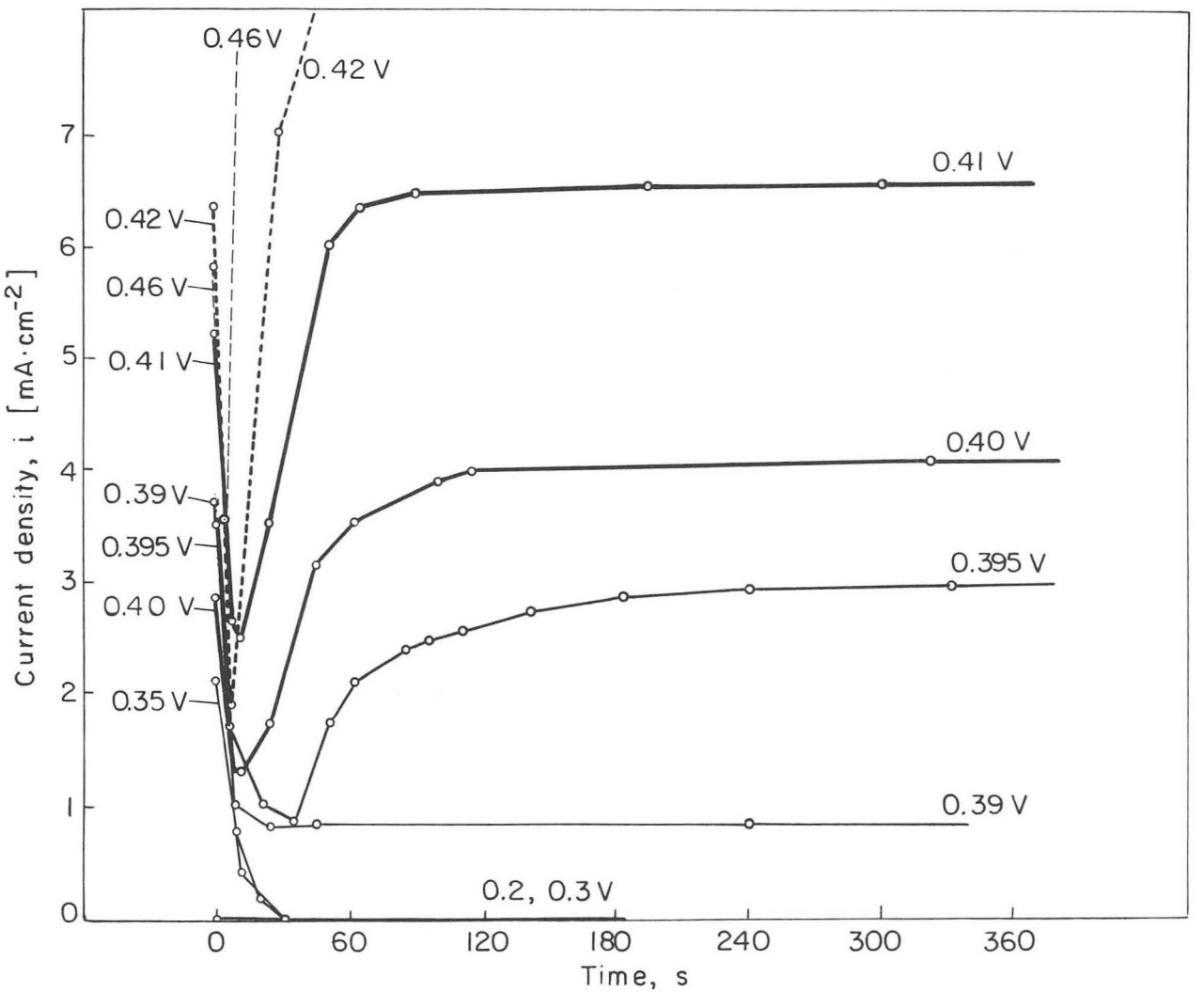

Fig. 4-19

XBL 815-5746

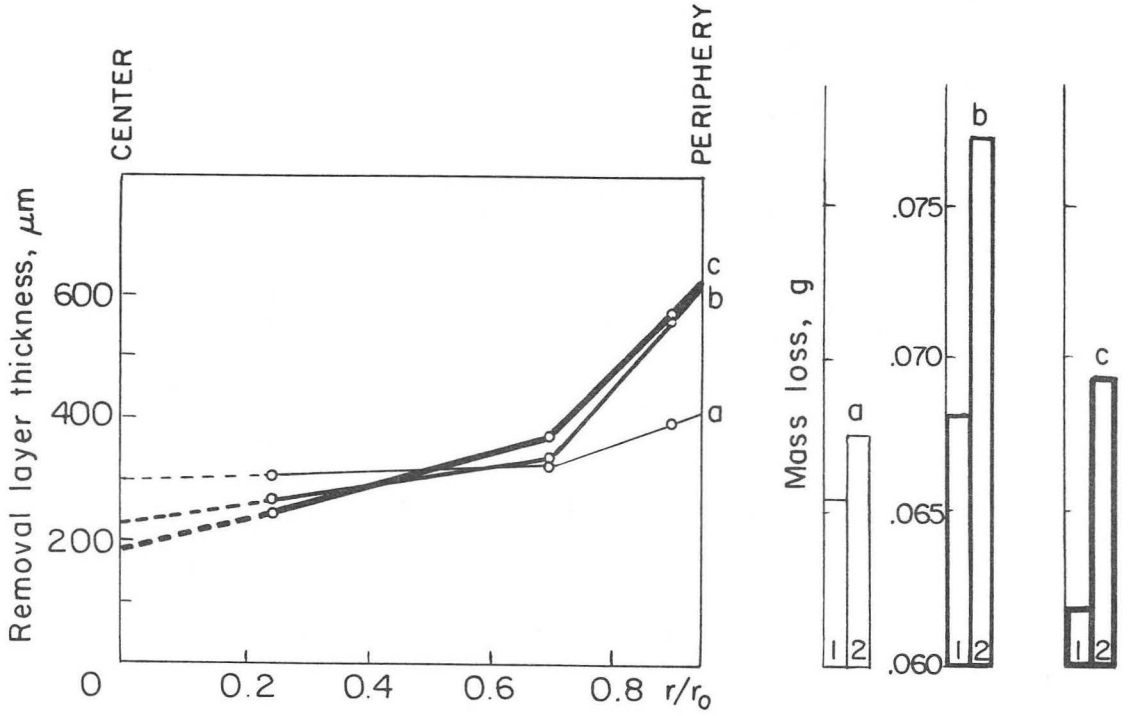

Fig. 5-1

XBL 815-5747

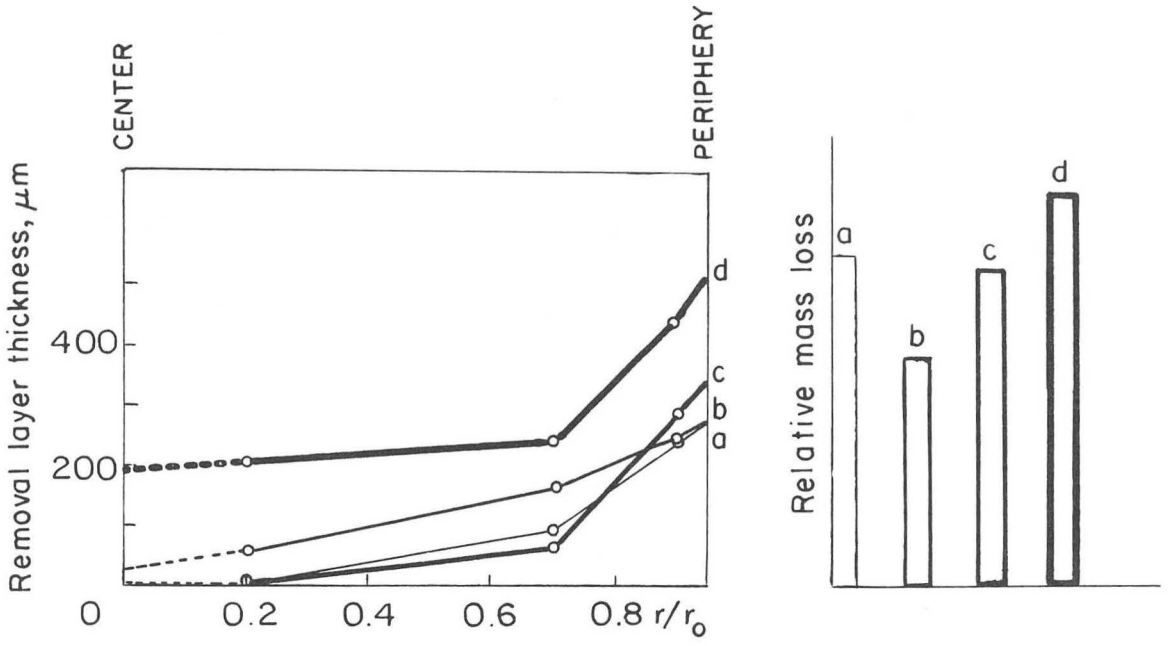

Fig. 5-2

XBL 815-5748

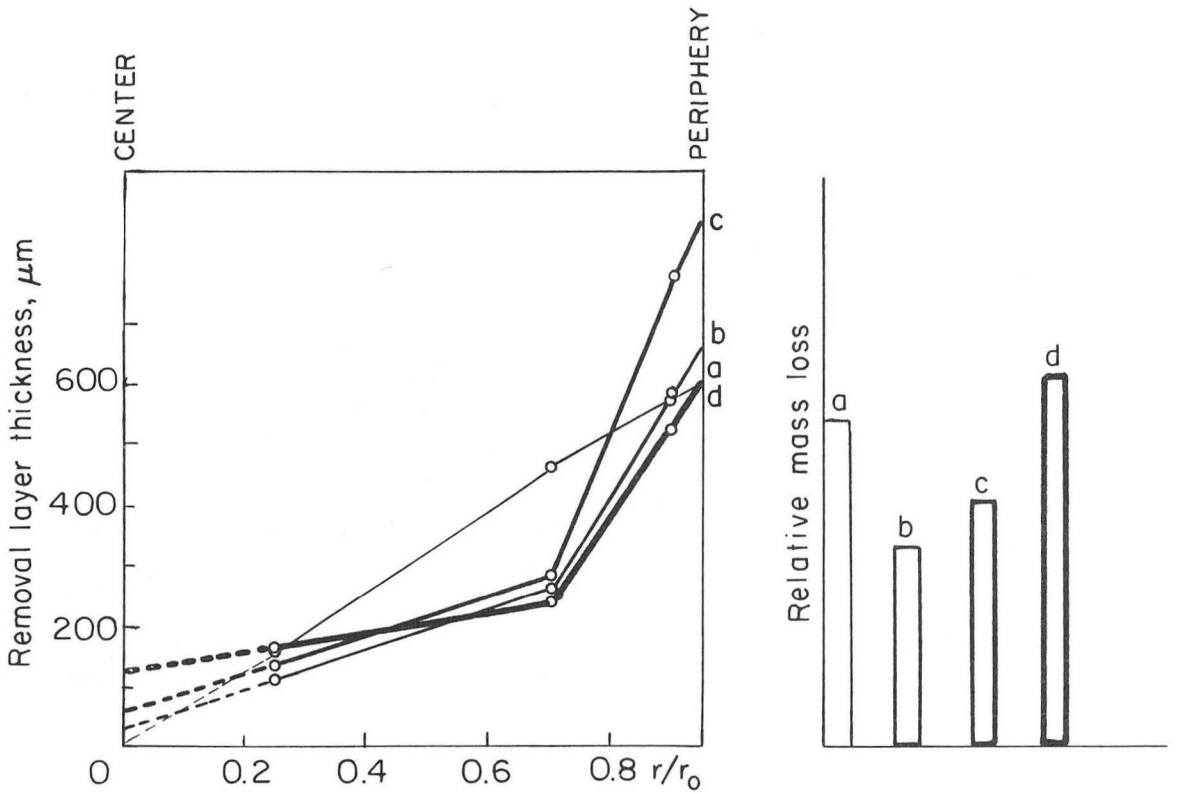

Fig. 5-3

XBL 815-5749

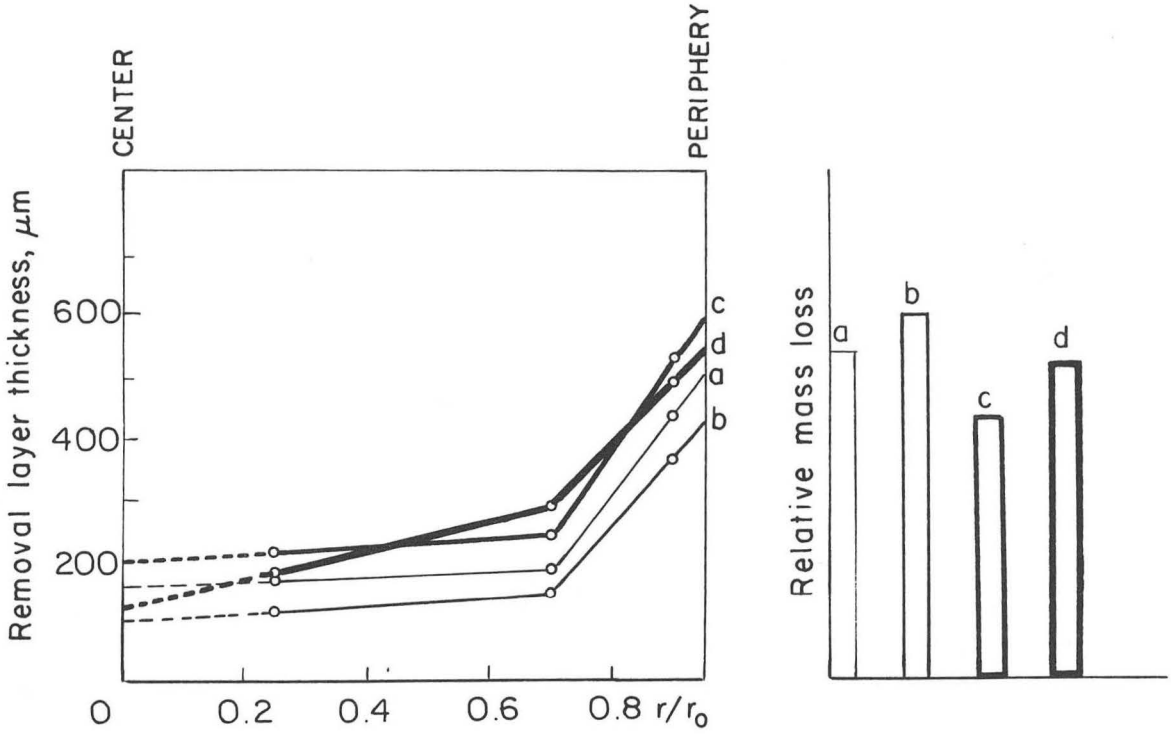

Fig. 5-4

XBL 815-5750

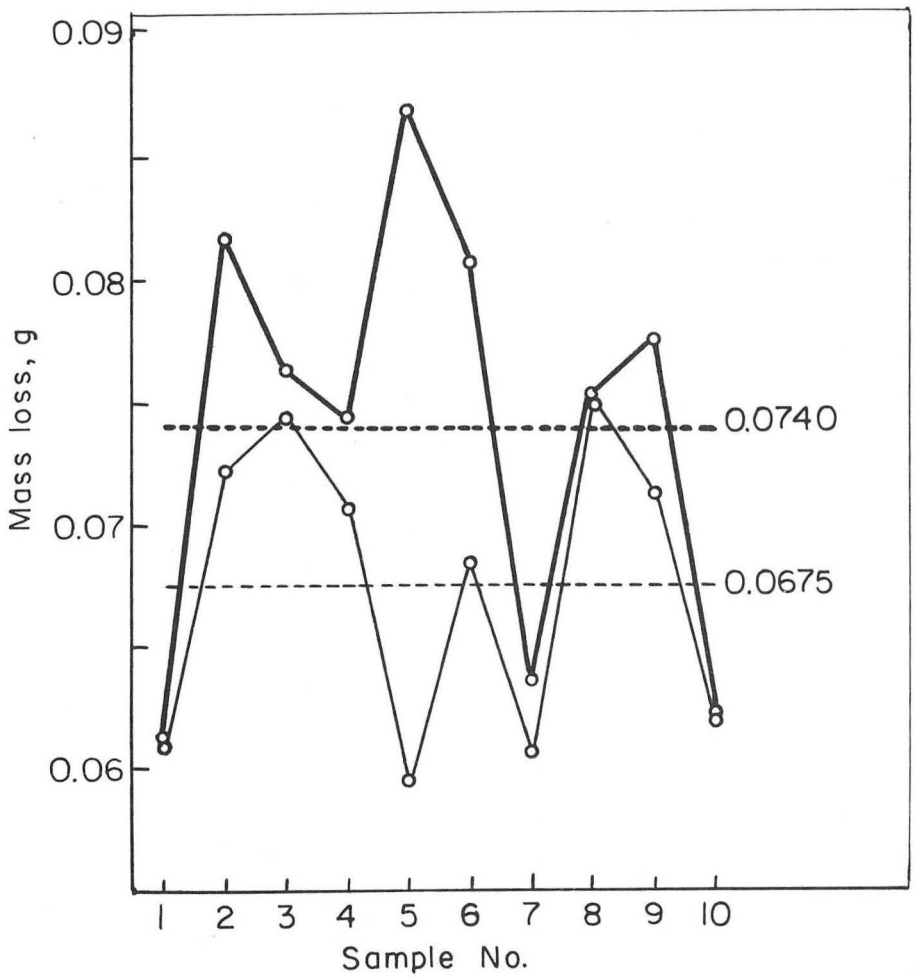

Fig. 5-5

XBL 815-5751

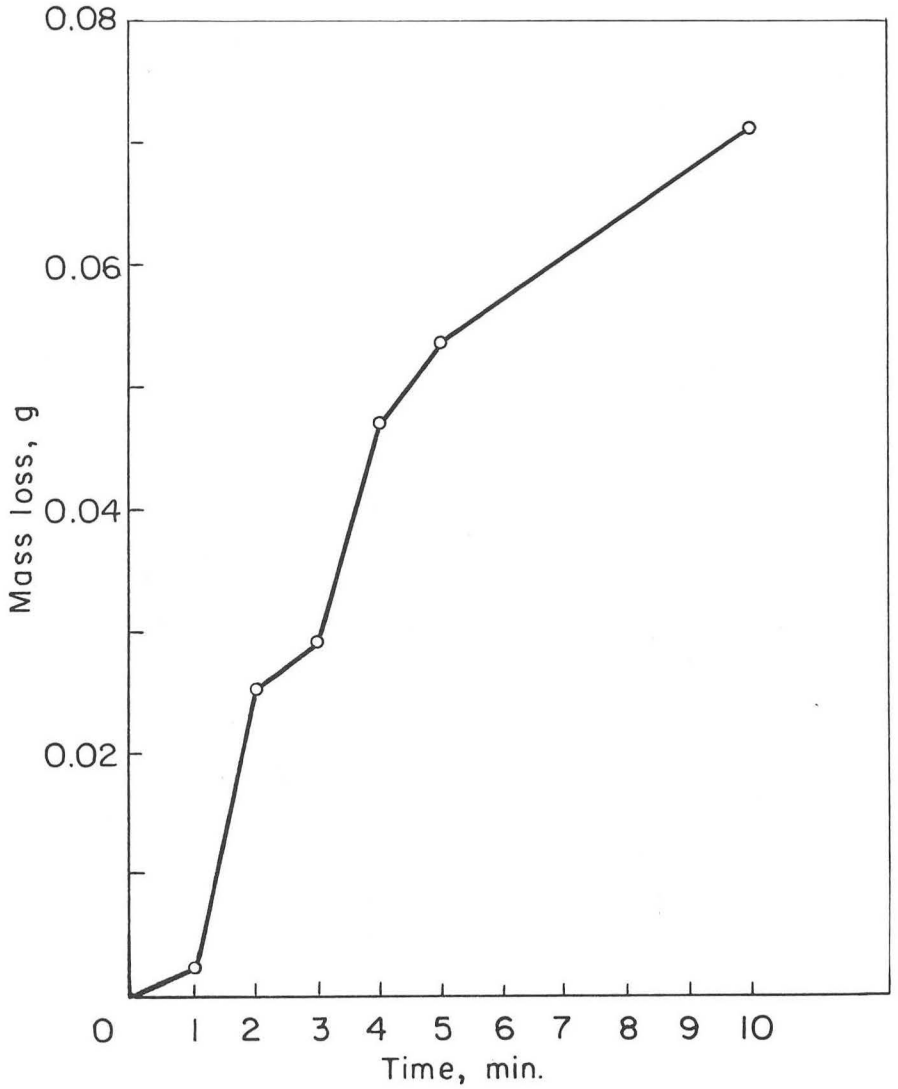

Fig.5-6

XBL 815-5752

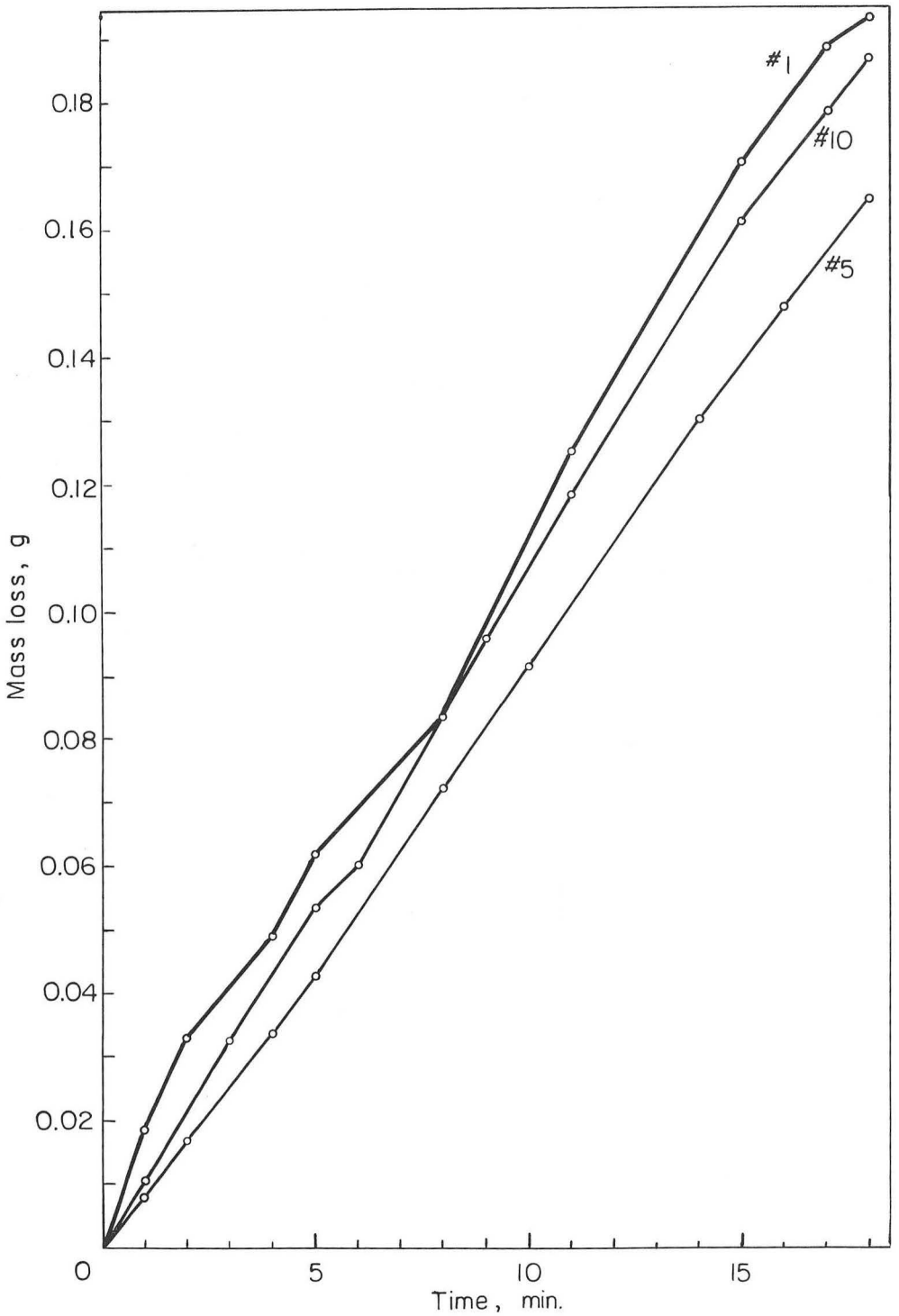

Fig. 6-1

XBL815-5753

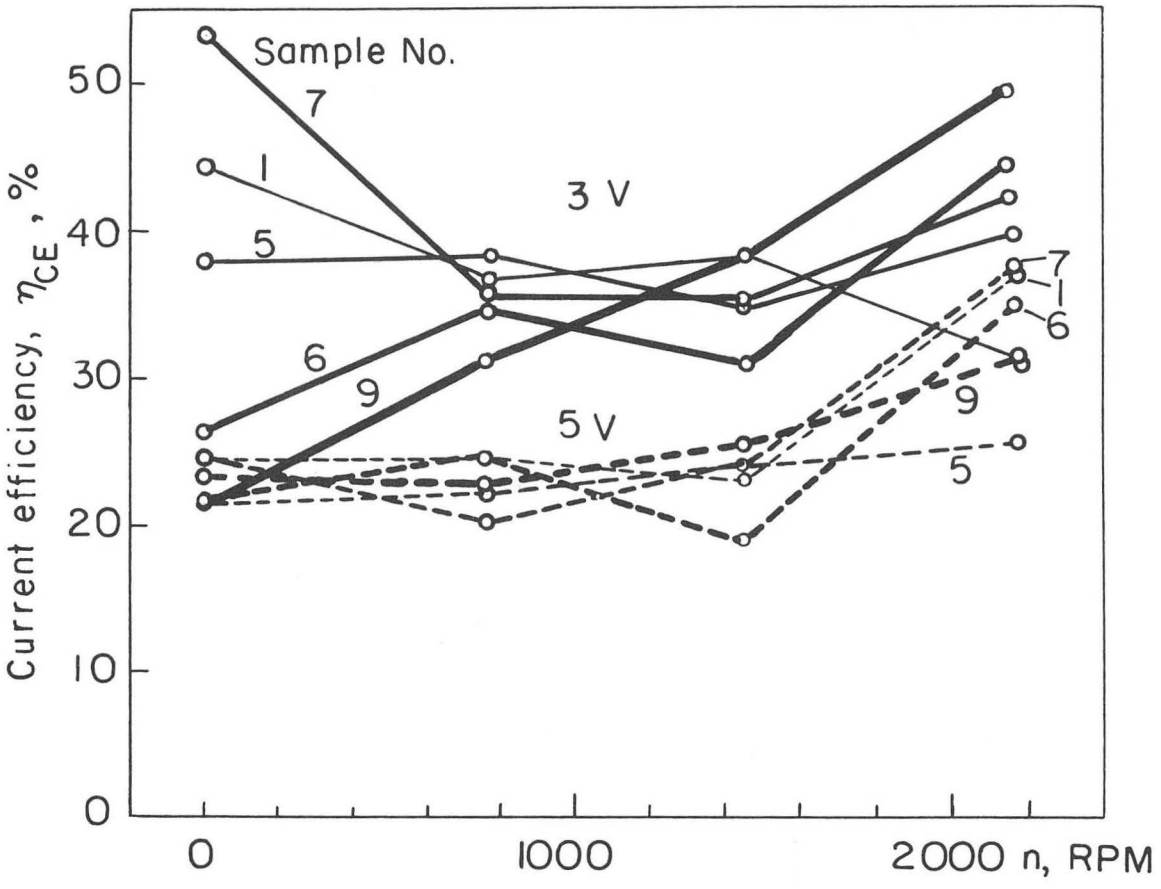

Fig. 6-2

XBL 815-5754

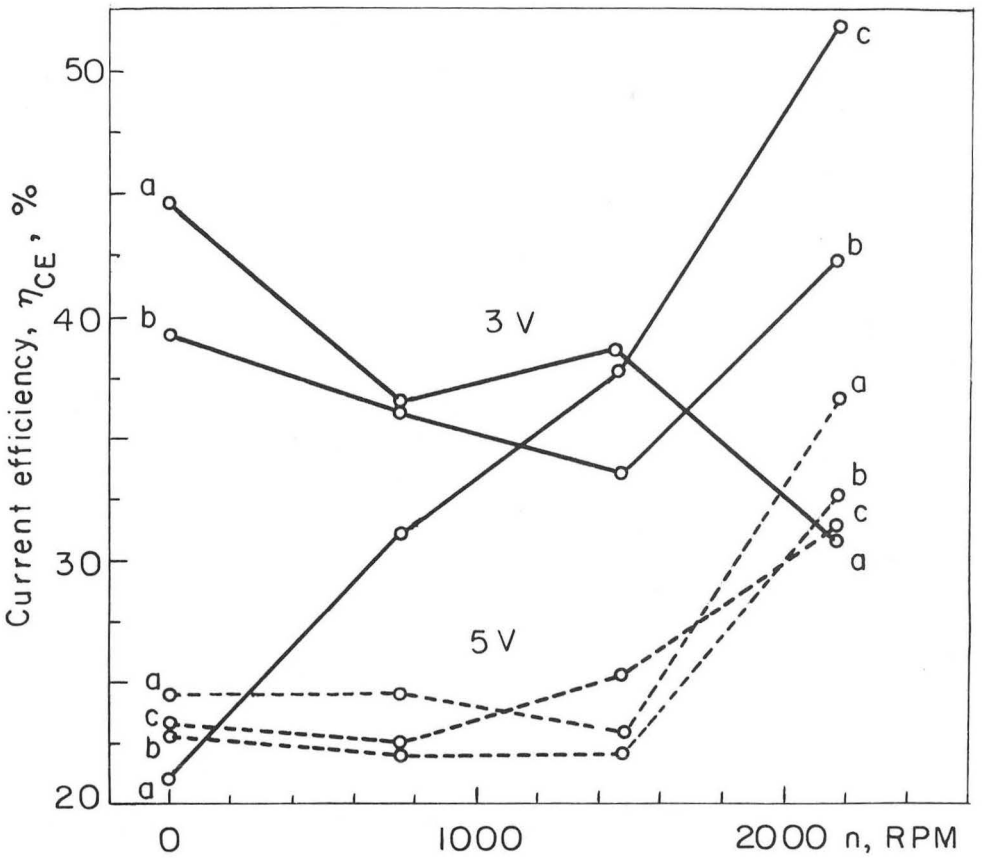

Fig. 6-3

XBL 815-5755

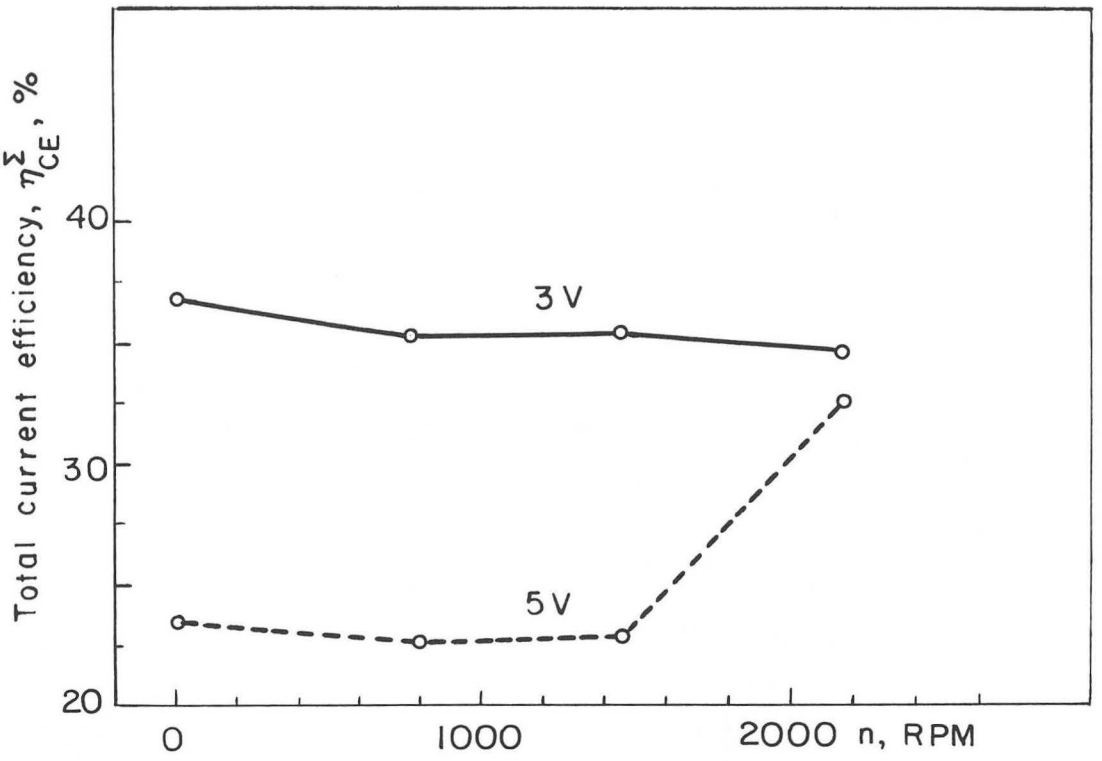

Fig. 6 - 4

XBL815-5756

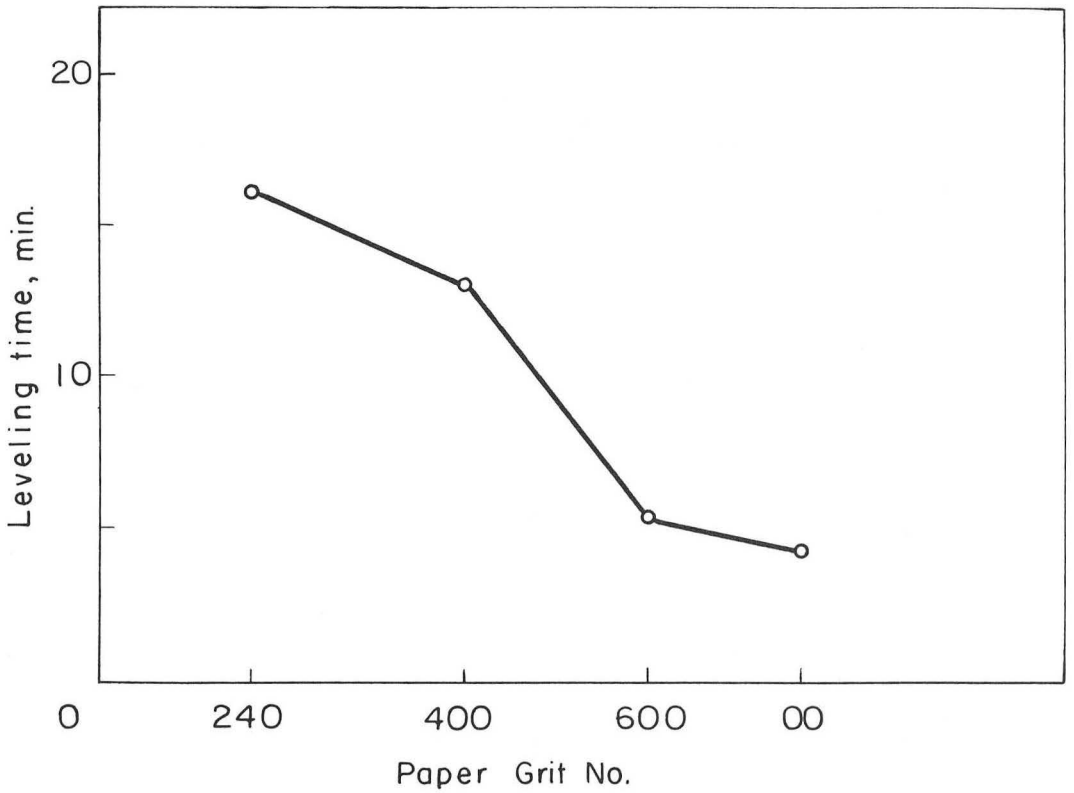

Fig. 7 - 1

XBL 815-5757

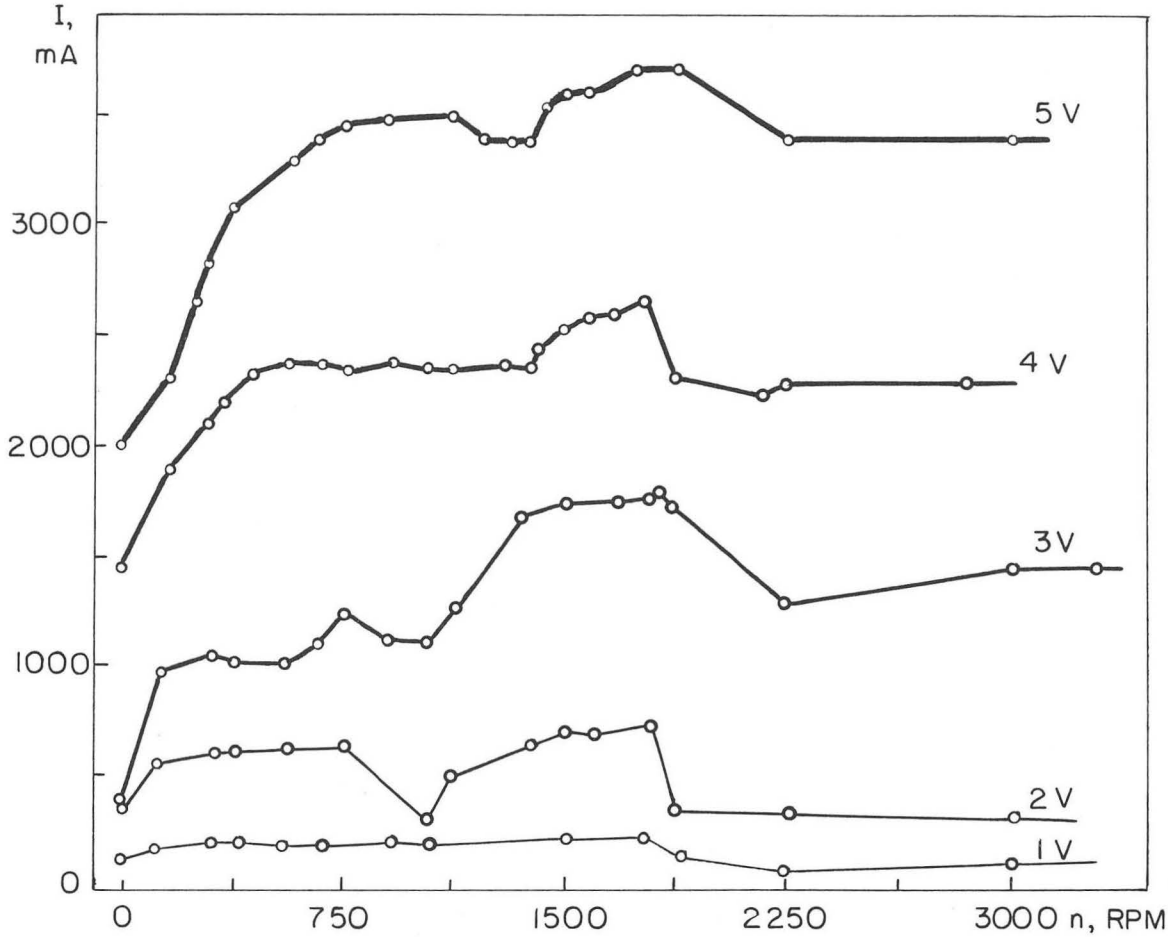

Fig. 8-1

XBL 815-5758

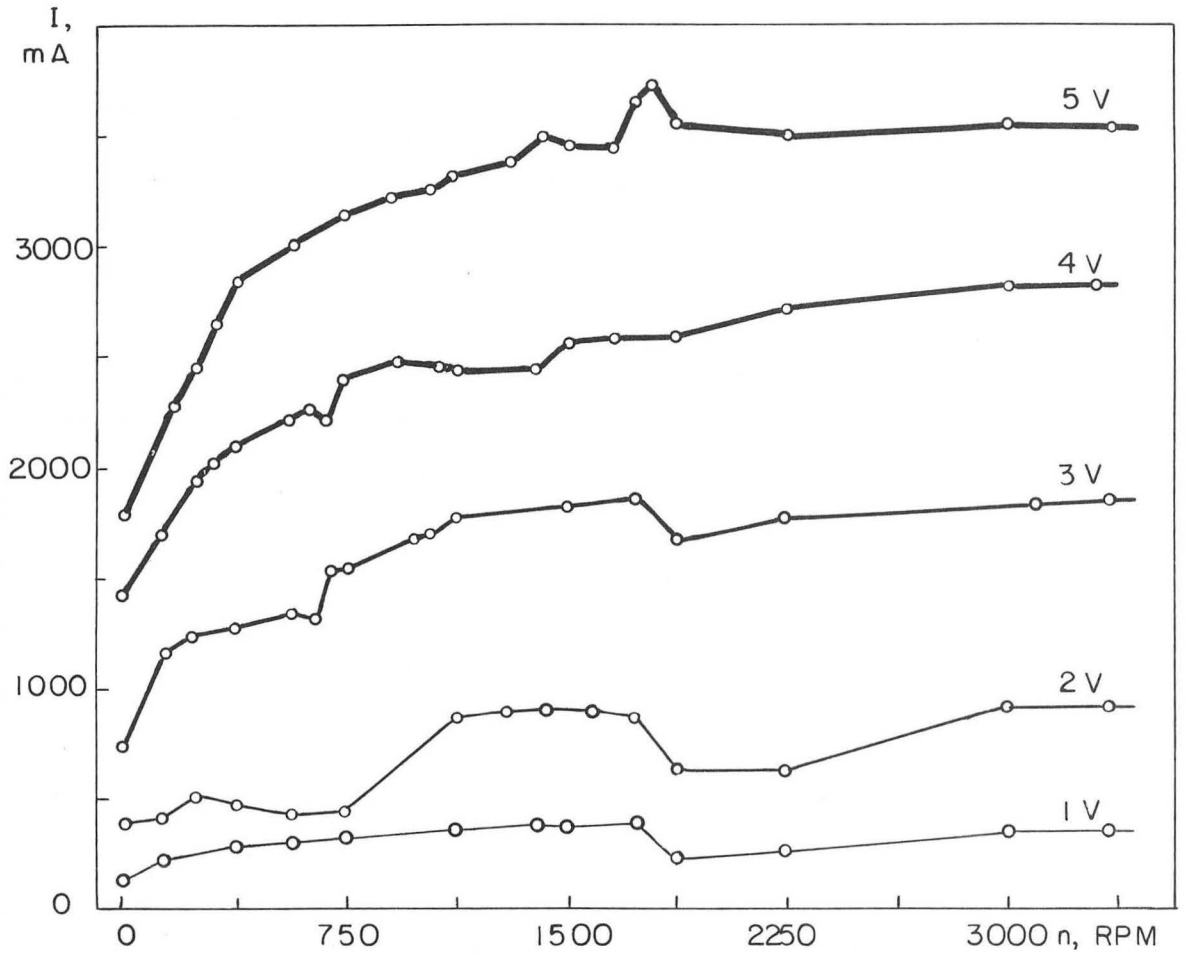

Fig. 8-2

XBL 815-5759

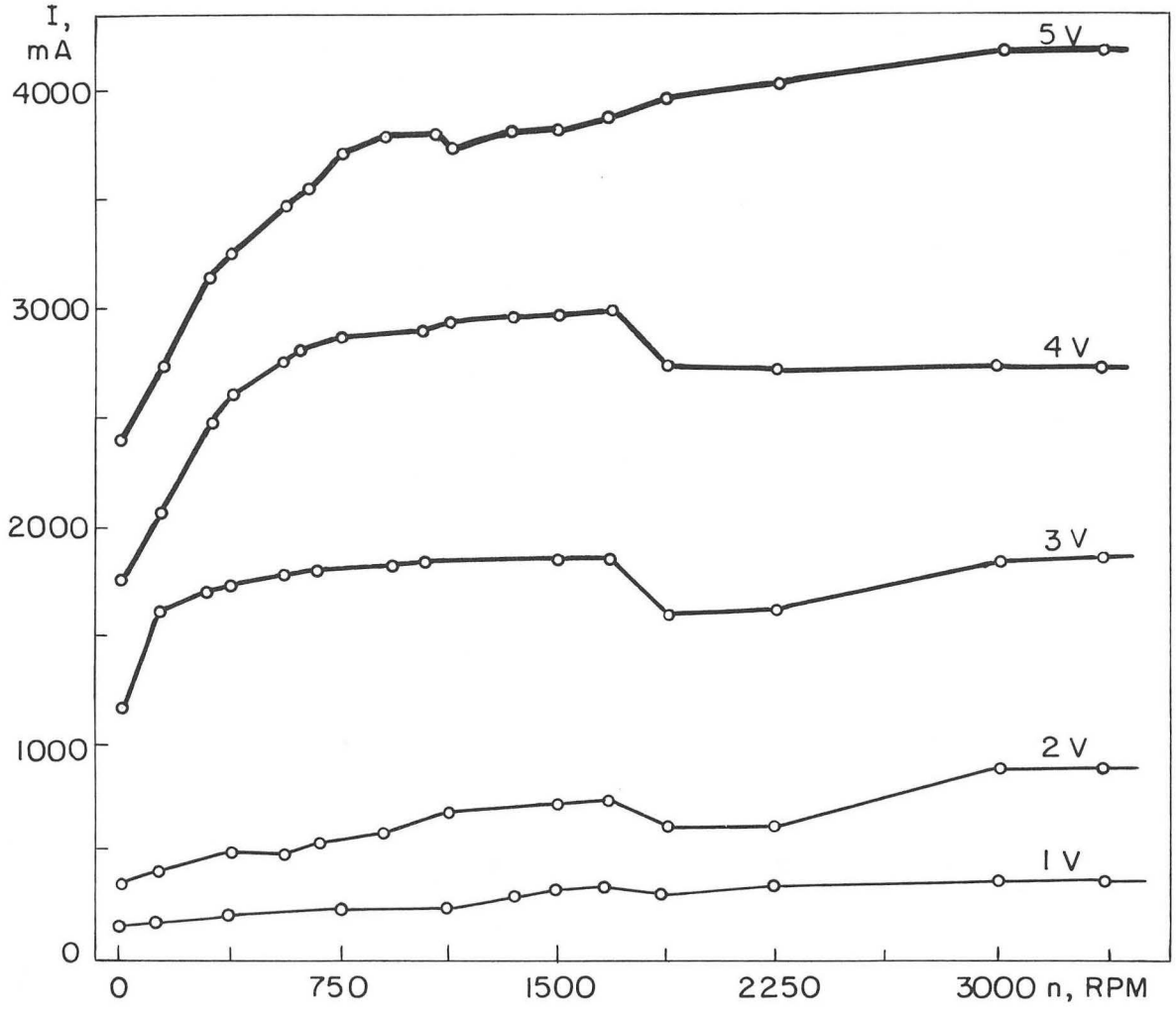

Fig. 8-3

XBL815-5760

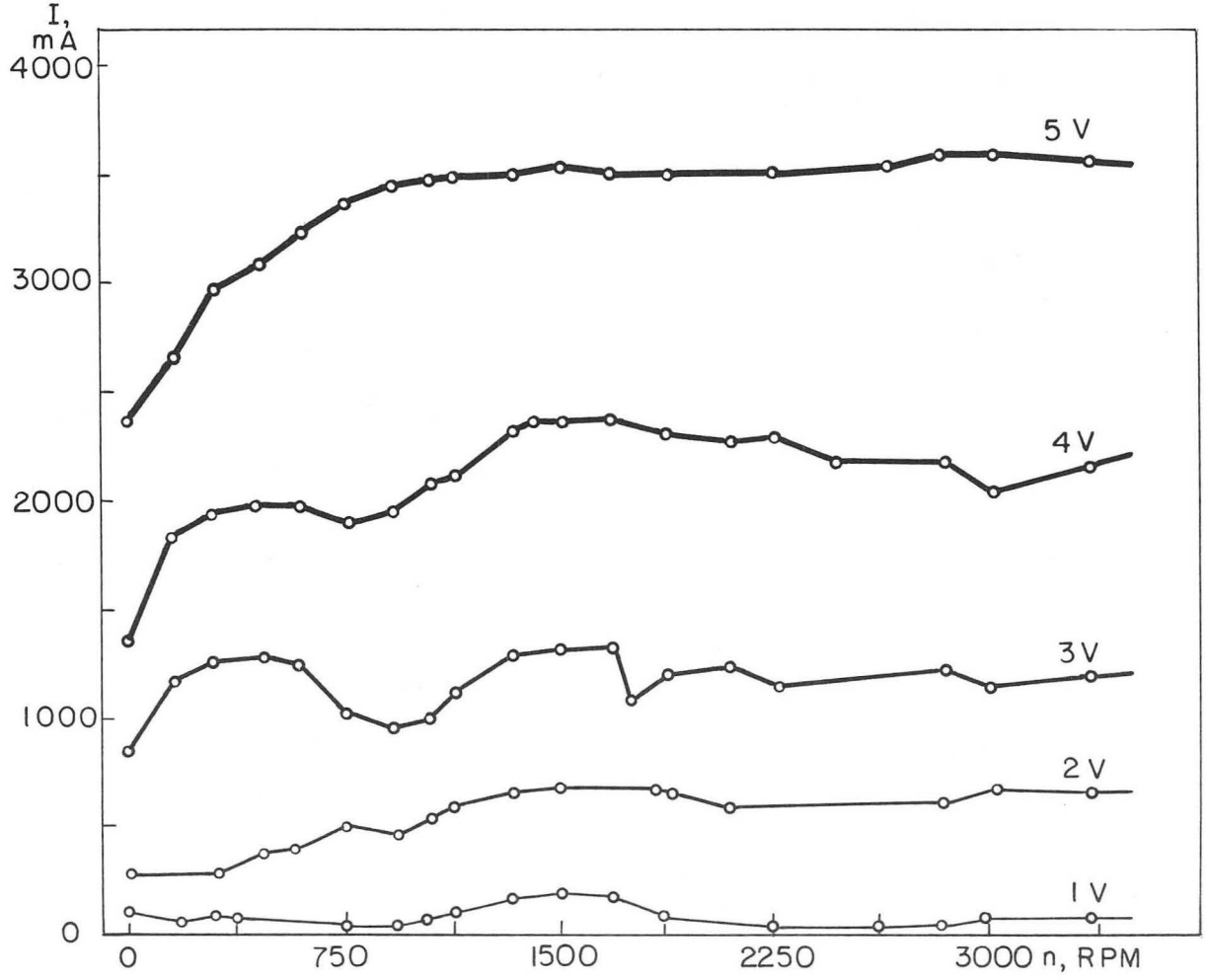

Fig. 8-4

XBL 815-5761

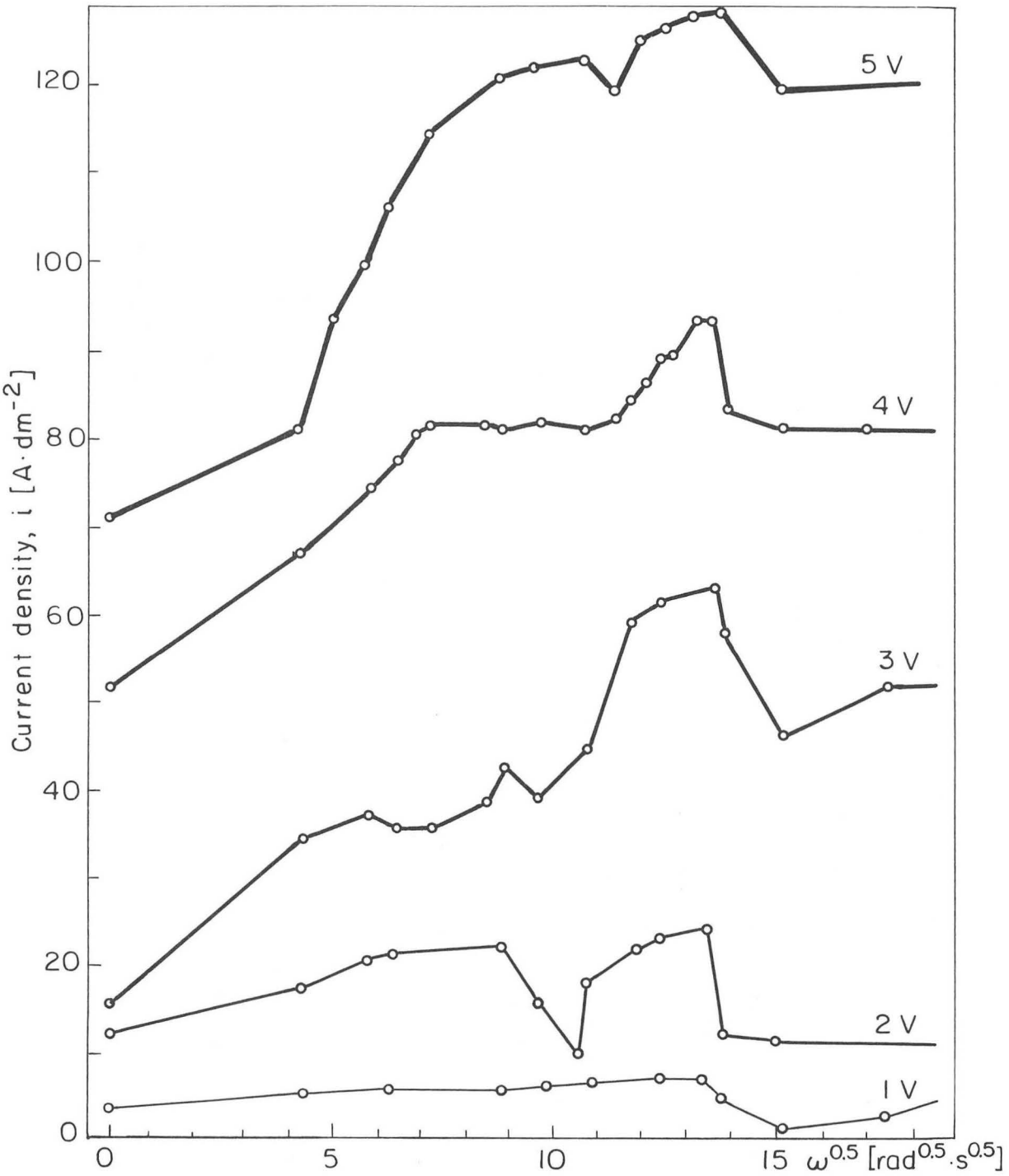

Fig. 8-5

XBL 815-5762

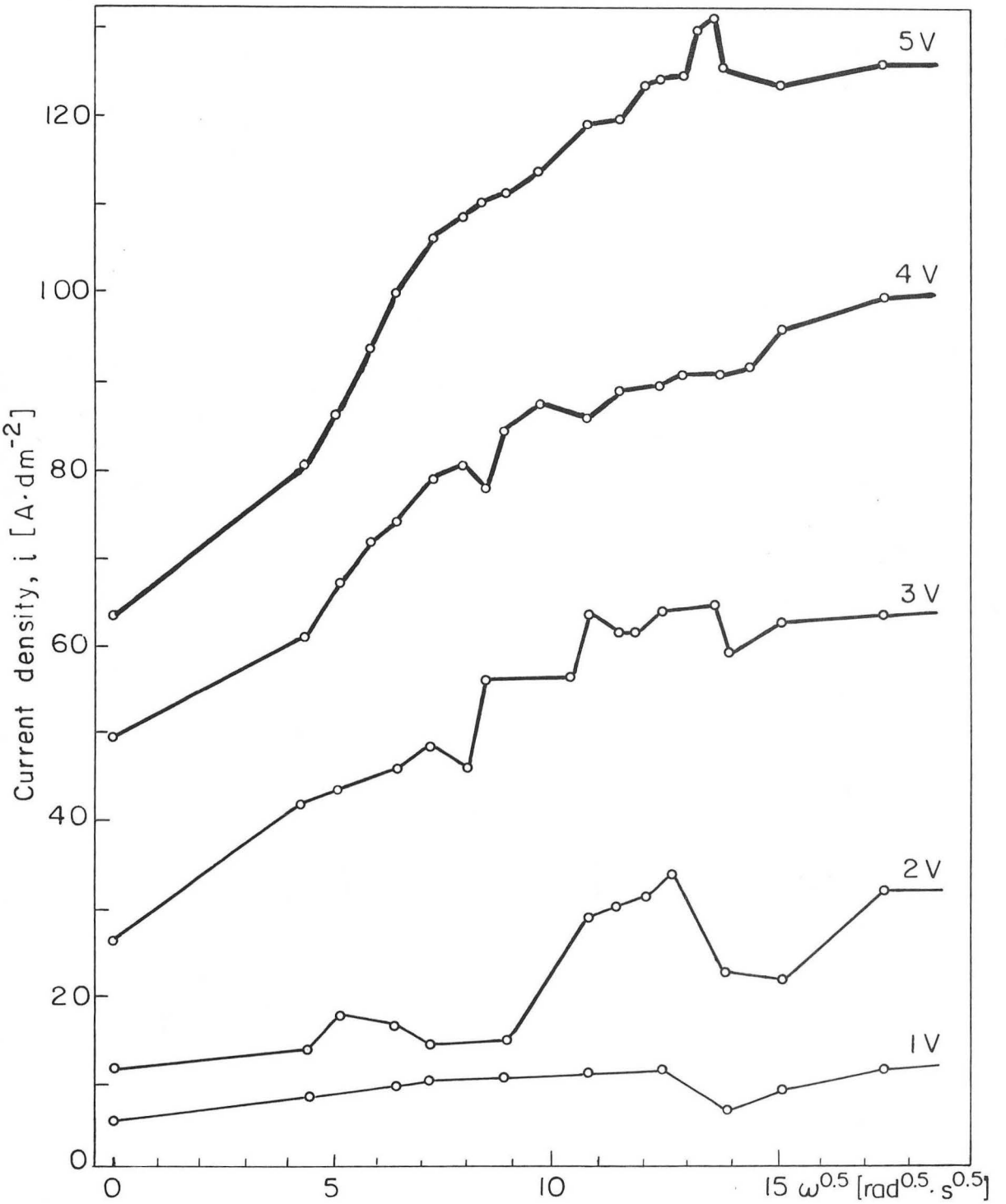

Fig. 8-6

XBL 815-5763

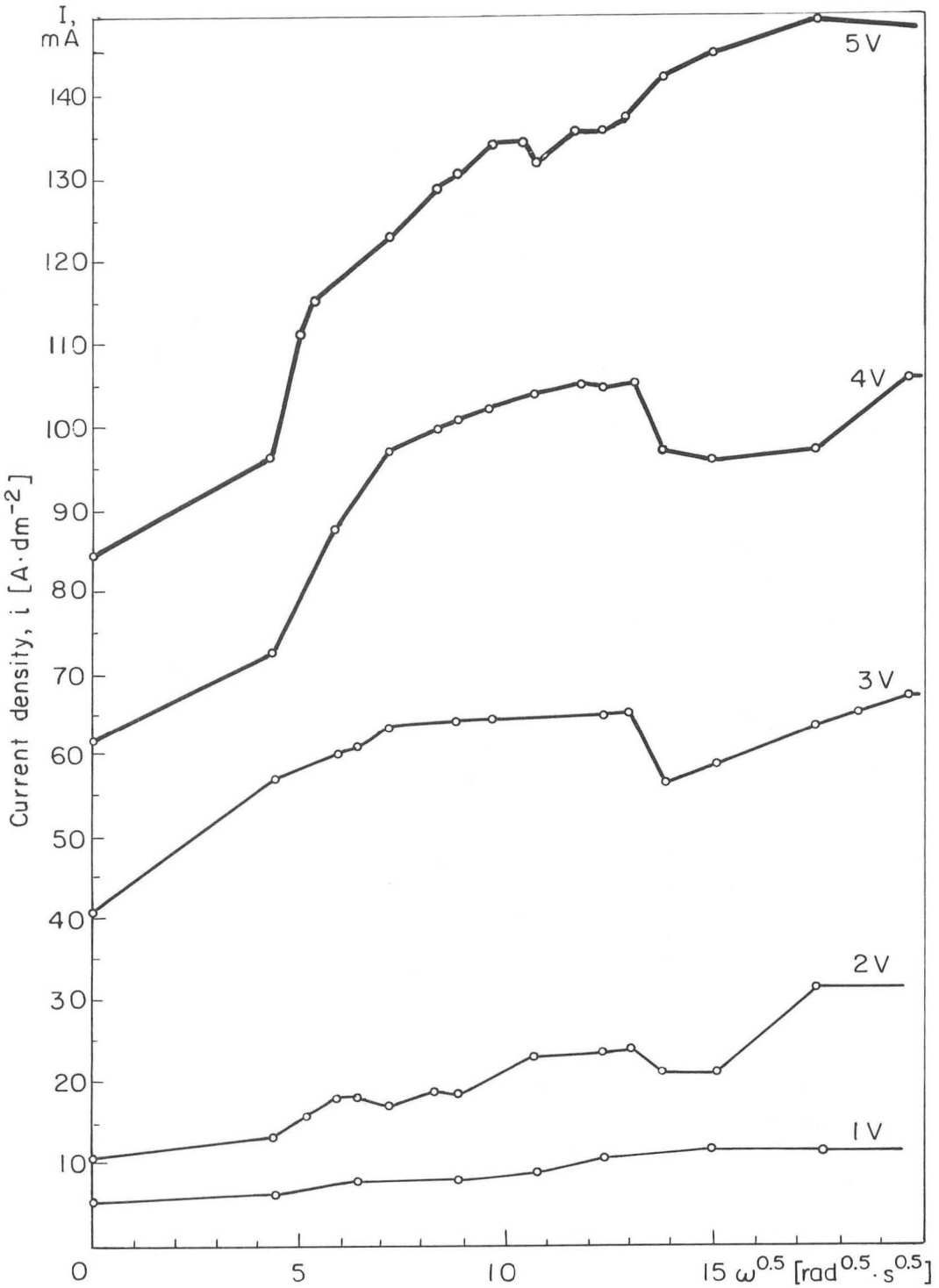

Fig. 8-7

XBL 815-5764

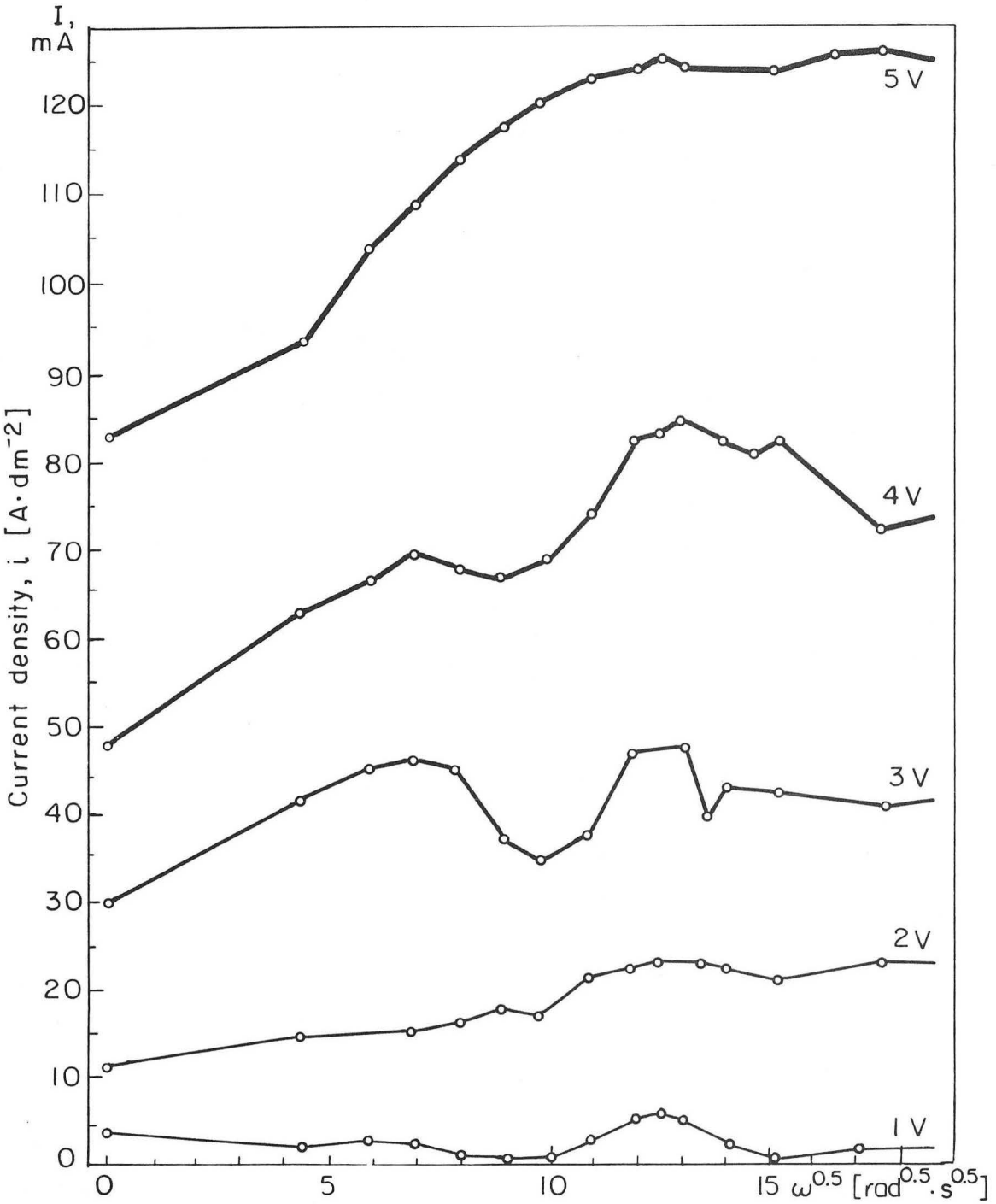

Fig. 8-8

XBL 815-5765

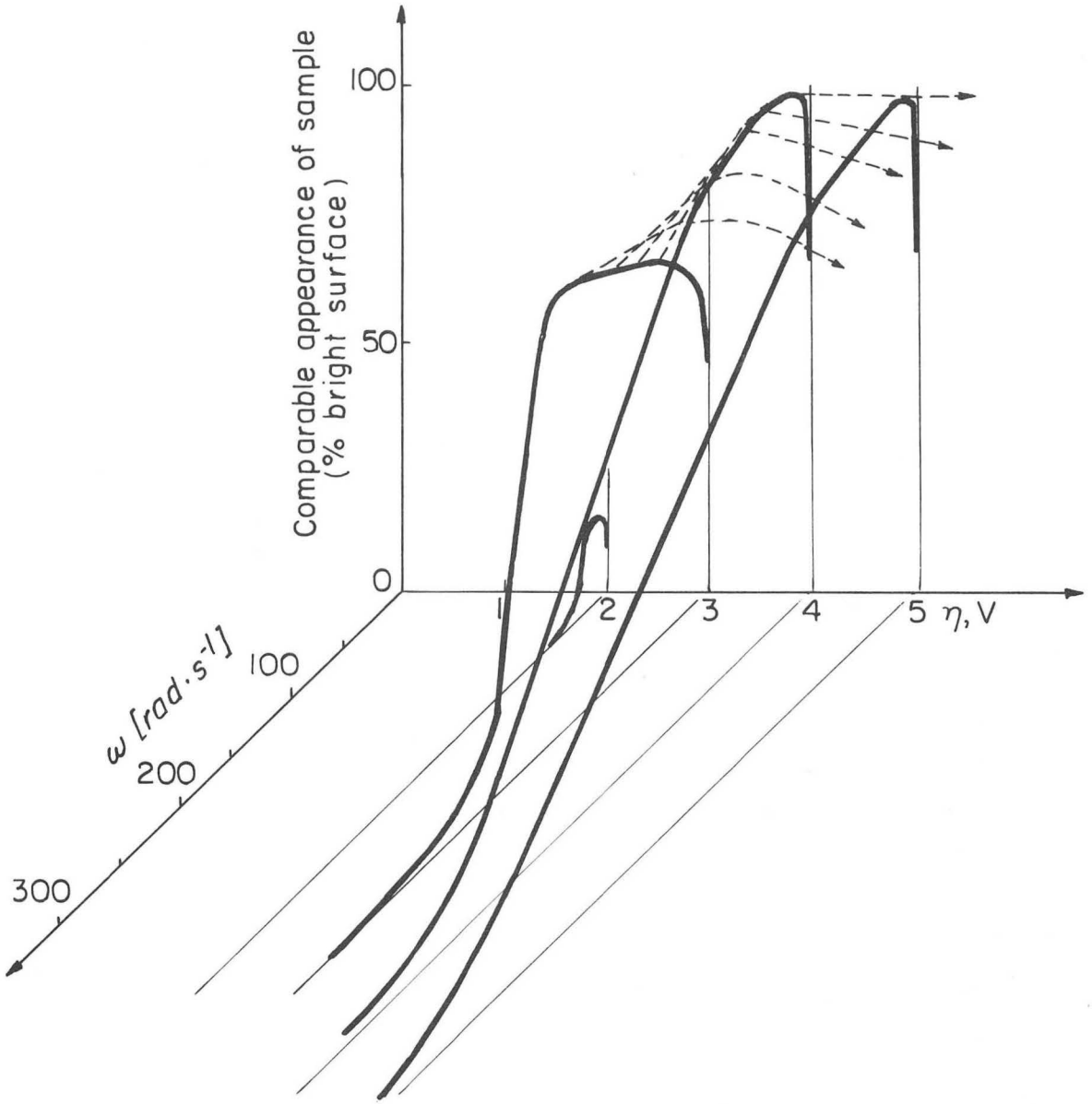

Fig. 9-1

XBL 815-5766

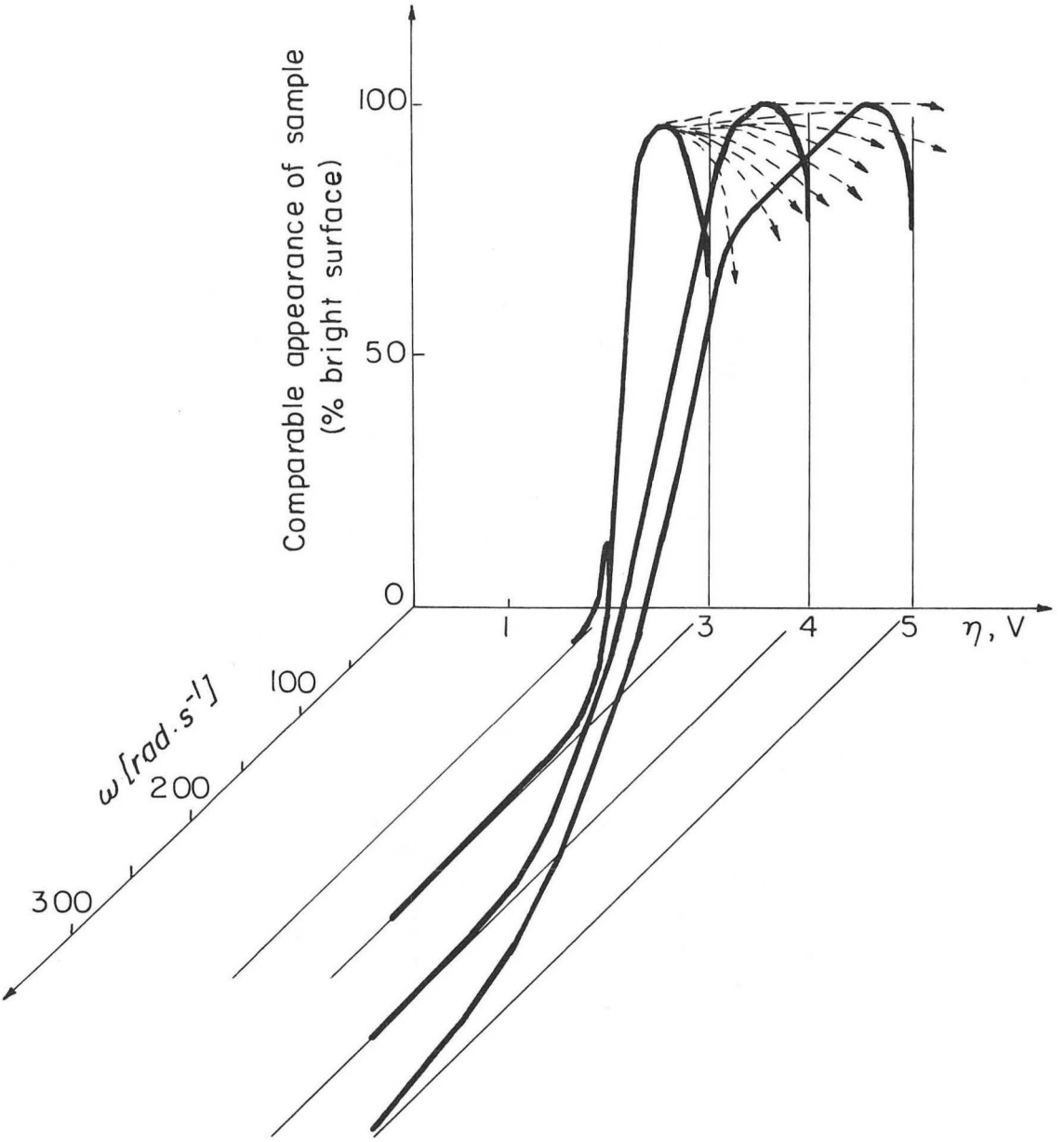

Fig. 9-2

XBL 815-5767

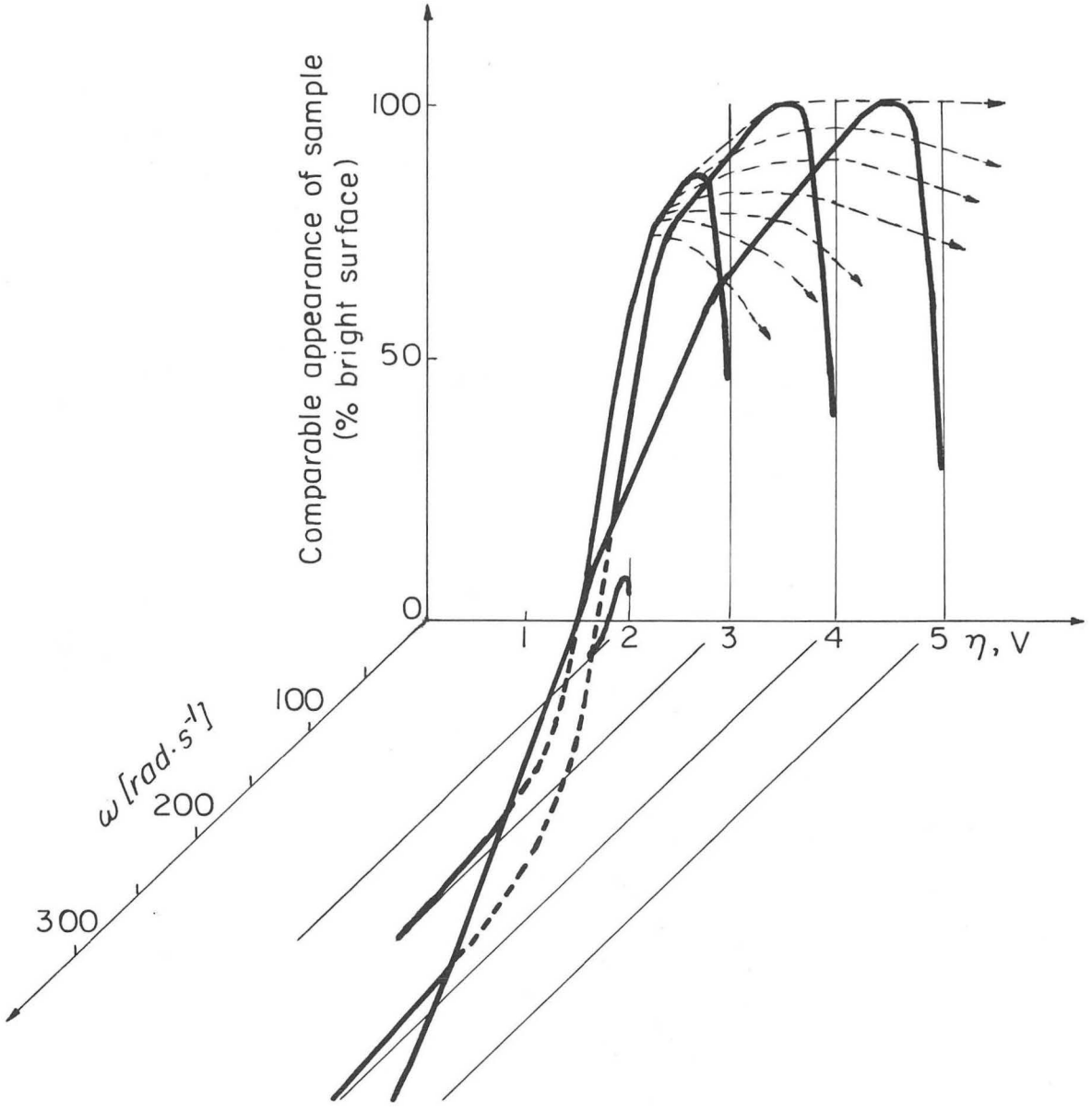

Fig. 9-3

XBL 815-5768

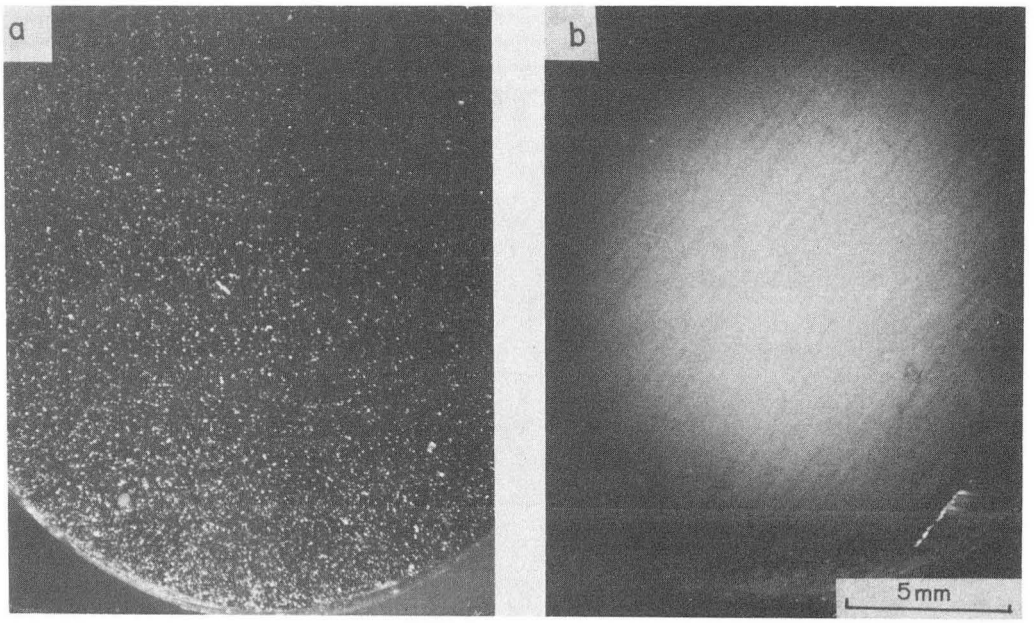

XBB 815-4760

Fig. 10-1

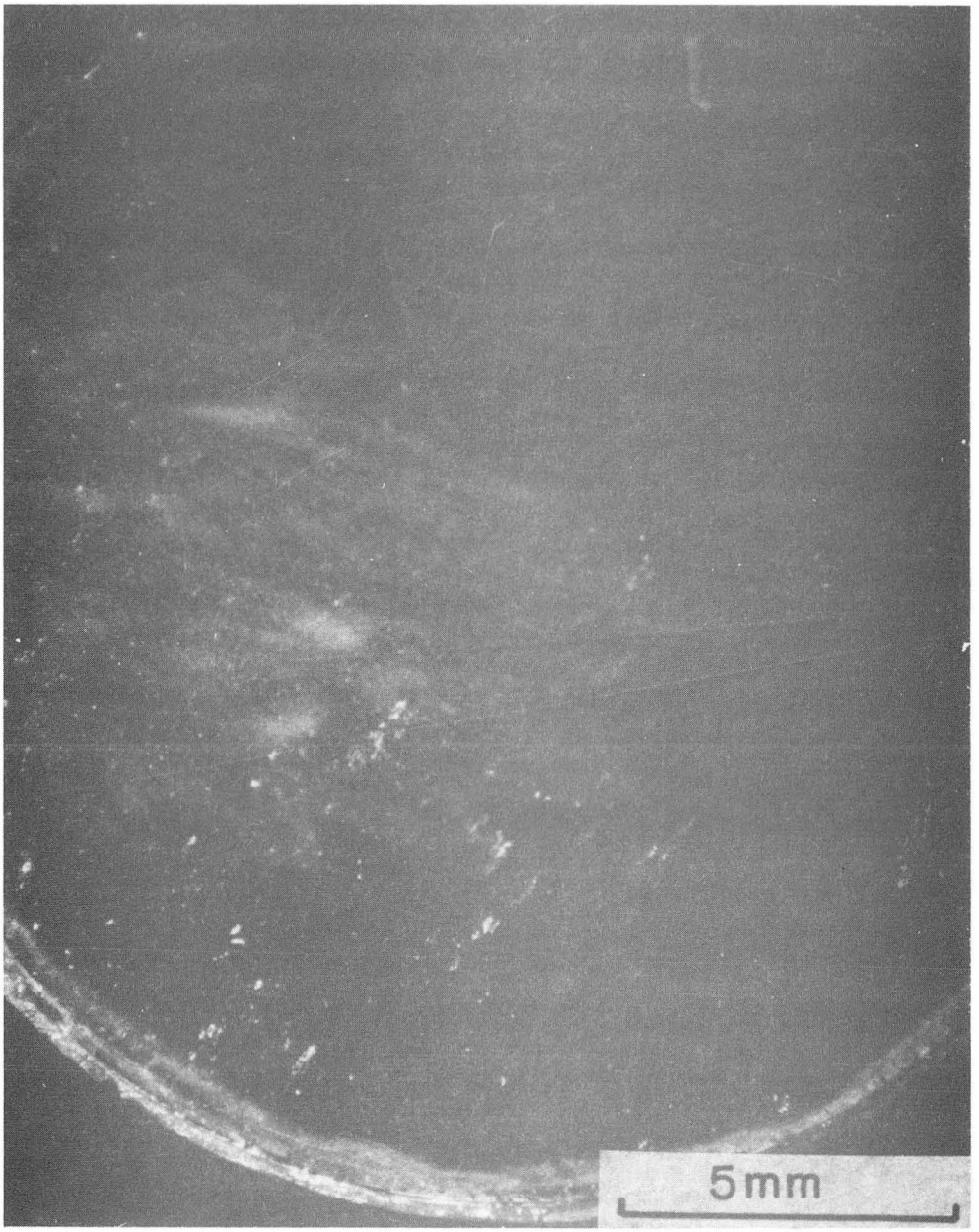

XBB 815-4758

Fig. 10-2

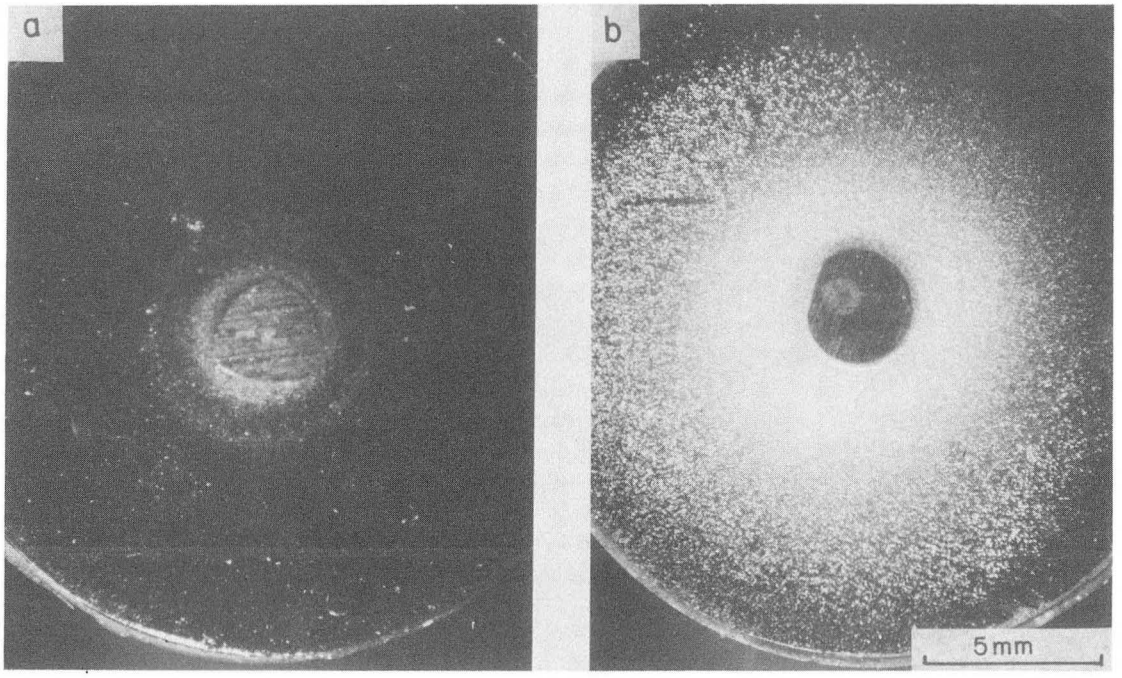

XBB 815-4761

Fig. 10-3

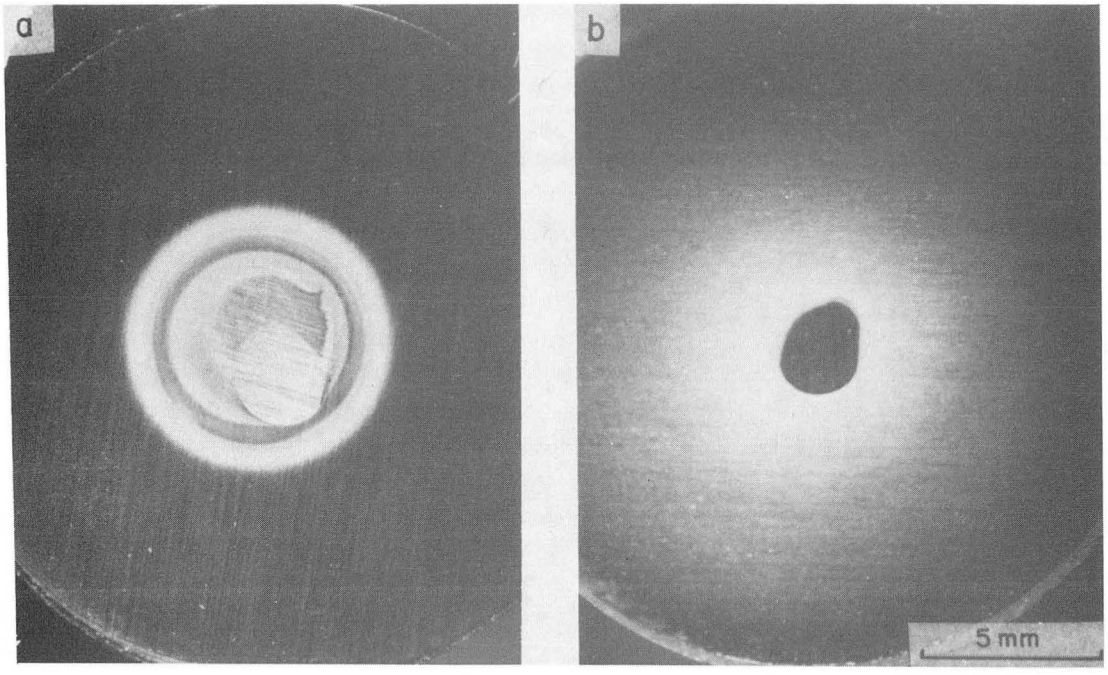

XBB 815-4754

Fig. 10-4

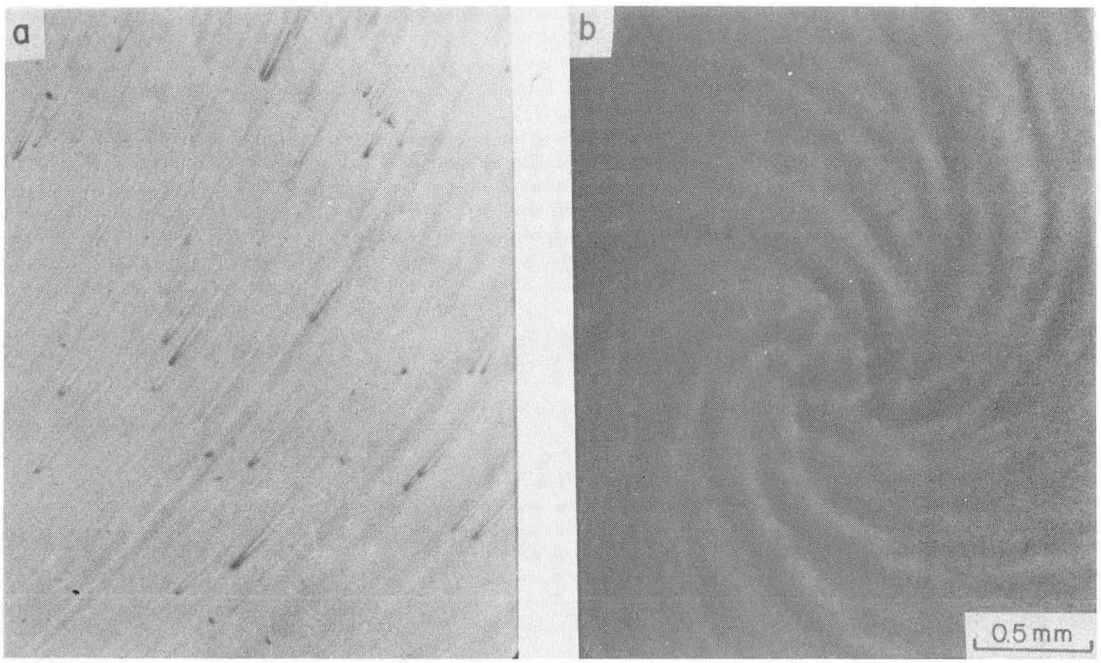

XBB 815-4756

Fig. 10-5

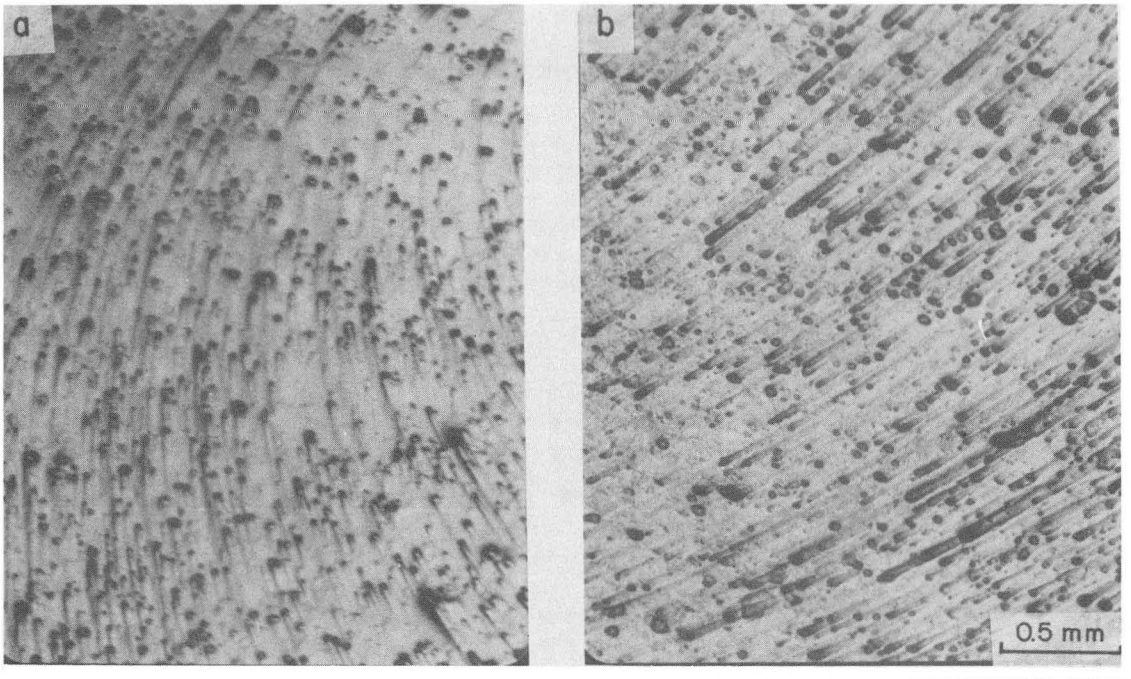

XBB 815-4762

Fig. 10-6

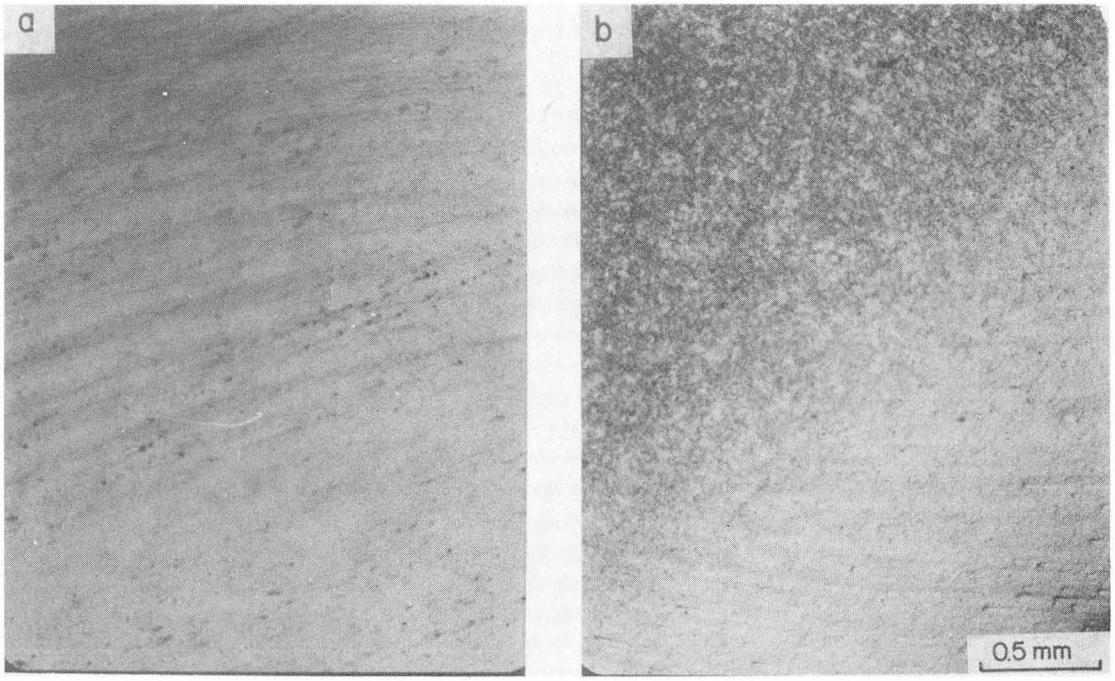

XBB 815-4765

Fig. 10-7

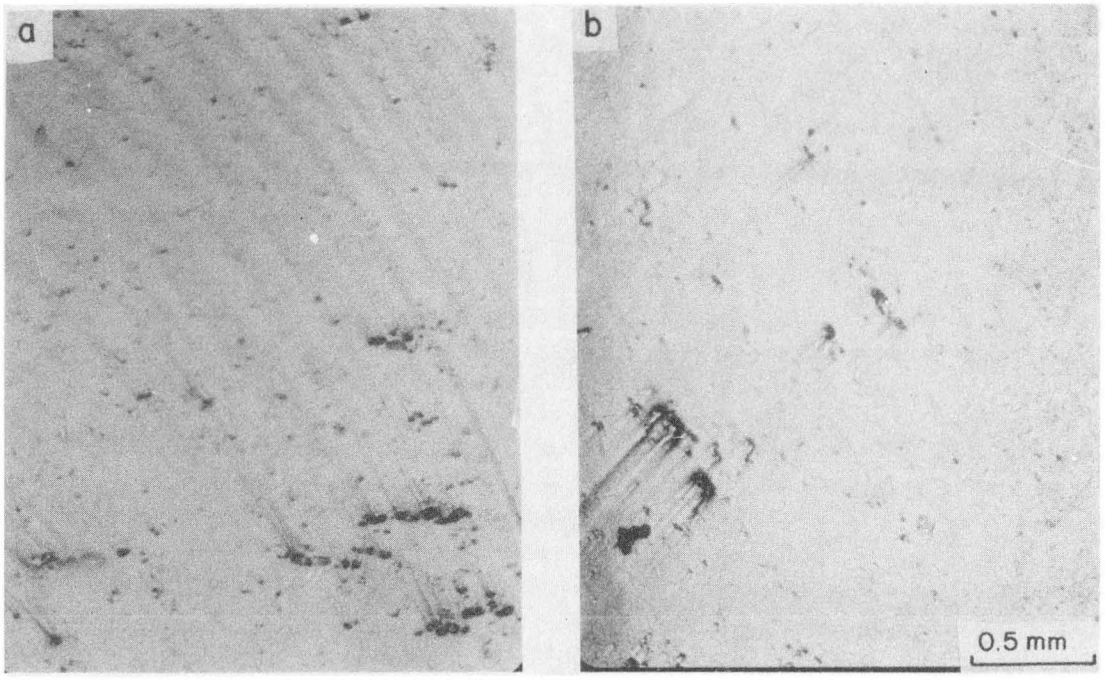

XBB 815-4765B

Fig. 10-8

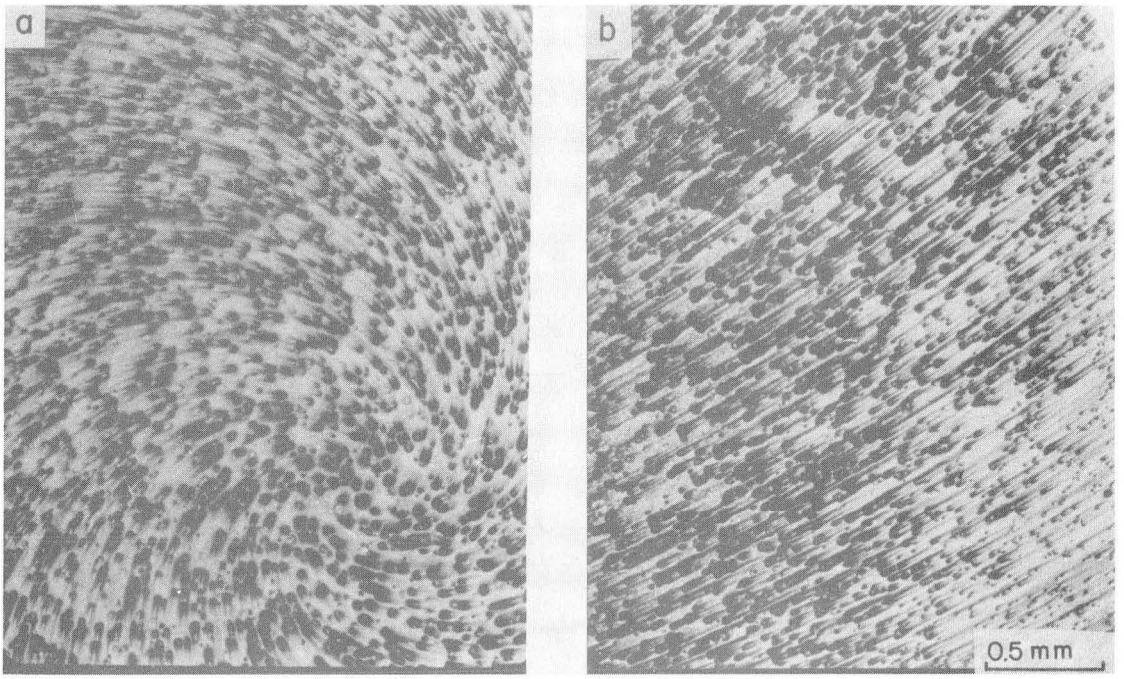

XBB 815-4765A

Fig. 10-9

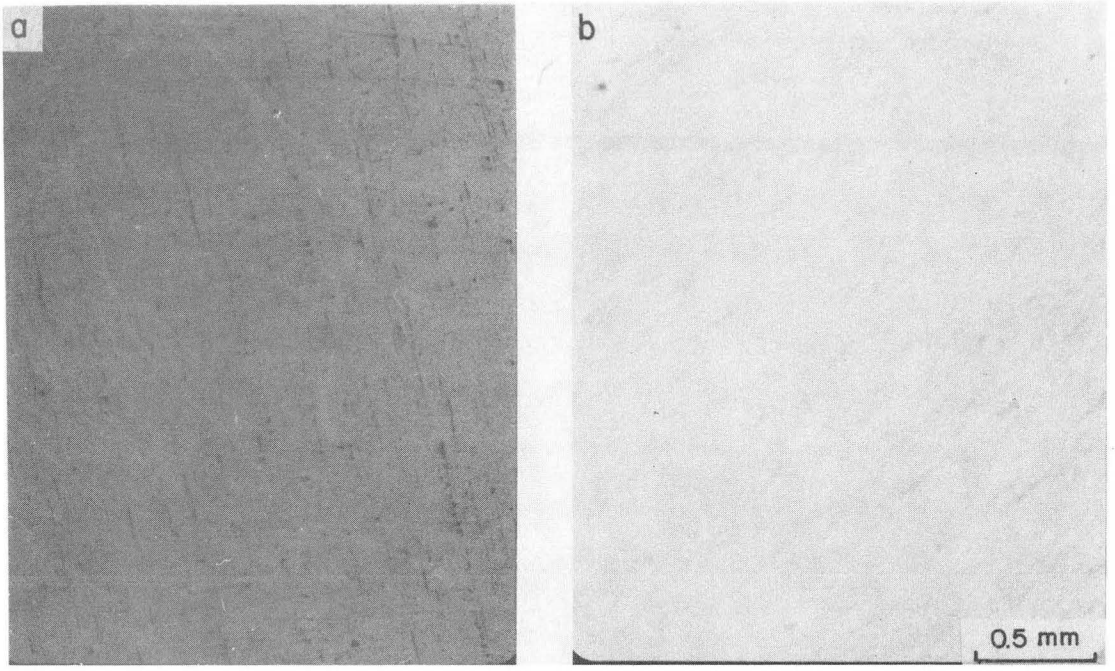

XBB 815-4755

Fig. 10-10

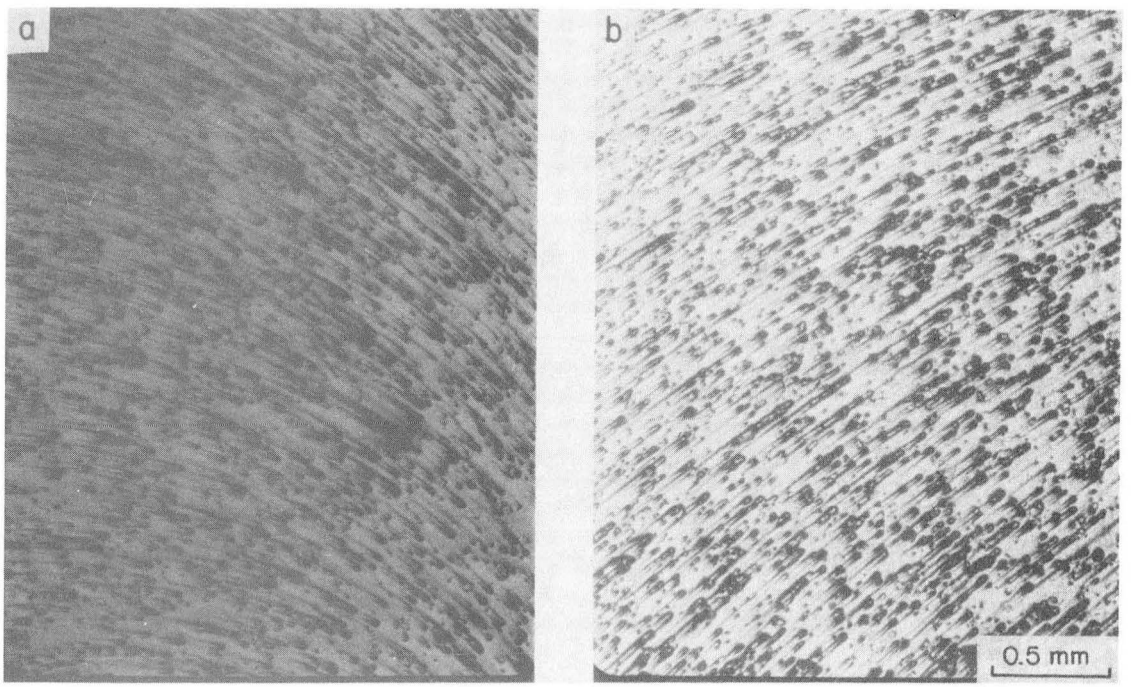

XBB 815-4763

Fig. 10-11

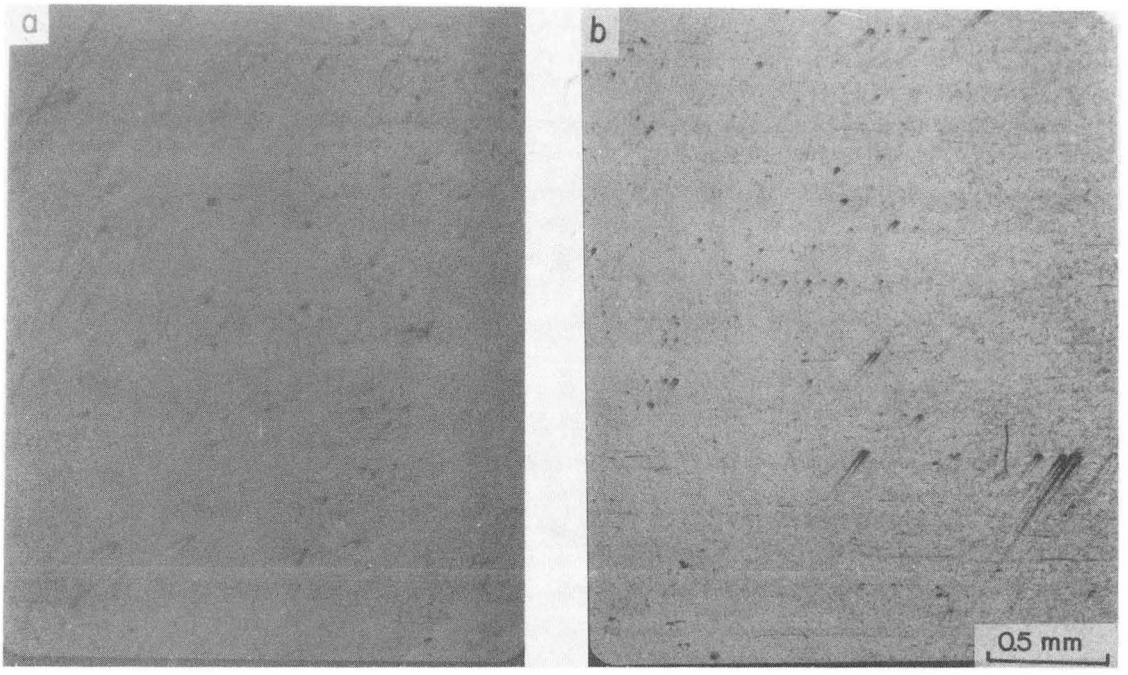

XBB 815-4757

Fig. 10-12

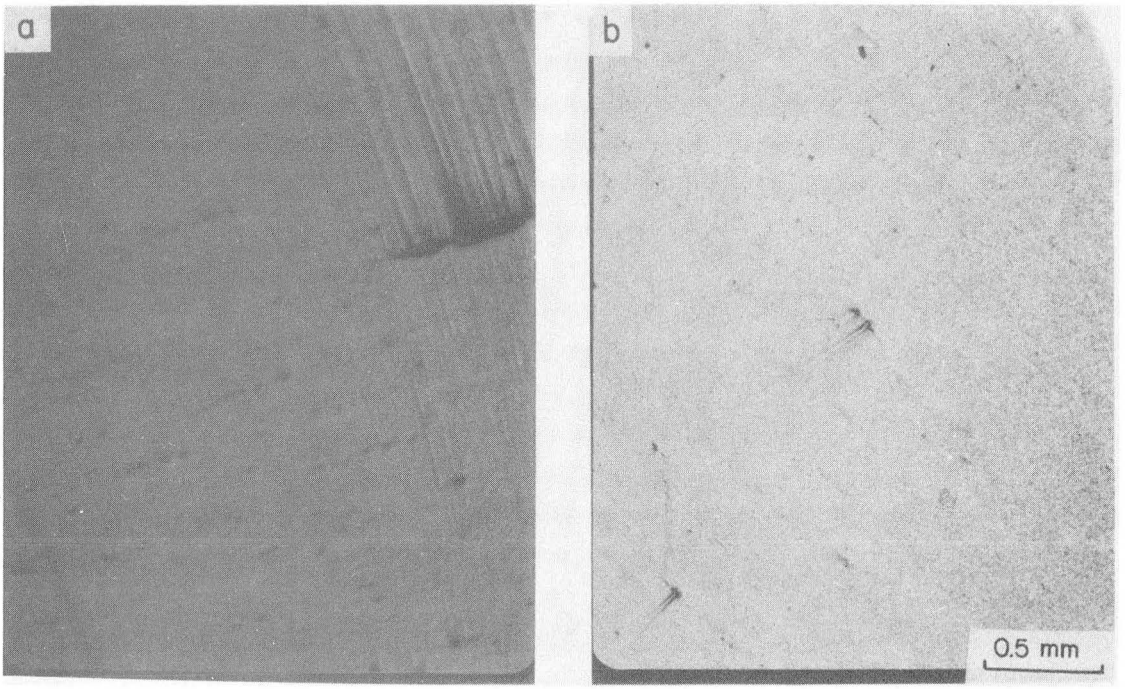

XBB 815-4764

Fig. 10-13

XBB 815-4759

Fig. 10-14

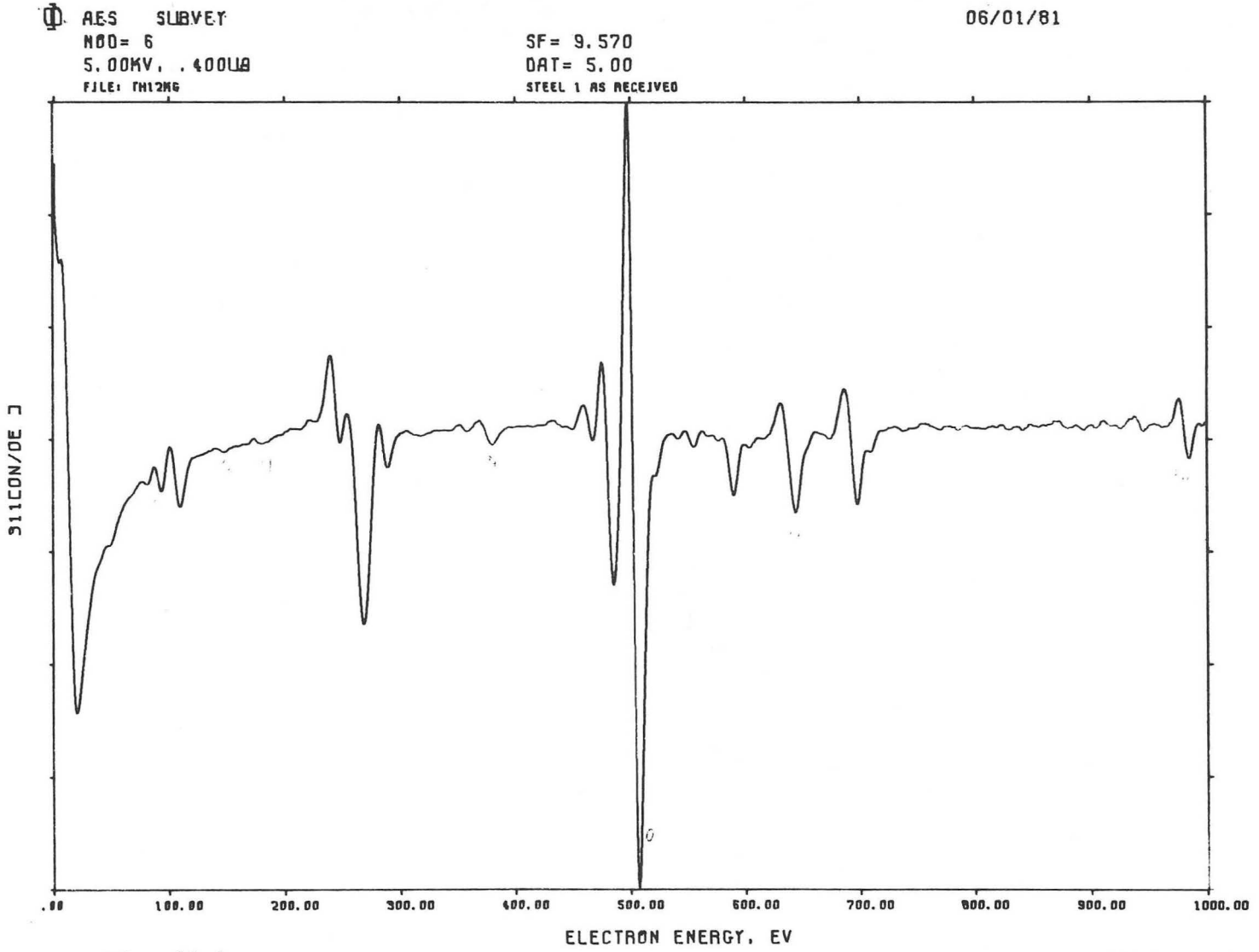

Fig. 11-1

XBL 816-10062

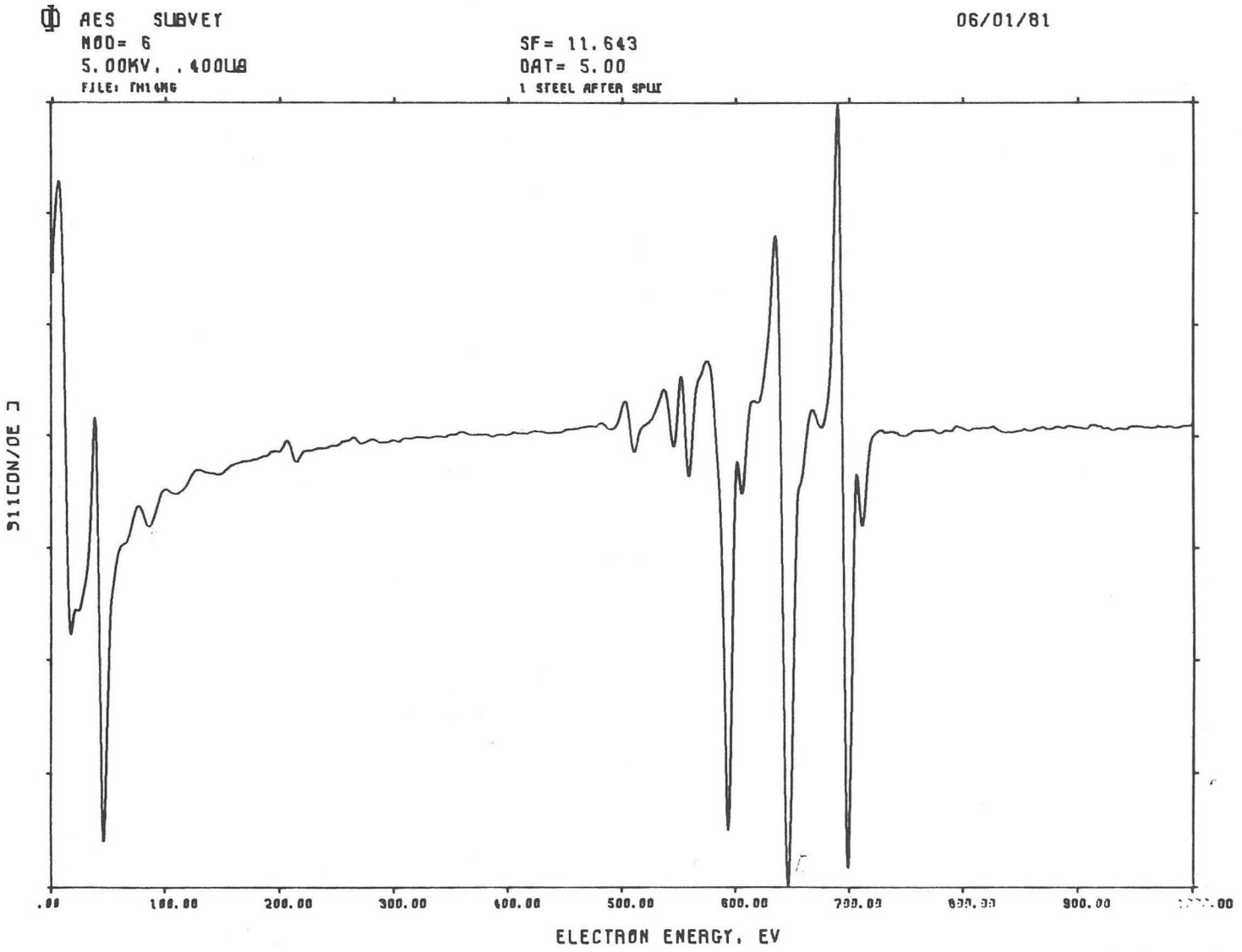

Fig. 11-2

XBL 816-10063

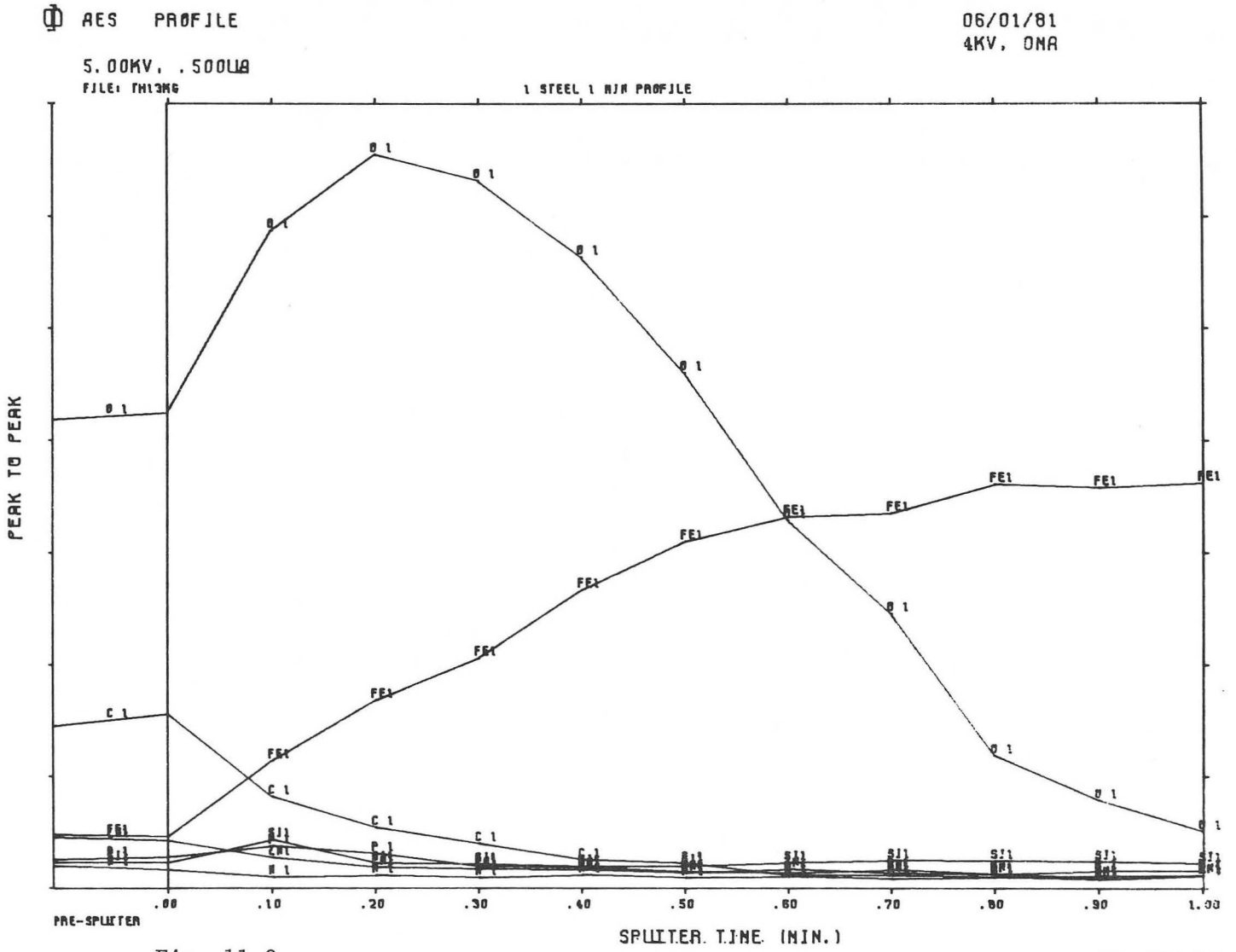

Fig. 11-3

XBL 816-10064

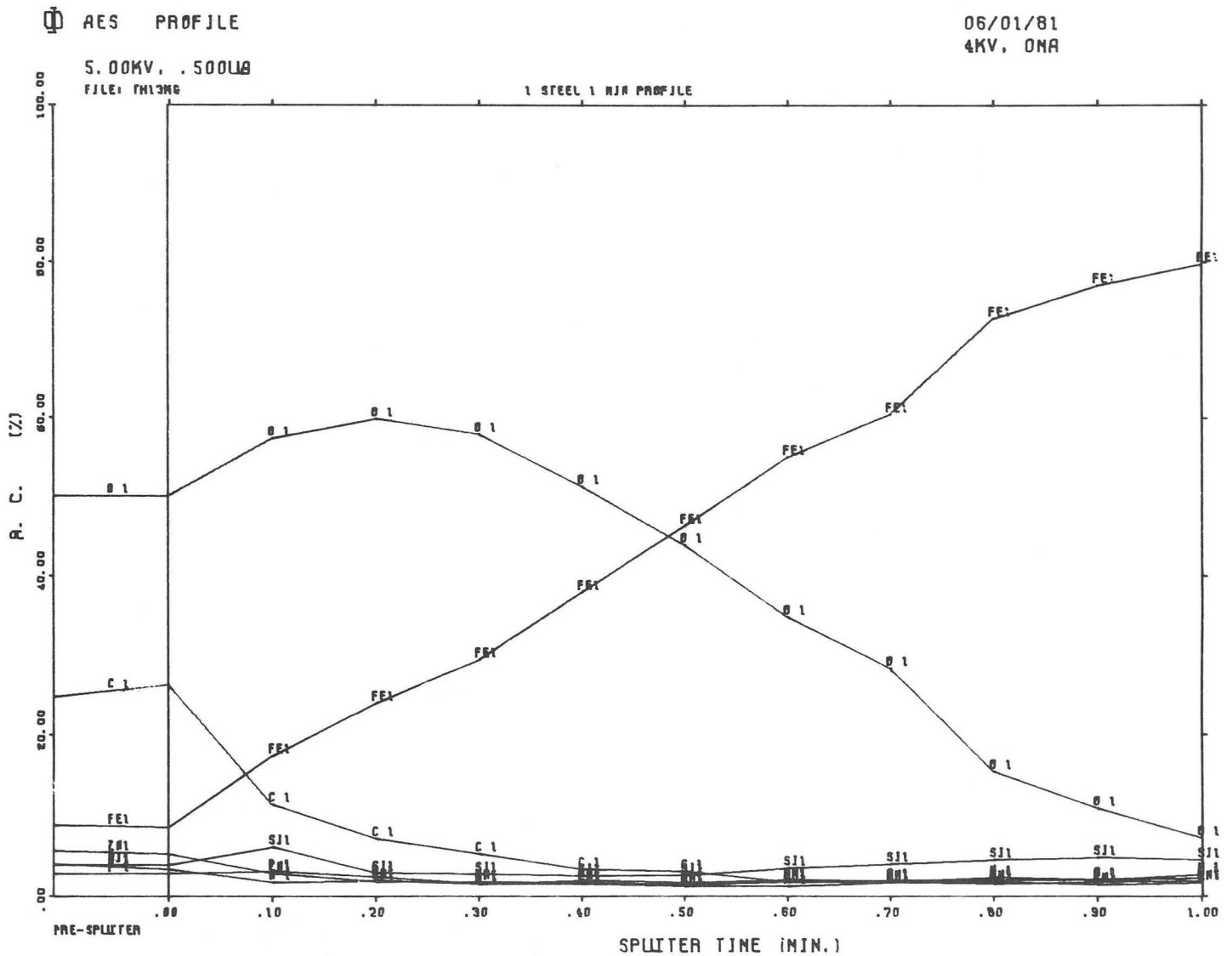

Fig. 11-4

XBL 816-10065

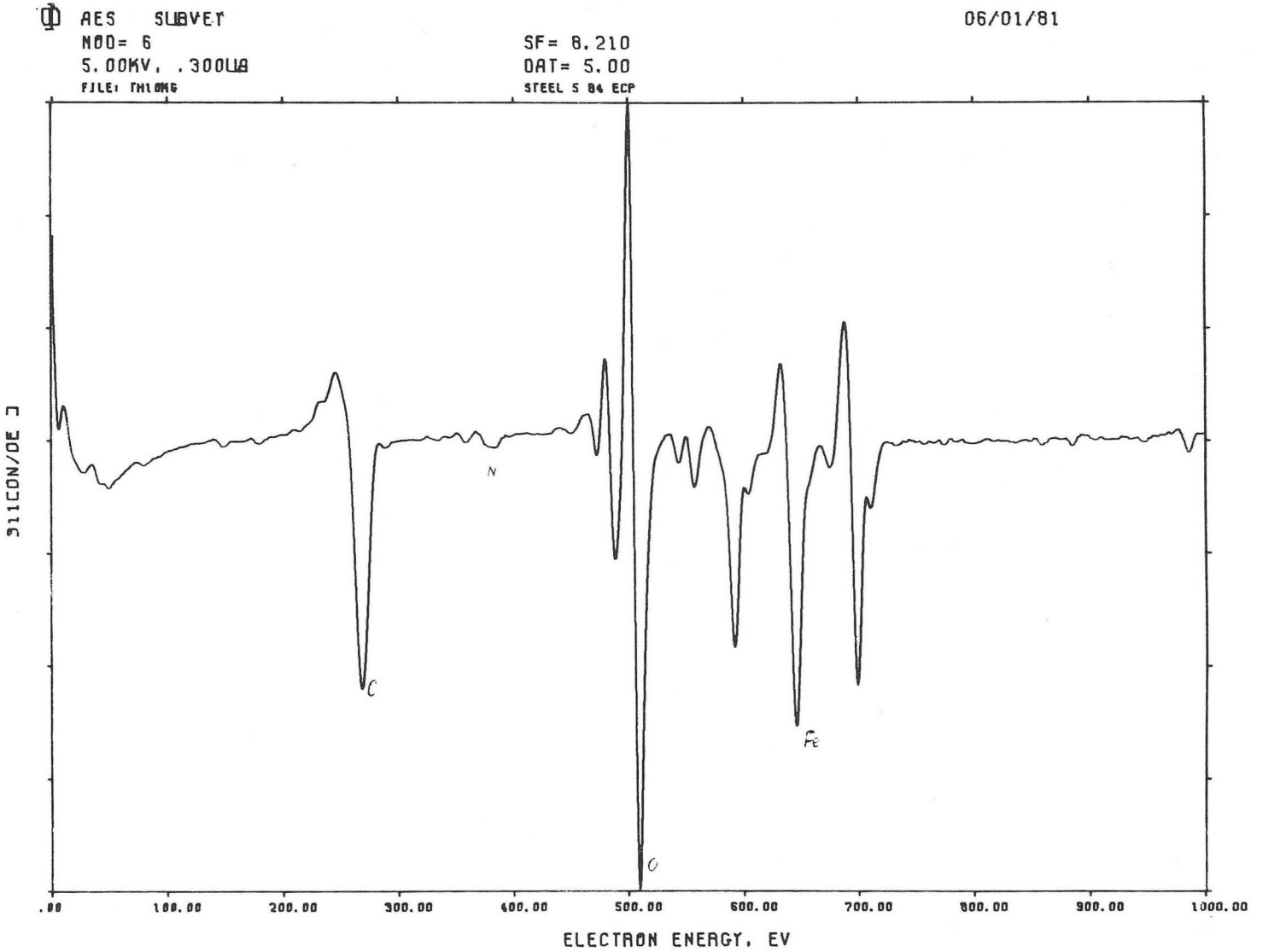

Fig. 11-5

XBL 816-10066

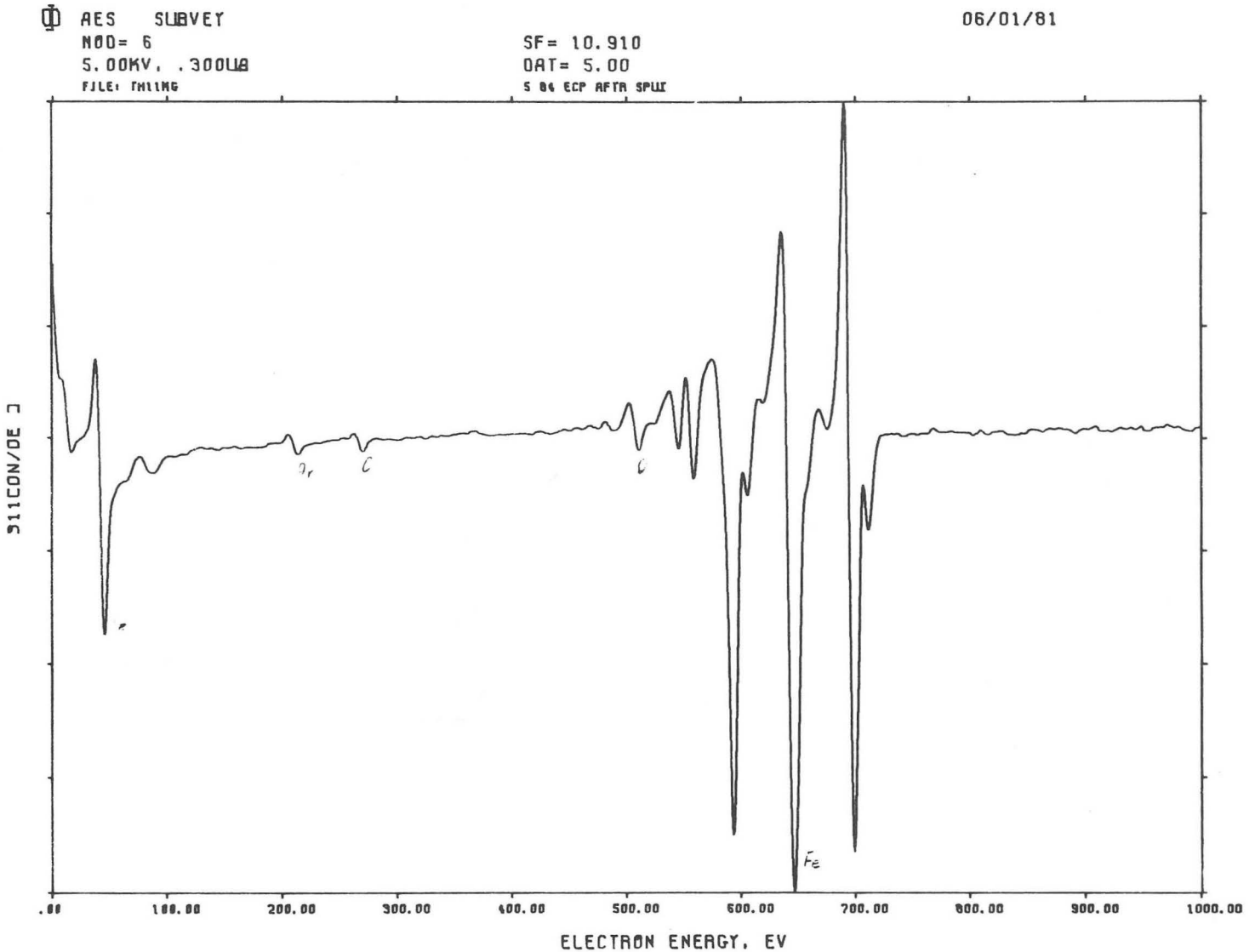

Fig. 11-6

XBL 816-10067

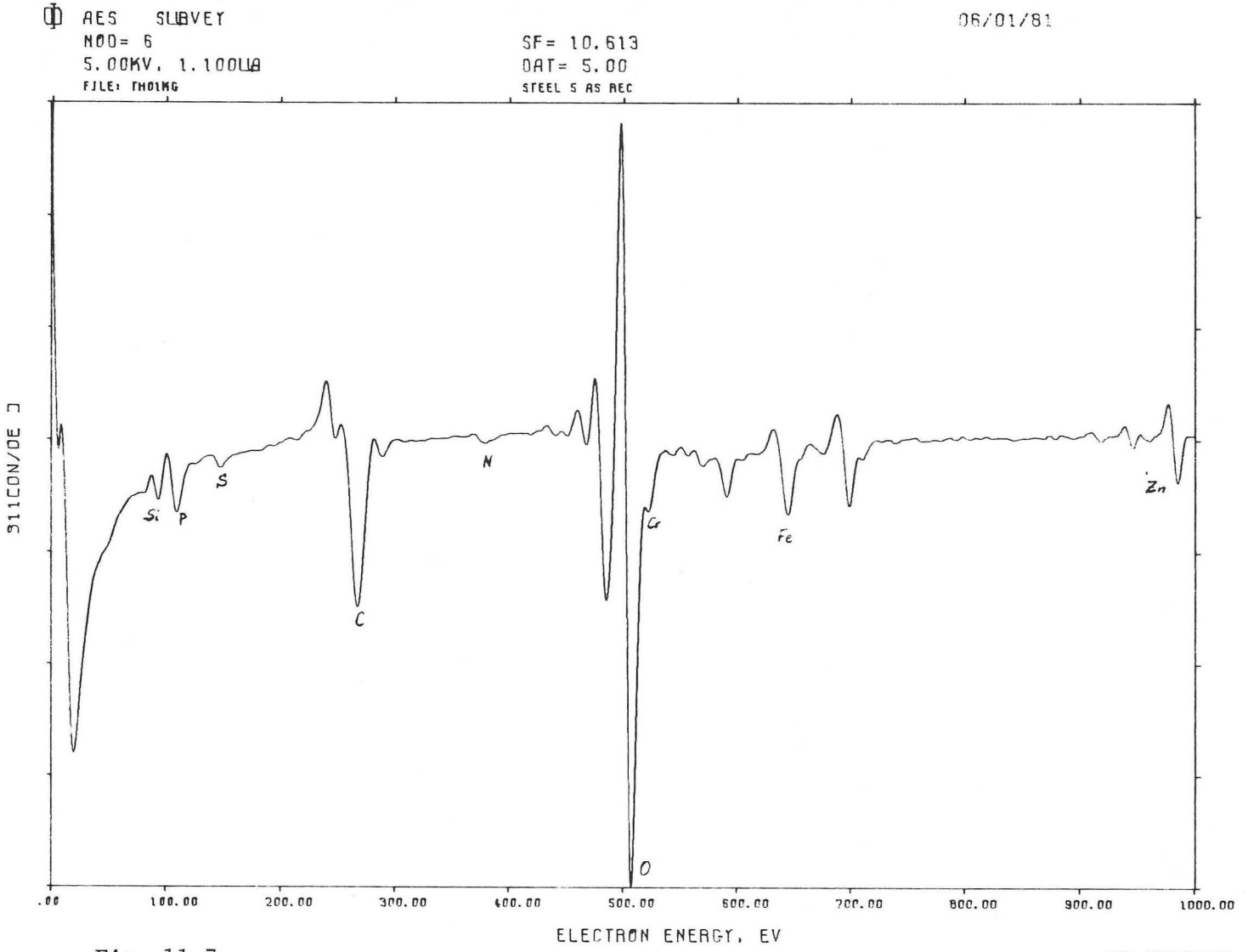

Fig. 11-7

XBL 816-10068

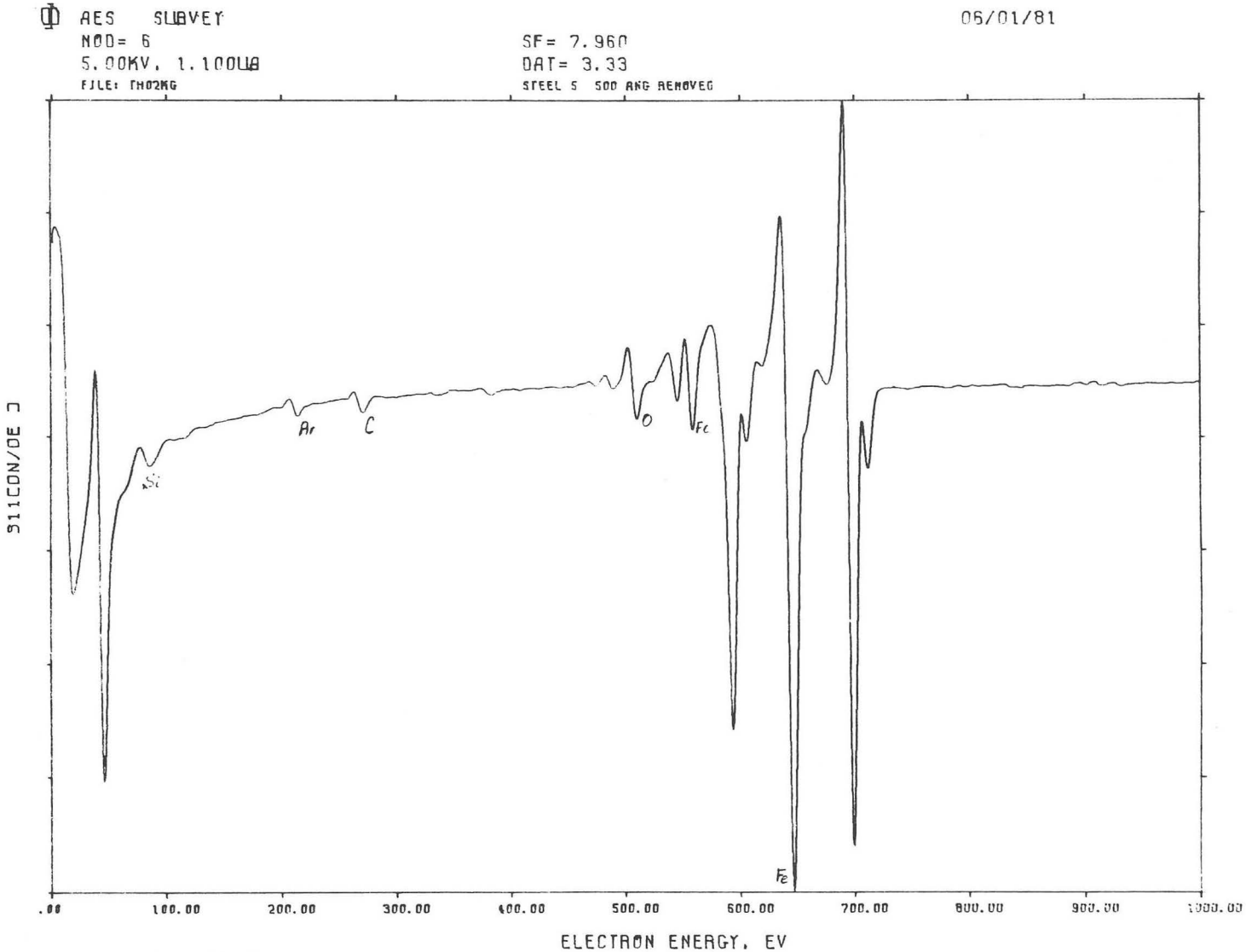

Fig. 11-8

XBL 816-10069

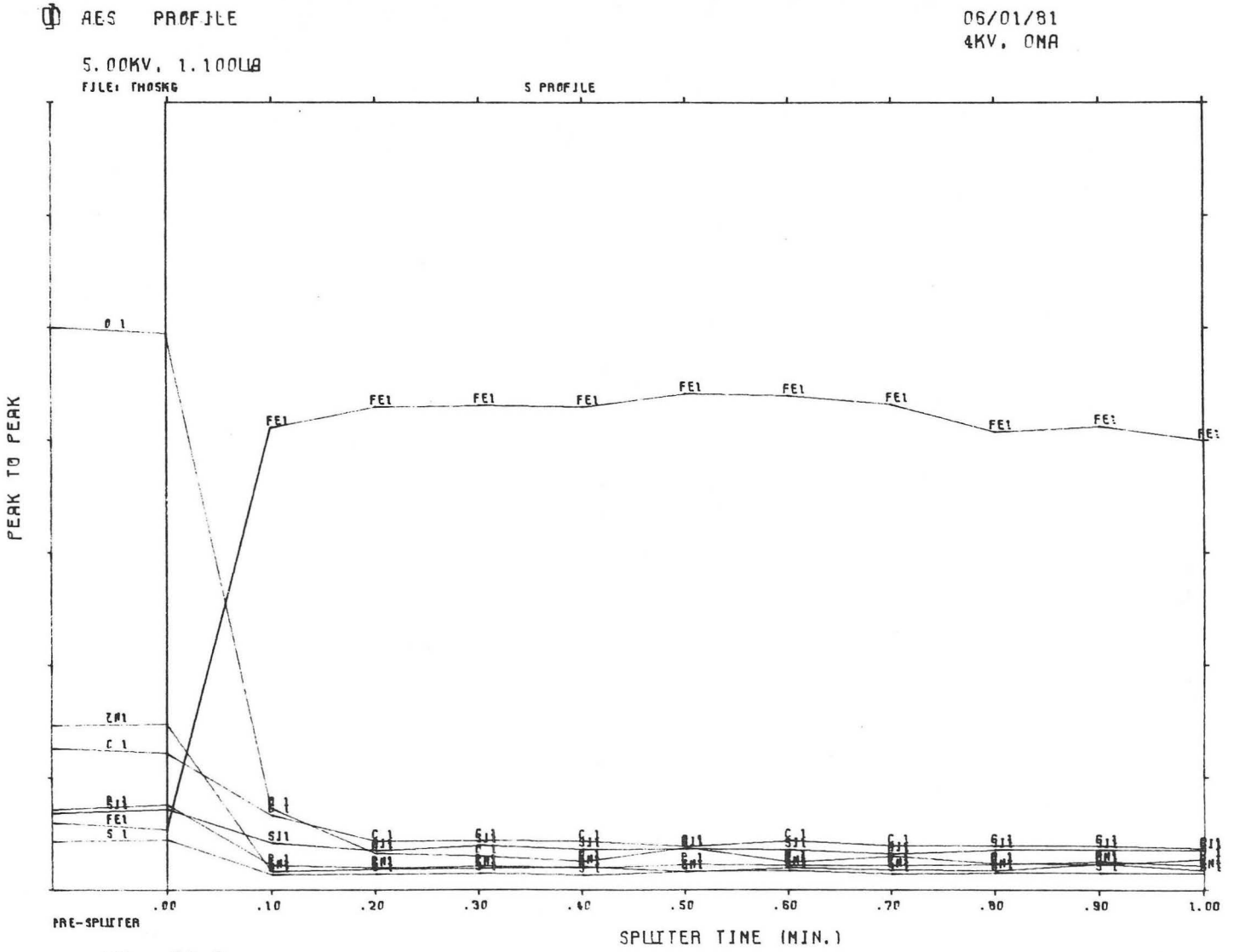

Fig. 11-9

XBL 816-10070

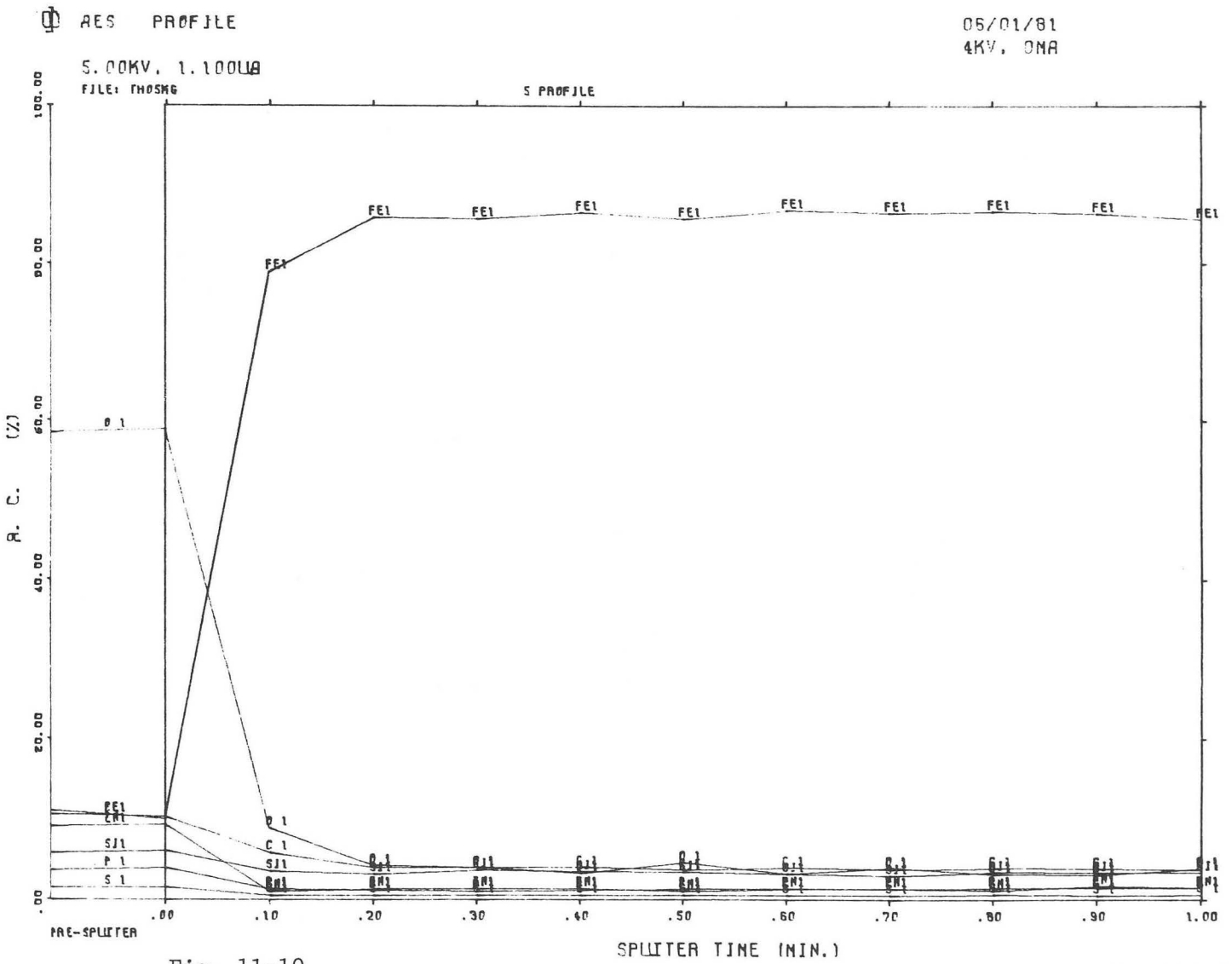

Fig. 11-10

XBL 816-10071

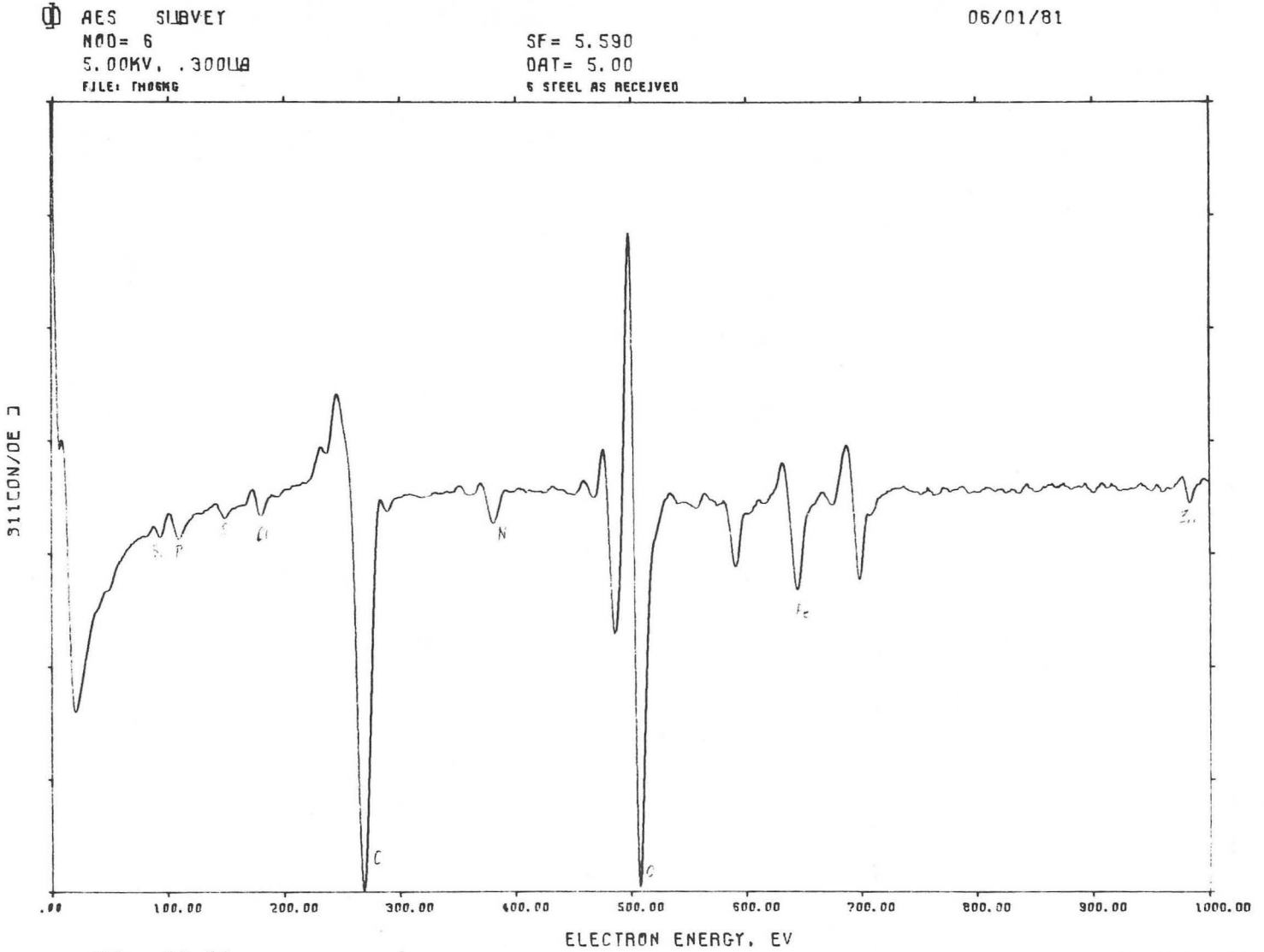

Fig. 11-11

XBL 816-10072

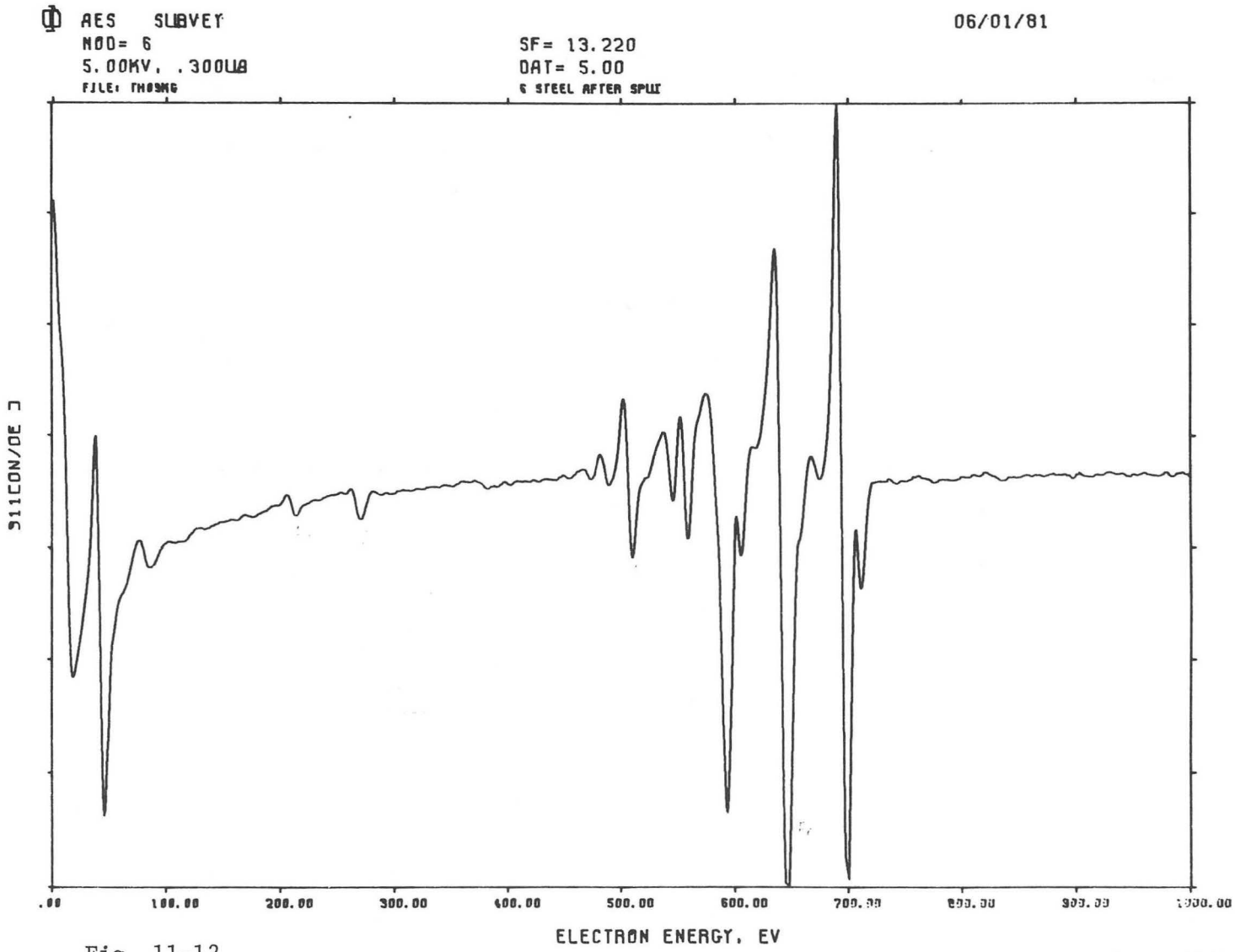

Fig. 11-12

XBL 816-10073

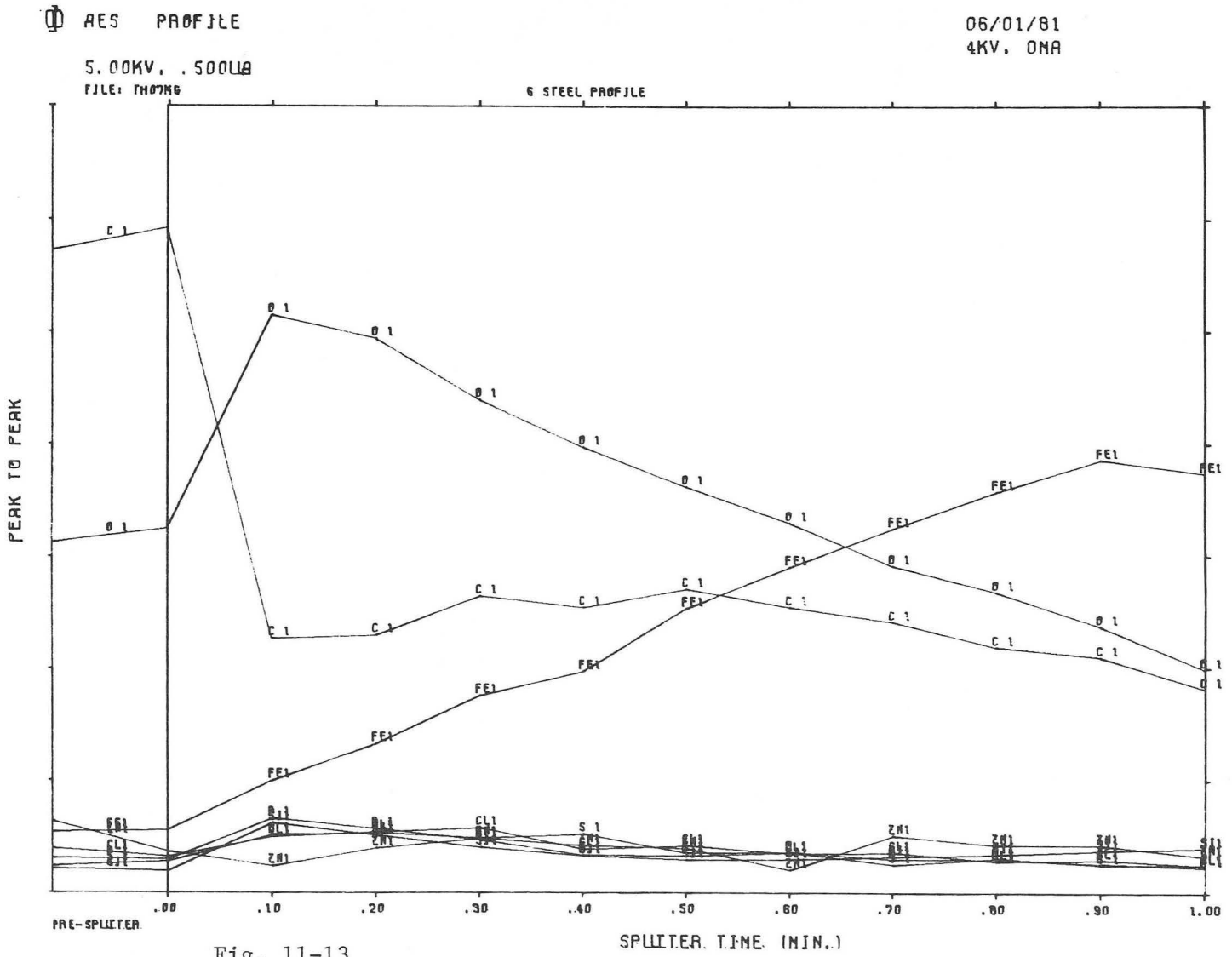

Fig. 11-13

XBL 816-10074

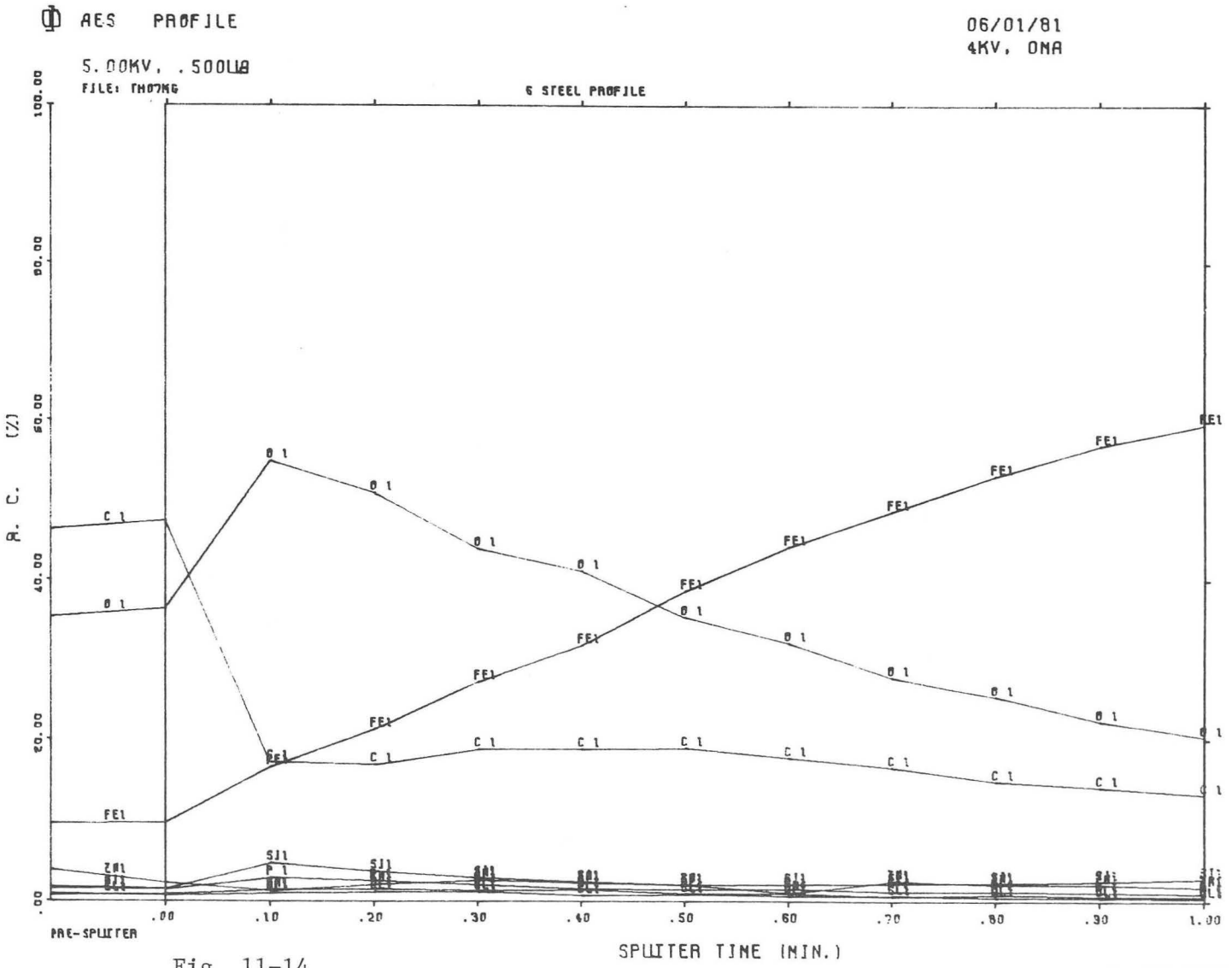

Fig. 11-14

XBL 816-10075

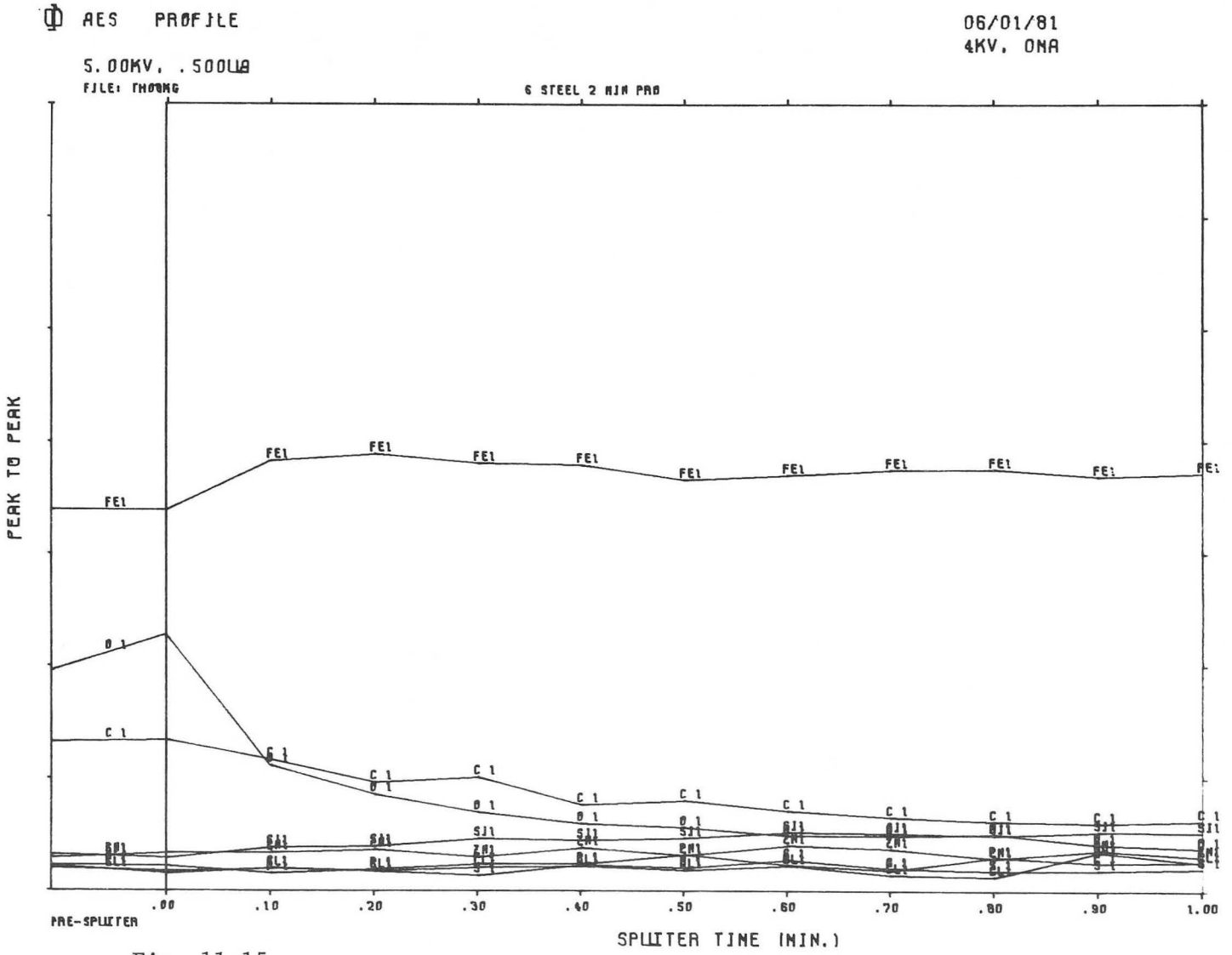

Fig. 11-15

XBL 816-10076

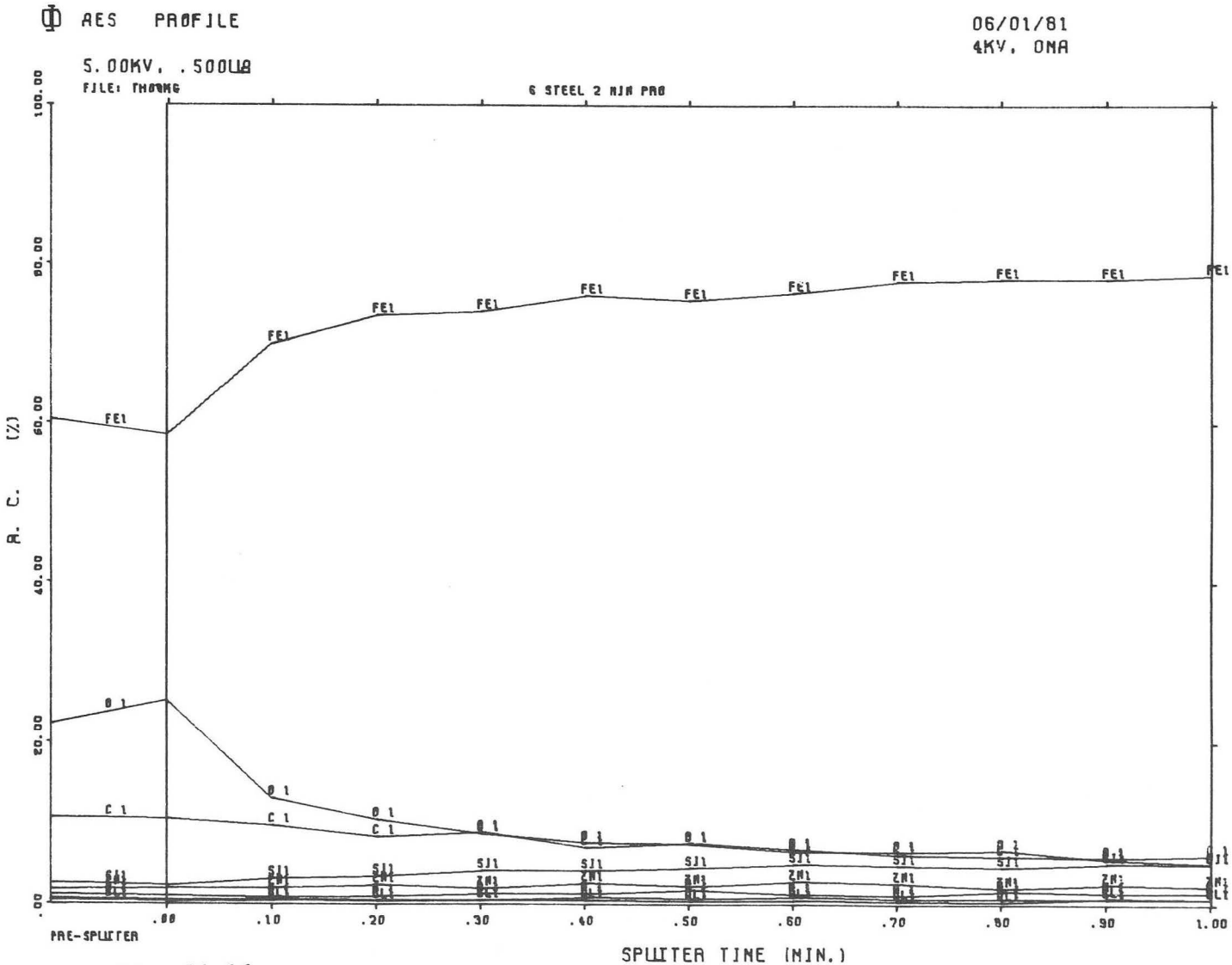

Fig. 11-16

XBL 816-10077

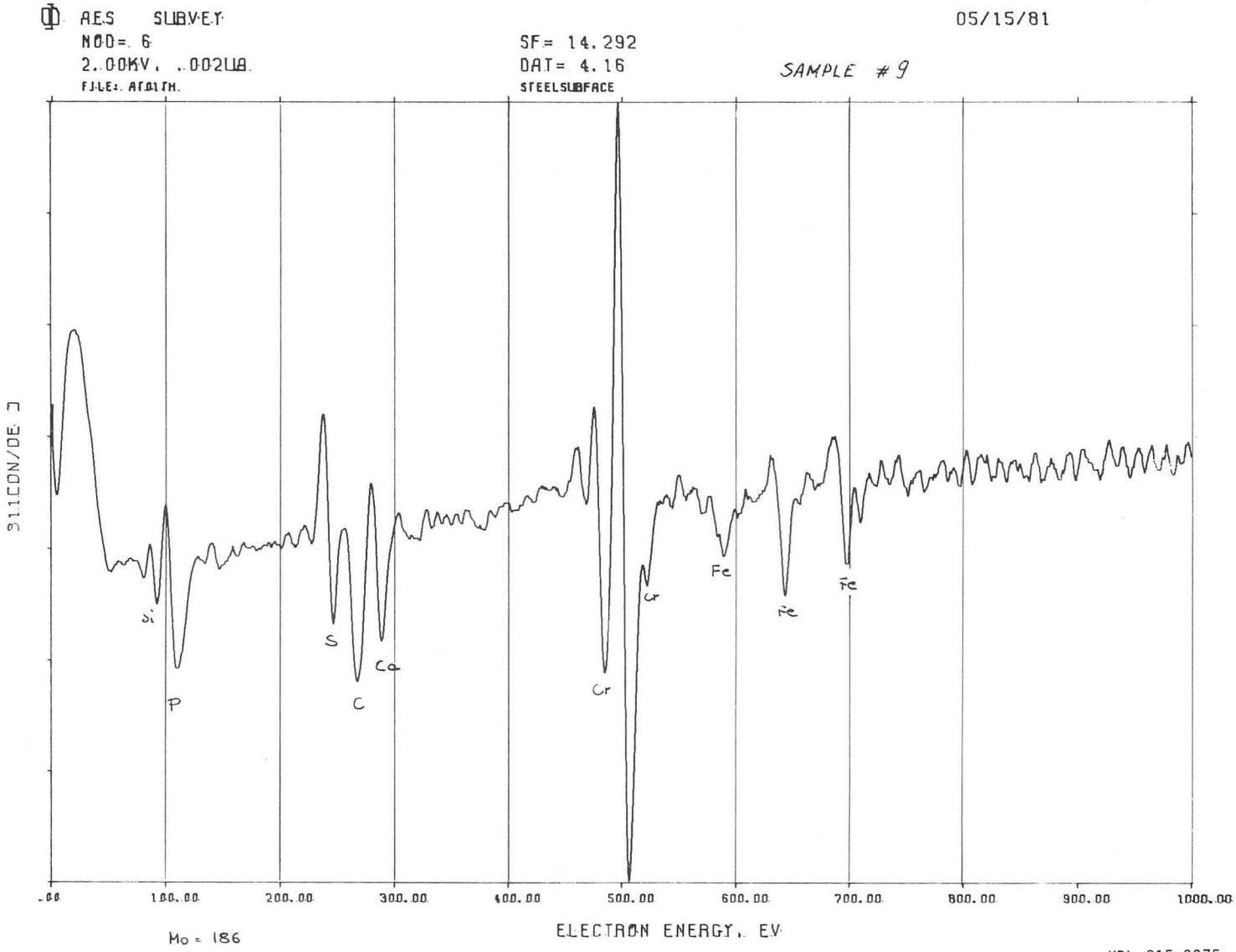

Fig. 11-17

XBL 815-9975

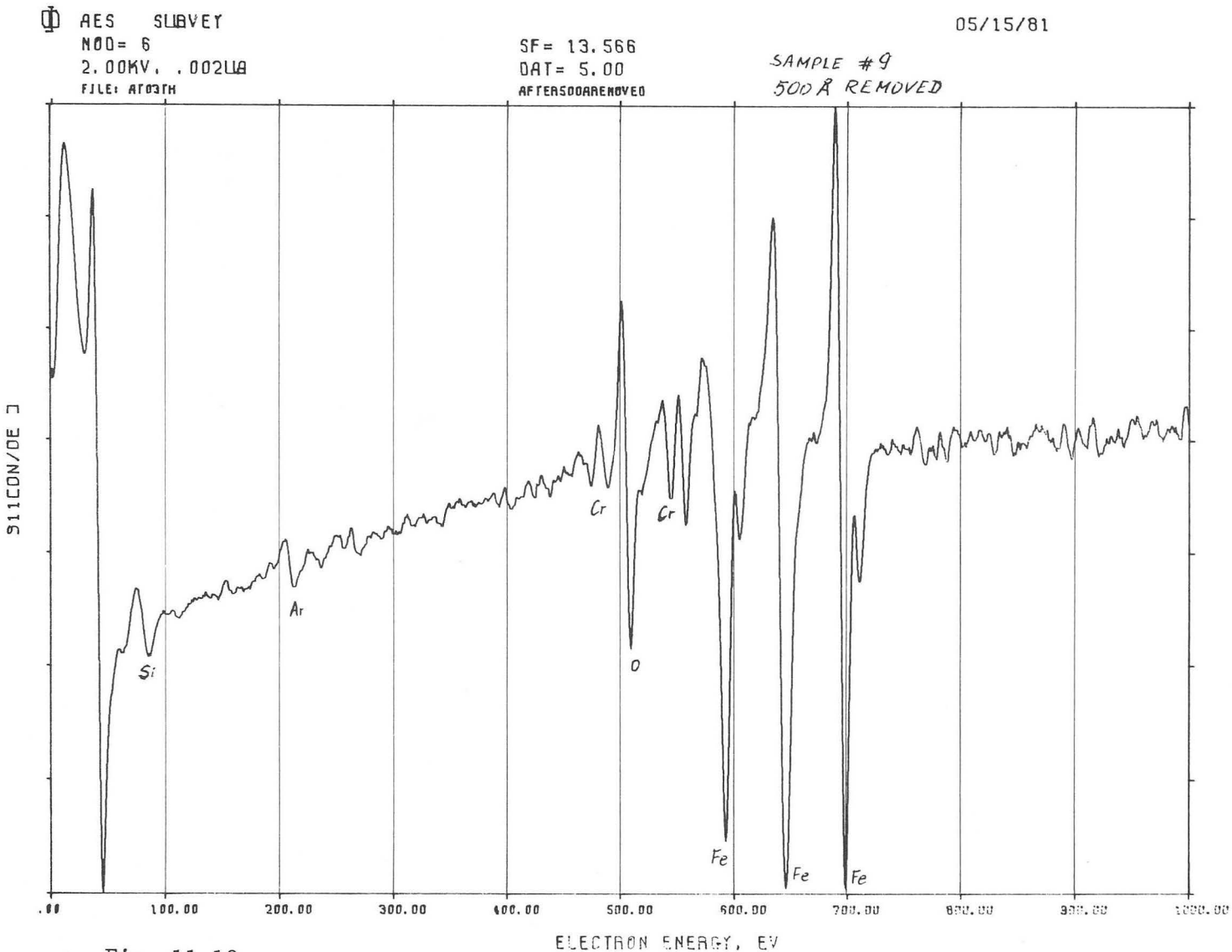

Fig. 11-18

XBL 815-9974

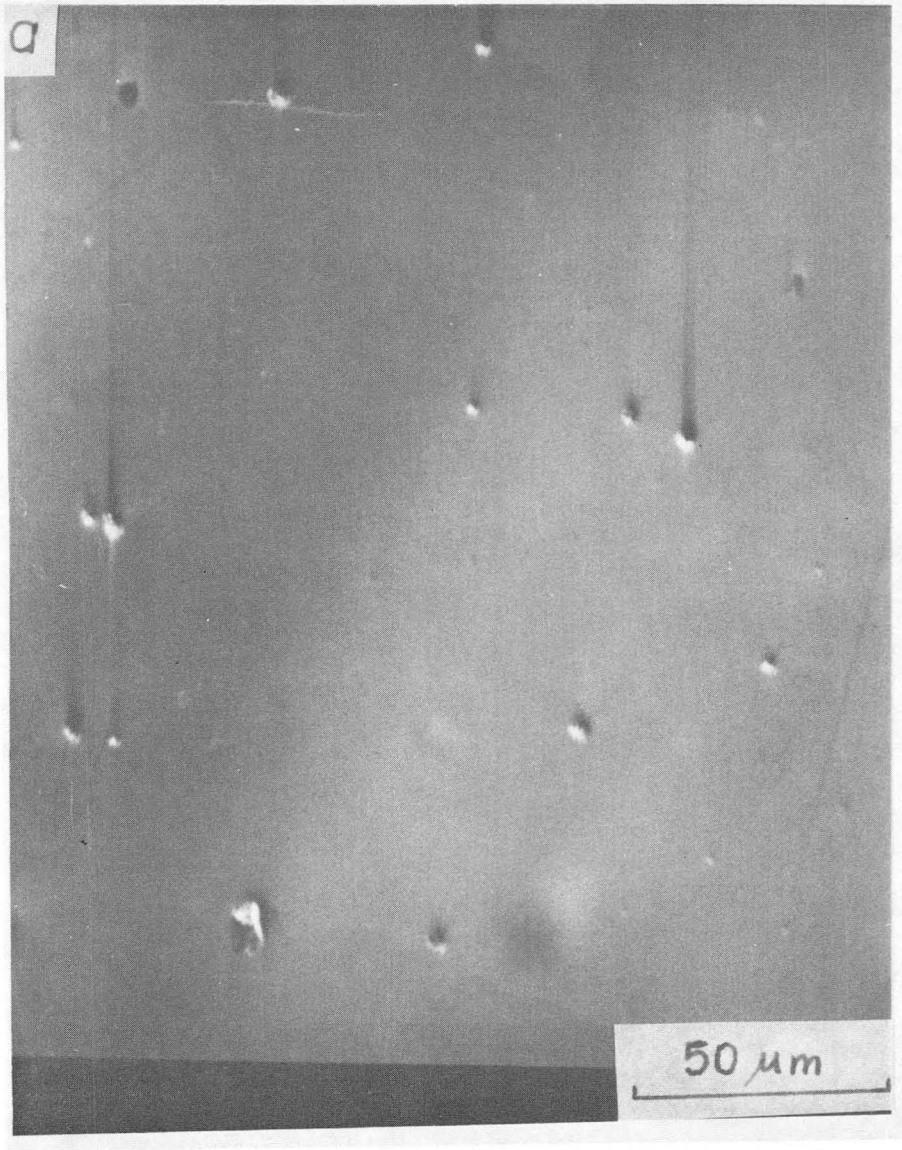

XBB 816-5081

Fig. 11-19

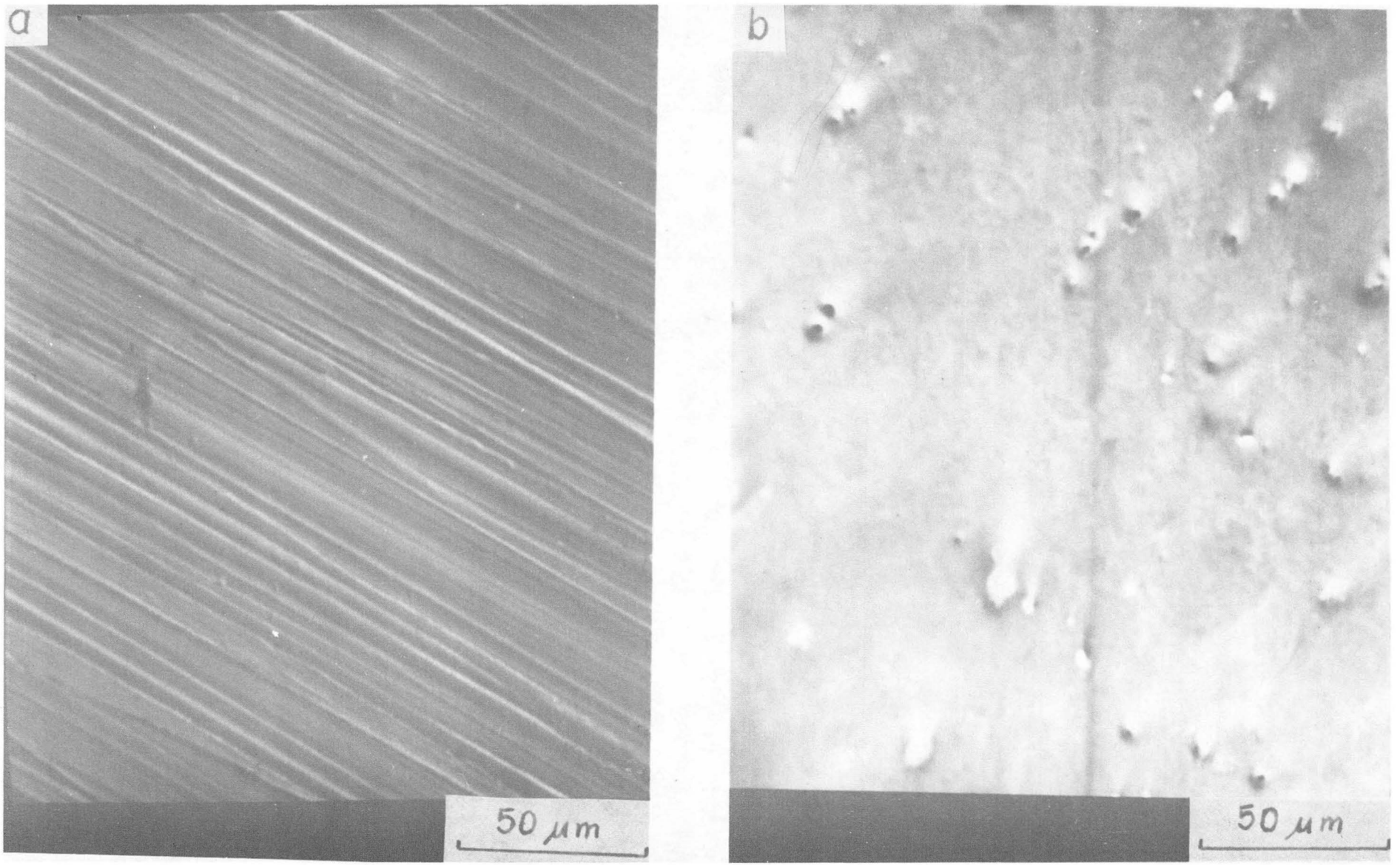

XBB 816-5080

Fig. 11-20

This report was done with support from the Department of Energy. Any conclusions or opinions expressed in this report represent solely those of the author(s) and not necessarily those of The Regents of the University of California, the Lawrence Berkeley Laboratory or the Department of Energy.

Reference to a company or product name does not imply approval or recommendation of the product by the University of California or the U.S. Department of Energy to the exclusion of others that may be suitable.

TECHNICAL INFORMATION DEPARTMENT
LAWRENCE BERKELEY LABORATORY
UNIVERSITY OF CALIFORNIA
BERKELEY, CALIFORNIA 94720